

CROSS-FREQUENCY COUPLING TRACKS MOTOR AUTOMIZATION AND EXECUTION IN THE HUMAN MOTOR SYSTEM

Dissertation

zur Erlangung des akademischen Grades

doctor rerum naturalium

(Dr. rer. nat)

genehmigt durch die Fakultät für Naturwissenschaften
der Otto-von-Guericke Universität Magdeburg

von Dipl.-Psych., Dipl.-Päd. Stefan Dürschmid
geb am 26. August 1979 in Magdeburg

Gutachter: Prof. Dr. Hermann Hinrichs
Prof. Dr. Klaus Lehnertz

eingereicht am: 14. November 2013
verteidigt am: 17. Juni 2014

“The ultimate physical substrate of memory formation and consolidation resides in alteration synaptic efficacy, which then alters the patterns of activity in large aggregate collections of cortical neurons”
(Hebb,1949)

List of Figures

1.1	The Motor System	8
2.1	Signal parameters	11
2.2	Frequency Analysis	12
4.1	Experimental paradigm	23
4.2	Trough-to-Peak ratio	25
4.3	Trial bin structure	28
4.4	Frequency coupling in ECoG	29
4.5	Parallel TPR-performance evolution	30
4.6	ROI-analysis	31
4.7	Performance related cortical clusters	33
5.1	MEG behavioral results	38
5.2	Change of paCFC in rPFC	39
5.3	Preferred frequencies in MEG recordings	40
5.4	Correlation of paCFC with reaction time across participants	42
5.5	Cross-regional granger causality	43
6.1	Experimental paradigm	49
6.2	Frequency analysis	53
6.3	Methods	55
6.4	Behavioral Results	59
6.5	θ -high γ variance	60
6.6	θ -high γ coupling	61
6.7	Individual Coupling Patterns	62
6.8	Effect of cognitive control	62
6.9	Variation of Coupling	71
6.10	Specificity of θ -high γ Coupling	72
6.11	Coupling/performance correlation	72
6.12	Phaseshift with cognitive control	73
6.13	θ Phase Resetting	74
8.1	Prediction as a function of θ phase	93
8.2	Grid coverage	94
9.1	Permutation test	100
9.2	paCFC for subgroups	101
9.3	Probability of Clusters of MEG-sensors	102

List of Figures

9.4	Dependence of Correlation on the number of trials	103
9.5	Test for equal variances	104
10.1	Anatomical location	106

Contents

1	Introduction	5
1.1	Outline of the thesis	5
1.2	Movement and the human brain	5
1.3	Learning	6
1.4	The motor system	6
1.5	Learning related changes in the motor system	7
2	General Methods to analyze Neural Correlates of Motor Learning and Automatization	9
2.1	Oscillations in the neuronal tissue	9
2.2	The θ and the high γ band: functions of slow and fast oscillations	13
2.3	Experimental and clinical constraints of invasive and non invasive recordings	14
2.4	The Hilbert Transform: Extracting phase and amplitude information	15
2.5	Phase-Amplitude Cross-Frequency Coupling	15
2.6	Testing and parametrization for occurrence of cross-frequency coupling	16
3	Working Hypotheses and Outline of Analyses	19
4	Oscillatory Dynamics during Motor Automatization: ECoG Recordings	21
4.1	Introduction	21
4.2	Methods and Materials	22
4.2.1	Patients	22
4.2.2	Experimental Paradigms	22
4.2.3	Data recording	24
4.2.4	Data pre-processing	24
4.2.5	Calculation of the Trough-to-Peak Ratio	25
4.2.6	Phase-Amplitude Coupling	26
4.2.7	ROI analysis	26
4.2.8	Separating performance from learning effects	26
4.3	Results	27
4.3.1	Phase amplitude cross frequency coupling	27
4.3.2	Covariation of paCFC with automatization	28
4.3.3	Discrimination of automatization from Random Performance Fluctuations.	31
4.4	Discussion of ECoG Results	32
4.4.1	Automatization and theta and high gamma activity	32
4.4.2	Biological mechanism	34

4.4.3	Conclusion	34
5	Oscillatory Dynamics during Motor Learning: MEG Recordings	35
5.1	Introduction	35
5.2	Methods and Material	36
5.2.1	Recording and Participants	36
5.2.2	Paradigm	36
5.2.3	Calculation of the theta-phase high gamma-amplitude Cross-Frequency Coupling.	36
5.2.4	Calculation of trial-by-trial paCFC	37
5.2.5	Granger causality	37
5.3	Results of MEG Recordings	37
5.3.1	Behavioral Results	37
5.3.2	Increase of paCFC in the contralateral (pre-)motor cortex	38
5.3.3	paCFC pattern in the right prefrontal cortex	39
5.3.4	paCFC/performance prediction in the right prefrontal cortex	41
5.3.5	Anatomical hierarchy	41
5.4	Discussion of MEG Results	42
6	Oscillatory Dynamics track Cognitive Control: Subcortical Recordings from the Nucleus Accumbens	47
6.1	Introduction	47
6.2	Methods and Material	48
6.2.1	Participants	48
6.2.2	Paradigm	48
6.2.3	Cognitive Control	49
6.2.4	Data Collection	50
6.2.5	General Data Analysis	51
6.2.6	Behavioral Data	51
6.2.7	Frequency analysis	51
6.2.8	Phase-Amplitude Cross-Frequency Coupling (PAC)	52
6.2.9	Preclusion of θ Phase Resetting	57
6.2.10	Specificity of θ -high γ Coupling	57
6.3	Results	57
6.3.1	Behavioral Results	57
6.3.2	Amplitude variation	58
6.3.3	High γ amplitude varies as a function of θ phase in the contralateral NAcc	58
6.3.4	Coupling strength reflects cognitive control	60
6.3.5	Functional Relation between PAC and Behavior	61
6.3.6	θ phase re-alignment	64
6.3.7	Specificity of θ -high γ Coupling	64
6.4	Discussion of DBS Results	64
6.4.1	Summary of Results	64
6.4.2	Interplay of Frequencies for integration of information	65
6.4.3	PAC is strongest following a decision	66

6.4.4	Differences in coupling phase	67
6.4.5	Conclusion	68
7	Summary and General Discussion	75
7.1	Summary of the experimental results	75
7.2	Perspectives for future research	77
	References	79
8	Appendix - ECoG recordings	91
9	Appendix - MEG recordings	95
9.1	Supplementary Methods	95
9.1.1	Calculation of Trough-to-Peak Ratio	95
9.1.2	Granger Causality	96
9.2	Supplementary Results	97
9.3	Probability not to respond	99
9.4	Equal variances	102
10	Appendix - DBS recordings	105
10.1	Procedure: surgery and deep brain stimulation	105
11	Curriculum Vitae	109
12	Publikationen	113
13	Selbständigkeitserklärung	115
14	Danksagung	117

List of Abbreviations

Ncl.	Nucleus
Ncll.	Nuclei
paCFC	phase-amplitude cross-frequency coupling
MVAR	multivariate autoregressive model
TPR	trough to peak ratio
EEG	Electroencephalography
MEG	Magnetoencephalography
ECoG	Electrocorticography
θ	theta
γ	gamma
α	alpha
NAcc	Nucleus Accumbens

Zusammenfassung

der Dissertation unter dem Titel:

CROSS-FREQUENCY COUPLING TRACKS MOTOR AUTOMIZATION AND EXECUTION
IN THE HUMAN MOTOR SYSTEM

vorgelegt von Dipl.-Psych., Dipl.-Päd Stefan Drschmid

Oszillatorische Phänomene erregten in den letzten Jahren ein großes Interesse innerhalb der Neurowissenschaften. Große Zellverbände im menschlichen Gehirn zeigen unterschiedliche zeitliche Entladungsmuster, die mit der Verarbeitung von Reizen und kognitiven Aufgaben in Verbindung gebracht werden. Man kann dabei langsame und schnelle Rhythmen unterscheiden, denen einerseits unterschiedliche Funktionen zugeschrieben werden, die andererseits jedoch aneinander gekoppelt zu sein scheinen. Das Phänomen der Kopplung über unterschiedliche Frequenzen wird in der gegenwärtigen Literatur als ein allgemeiner Organisationsmechanismus gesehen, der es dem menschlichen Gehirn unter anderem ermöglicht zu lernen. In dieser Arbeit untersuche ich am Beispiel motorischer Lern- und Automatisierungsprozesse, ob ein solcher Zusammenhang tatsächlich hergestellt werden kann.

Über motorisches Lernen gelingt es dem Menschen, nach einer Zeit des wiederholten Trainings, Bewegungen exakter, schneller und effektiver einzusetzen. Das motorische System im menschlichen Gehirn, das neben der Ausführung auch das Lernen von motorischen Bewegungen vermittelt, besteht aus weit verteilt liegenden Arealen, die unterschiedliche Aufgaben haben. In drei Studien untersuche ich einen Teil dieser sehr unterschiedlichen Gehirnbereiche hinsichtlich der Kopplungsphänomene zwischen langsamen – z.B. der *theta* Aktivität (θ : 4-8Hz) – und schnellen Frequenzen – z.B. der *gamma* (γ) und high *gamma* Aktivität (> 40 Hz) – und ihrer Relevanz für das motorische Lern- und Automatisierungsvorgänge.

An den Studien nahmen sowohl gesunde Probanden und Epilepsiepatienten an einfachen Experimenten zum motorischen Lernen teil, wobei mit verschiedenen invasiven (elektrokortikographisch – ECoG; subkortikal im Kontext der Tiefenhirnstimulation) und nicht-invasiven (magnetoenzephalographisch – MEG; elektroenzephalographisch – EEG) Aufnahmetechniken die Gehirnantworten aufgezeichnet wurden. Dabei zeigte

Contents

sich, dass sich die Kopplung in enger Beziehung mit einem sich verbessernden motorischen Verhalten in kortikalen Arealen veränderte, die eng mit der Ausführung und dem Lernen von Bewegungen in Verbindung stehen. Außerdem steht die Stärke der Frequenzkopplung im subkortikalen Nucleus Accumbens in einem engen Verhältnis zur Schwierigkeit der motorischen Aufgabe.

Zusammenfassend zeigen die in dieser Arbeit vorgestellten Untersuchungen eine direkte Beziehung zwischen der frequenzbasierten Kopplung zwischen Hirnarealen und dem Lernen im menschlichen Gehirn.

Im ersten Teil der Dissertation werden die allgemeinen Methoden zur Analyse neuronaler Korrelate der Verbesserung der motorischen Performanz beschrieben. In diesem Zusammenhang werden die spezifischen Annahmen über die funktionelle Rolle der unterschiedlichen Frequenzbänder neuronaler Oszillationen, die Methoden um die spezifische Merkmale der Frequenzbänder zu bestimmen und die Tests zur Überprüfung der statistischen Signifikanz der oszillatorischen Veränderung erörtert. Im anschließenden Teil werden die Hypothesen vorgestellt, die aus gegenwärtigen wissenschaftlichen Studien abgeleitet wurden. Jedes der folgenden Kapitel umfasst eine Studie bezüglich oszillatorischer Veränderung im menschlichen Gehirn. In jedem Kapitel werden die Ergebnisse jeder Studie diskutiert. Im letzten Teil der Dissertation werden die Ergebnisse zusammengefasst und ein Ausblick auf die zukünftige Forschungsfragen gegeben.

Abstract

of the PhD-Thesis:

CROSS-FREQUENCY COUPLING TRACKS MOTOR AUTOMIZATION AND EXECUTION
IN THE HUMAN MOTOR SYSTEM

by Dipl.-Psych., Dipl.-Päd Stefan Drschmid

Oscillatory phenomena in the human brain aroused great interest in the last years within the field of neuroscience. Large assemblies of neurons show different temporal action firing patterns, which are associated with the processing of stimuli and cognitive tasks. These temporal patterns can be divided into fast and slow rhythms to which different functions are attributed. Furthermore, the fast and slow rhythms seem to be coupled to each other. This frequency coupling is described as a general mechanism of organization which enables the human brain to learn. In this thesis I investigate in the context of processes of motor learning and automatization whether such an association can be established.

During motor learning in repeated training sessions humans succeed in more precise and faster movements which is mediated by the motor system in the human brain. This system which mediates the execution and learning of movements comprises spatially dispersed brain areas engaged in different tasks. In three studies I investigate parts of these different brain areas regarding the coupling between slow – e.g. *theta* activity (θ : 4-8Hz) – and fast oscillations – e.g. *gamma* (γ) and high *gamma* Aktivität ($> 40\text{Hz}$) – and its relevance for processes of motor learning and automatization.

In the studies presented here both healthy and epilepsy patients participated in simple motor learning experiments while the brain responses were recorded with different invasive (electrocorticographic – ECoG; subcortical within the context of deep brain stimulation – DBS) and non-invasive (magnetoencephalographic – MEG; electroencephalographic – EEG) recording techniques. In these studies motor performance improvement can be seen in a tight relationship with the coupling between slow and fast frequencies in cortical areas associated with motor learning and execution. Furthermore, the strength of frequency coupling in the subcortical Nucleus Accumbens is related to the difficulty of the motor task.

1 Introduction

1.1 Outline of the thesis

The present thesis deals with the coupling between slow and fast frequencies in the human brain which is called Cross-Frequency Coupling. Specifically the coupling between the phase of the θ and the amplitude of high γ activity in cortical and subcortical regions is investigated regarding its functional role in human behavior. In the first part the general methods to analyze neural correlates of motor performance improvement are described. In this context the specific assumptions of the functional role of frequency bands of neuronal oscillations, the methods to extract features of frequency bands and the tests to assess the statistical significance of oscillatory dynamics are discussed. In the next part the hypotheses derived from the recent scientific studies and the analyses used are introduced followed by three chapters each comprising one study on oscillatory dynamics in the human brain. The results of each study are discussed in each chapter. In the last part the results of all studies are summarized and perspectives for future research are given.

1.2 Movement and the human brain

The word *movement* describes the change of the position of an object relatively to the actual position across time. In several ways it is important that human beings are endowed with the capability to move themselves and objects. Without it, it is hardly conceivable that human beings had evolved at all, if for instance our ancestors were not capable to escape from enemies and to acquire food. One particular example of learned movement patterns is playing piano which requires a high flexibility of finger movements. This includes pressing different keys in a defined order with different fingers, integrating the action of both hands or withholding action if a rest is required. Practicing an unknown melody starts with “stumbling” across the notes and ends with a fluent movement.

In general, movements are essential since they are used to interact with the physical and social environment. The use of instruments is advanced in such an extent that we all are *potentially* capable of playing piano. *Potentially* here means that, if done repeatedly, humans tend to improve their performance. This improvement is the result of experience, which one can rely on, indicating the formation of memory which is established during learning.

1.3 Learning

In this section the process of learning is explained by the examples “playing piano”. To simply improve or to be a perfect piano player it is necessary to practice, leading to a gradual improvement. In turn, this indicates that the human brain which mediates motor performance changes gradually over time. To “know” how to perform a piano concert is “simple” examples of learned motor skills. And these well-established or learned motor skills results from practice. Practice points to the most important characteristic of learning namely, that it deals with a process. In this process longlasting changes are embedded in the behavior as a result of experiences (Fitts and Posner, 1973b; Pollmann, 2008). At the end, skills are so highly overlearned that the tremendous practice of walking in childhood is forgotten. However, to come to be an expert of a motor task different phases have to be passed before showing overlearned and automated performance. Starting with a *cognitive* phase the learner has to apply attention to the task before in the *intermediate* phase new behavioral patterns emerge which are increasingly automated in the last phase. And most important: learning should be visible in overt behavioral changes like faster or more precise responses. Nevertheless, behavioral patterns, even though automated, should remain flexible in nature to effectively react to changes in the environment. A very complex system is needed, which mediates motor execution to show overt behavior, motor learning to show changes in overt behavior and action monitoring to adjust overt behavior when necessary.

One interesting phenomenon is that motor learning enables to improve performance without being able to make an *explicit* statement about the single steps during pole-vaulting when becoming an expert. But one can *implicitly* recall the whole sequence of pole-vaulting. The major difference is that some memory contents are explicit in that sense that the participant can make a statement about the content (“who composed a piano concert?”) while it is called PROCEDURAL memory to be able to repeatedly play the entire concert without making any mistake. On the other hand explicit and implicit memory occur in the same process of learning, however, at opposite parts of the continuum. For example, explicit memory already occurs in the early cognitive phase of skill acquisition when attention is applied: “I know which note follows in a given part of the concert, but I fail to repeatedly produce the entire sequence”. Following extensive training the player tends to “know” how to produce a sequence without committing an error, but could fail to report which note is the next when asked. This supports the hypothesis that both are partly related to each other (Willingham and Goedert-Eschmann, 1999). Therefore, despite the explicit-implicit differentiation, in this thesis the intention is not to discriminate between the two experimentally, but to investigate the accompanying neuronal changes of this time-discrete process of learning.

1.4 The motor system

As indicated by such diverse task as execution, learning and monitoring: the human motor system is not a unit in the sense of a single circumscribed central region. It consists of dispersed cortical, sub-cortical and cerebellar regions all assuming different

tasks (see FIGURE 1.1). For example the cerebellum coordinates and adjusts the course of the movement (Trepel, 2004), to acquire the optimal internal model for a movement (Penhune and Steele, 2012). This is achieved by signalling the discrepancy between the actual sensory consequences of movements and their prediction by means of an efference copy of the motor command (Blakemore et al., 2001). Sub-cortical movement related regions are the basal ganglia, which encompass several nuclei (Ncl.) as the striatum – with the Ncl. caudatus and the putamen and the Nucleus accumbens as part of the ventral striatum – and the pallidum. Even though frequently associated with reward coding the Nucleus Accumbens can also be seen as part of the motor system due to the mediation of movement planning (Mogenson et al., 1980; Grace, 2000) and adjustment of response strategies (Münte et al., 2007). Furthermore, the basal ganglia are extended by several authors by the Ncl. subthalamicus and the substantia nigra (Trepel, 2004). The striatum and the pallidum are in pairs in the developed brain. However, they stem from the same predisposition and are separated later during the development of the human brain. This explains the largely resembling functions of the bilateral regions. The integration of motor impulses and the scaling of learned motor programs (Scheidt et al., 2012) are ascribed to this sub-cortical structure. It is important to note that impulses coming from the cortex are mainly suppressed by the striatum, wherefore, the striatum can be seen as an inhibitory unit in the processing of motor information. Together with the striatal representation of stimulus-response associations Penhune and Steele (2012) this structure seems to be necessary for action monitoring. In contrast, the pallidum with the medial and lateral segment has a more excitatory effect (Trepel, 2004) and holds connections with the thalamus, which project to the motor cortex. The output Ncl. of the basal ganglia, the medial segment of the internal globus pallidus, inhibits the thalamus by GABAergic (γ Aminobutyric Acid) neurons. On the cortical layer an important unit within the motor system of the human brain is the motor cortex situated in the posterior part of the frontal lobe. The motor cortex can be distinguished between the primary, supplementary and pre-motor cortex. From the motor cortex the motor impulses are “travelling” across the corticospinal and the corticonuclear tract to the contralateral motor execution organs (Trepel, 2004). In sum, this gives a brief outline of the complexity of the motor system whose parts are differently affected by motor learning.

1.5 Learning related changes in the motor system

Motor learning was investigated with quite diverse paradigms (serial response time task (Nissen and Bullemer, 1987), finger opposing task (Wessel et al., 1995), rotary pursuit task (Lordahl and Archer, 1958)) and diverse recording techniques. A great deal of research was conducted to discover cerebral changes across several training sessions with fMRI¹ and PET². In a series of experiments Grafton et al. (1992) investigated

¹functional magnetic resonance imaging

²Positron emission tomography: a technique of nuclear medicine in which the regional cerebral blood flow is recorded resulting in a good spatial resolution however, at the expense of a temporal resolution. Both recording techniques have good spatial accompanied by a poor temporal resolution.

General Introduction

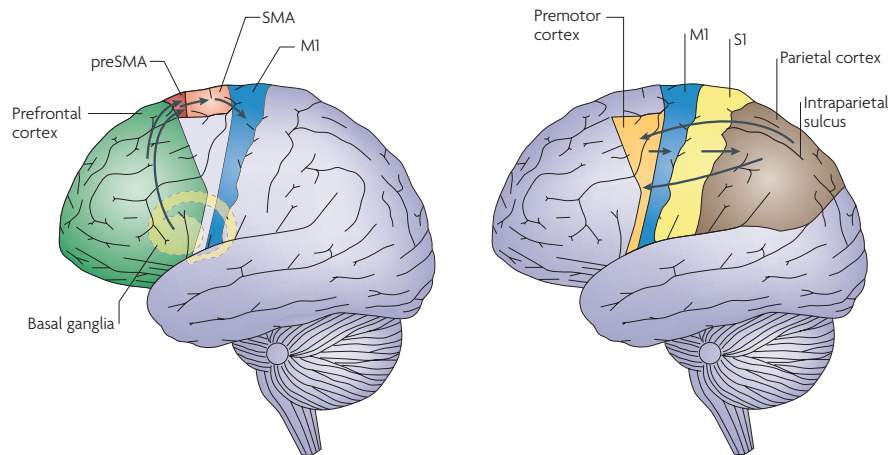


FIGURE 1.1:

Depiction of brain circuits involved in voluntary actions. This figure was taken from Haggard (2008)

procedural motor learning using PET. They found that execution and learning mediating areas show a great overlap and that motor learning is embedded in a widely distributed network of motor execution related areas. Motor execution involved cerebellar, striatonigral, and cortical areas encompassing the contralateral primary motor cortex and the supplementary motor area, which showed learning associated changes. Furthermore, during early learning rCBF increased for example in premotor and prefrontal areas while rCBF decreased in visual areas. Probably, this opposed effect marks the transition from the cognitive to the automated phase, when new behavioral patterns emerge. Nudo et al. (1996) additionally showed for the primate cortex that M1 is changeable during the course of life - a necessary prerequisite for learning - and cortical sectors expand after training supporting the notion that learning can be associated with the motor cortex. Bangert et al. (2006) showed in musicians that lifelong practice leads to enhanced activity in networks shared with non-musicians. Schendan et al. (2003) found memory, the product of learning, associated with activation of the mediotemporal lobe which suggested to them to be evidence of the involvement of the hippocampus in the formation of higher order associations both in implicit and explicit memory.

2 General Methods to analyze Neural Correlates of Motor Learning and Automization

In the last decades the repertoire of methods to unravel the brain functions has extended tremendously. Generally, on the one hand methods can use the brain's metabolism as the fMRI or the PET. These recording techniques have a good spatial resolution, but lack to discriminate ongoing processes in the human brain in the temporal dimension due to the poor temporal resolution. On the other hand, recording techniques as the EEG¹, ECoG² and the MEG³ which pick up electrical properties of the neuronal tissue, capture ongoing fluctuations in the human brain with a high temporal resolution in the range of milli seconds. In this thesis these recording techniques with a high temporal resolution are used since the oscillatory dynamics of interest here occur in a temporal range of milliseconds. The characteristics determining the signal recorded are illustrated in the next section.

2.1 Oscillations in the neuronal tissue

The human brain shows a hierarchical organization of different cortical, subcortical and cerebellar areas which can also show parallel information streams. Each brain site can be seen as a accumulation of neuronal cells releasing and reuptaking neurotransmitter via synapses. This leads a neuron to fire according to the temporal dynamics of the availability of neurotransmitters and hence the dynamics of the synaptic process (Pfurtscheller and da Silva, 1999). A given cell changes its state rhythmically and hence oscillates. Additionally to the dependence of processes between two interconnected neurons, the oscillation of a neuron depends on the intrinsic membrane properties. *Oscillation* means that this cell recurrently goes through hyperpolarization and depolarization both describing a deviation of a cell from its resting potential. When a cell is stimulated by the ion movements via the synapse or the cell membrane, the cell is depolarized, which can be explained by the influx of Na^+ ions. This in turn opens K^+ channels which release K^+ ions and mediates the hyperpolarization and hence the restoring of the resting potential. Due to this process, also called an action potential, neurotransmitter are released by which information is exchanged between neurons. Most probably, cells in the same assembly show the same pattern of state

¹electroencephalogram

²electrocorticogram

³magnetoencephalogram

changes and which is called *synchronisation*. But it is also plausible that an assembly of cells or two assemblies desynchronize in their action potentials. A desynchronization is often interpreted in that way that cells are not engaged in the same processing step. Synchronization of neurons leads to the local field oscillations (Chrobak and Buzsáki, 1998) which is the basis of the macro-electrode recordings and subject of the next paragraph.

Since the first electroencephalographic recordings (Berger, 1929) in humans it was well established that human neuronal tissue oscillates (Singer, 1993). The term oscillations refers to the ongoing fluctuations of field potentials⁴ which can be registered by means of invasive and non-invasive macroelectrodes. It is fairly easy to recognize those fluctuations by eyeballing what EEG/ECOG macroelectrodes or MEG sensors pick up. The signal recurrently passes through peaks and troughs (see FIGURE 2.2). The course through troughs and peaks is determined by several different characteristics as the amplitude or the “strength” of the oscillation (Busch, 2005), or the frequency (see FIGURE 2.1). The latter defines how often the signal passes through troughs and peaks within a temporal unit. The frequency is given in Hertz (Hz) and states the number of cycles per second. For example, an oscillation of 6 Hz means that the recorded signal passes six times through a cycle (see FIGURE 2.1). Furthermore, the oscillation is defined by the phase of the signal at a given point in time. However, in FIGURE 2.1 and 2.2 it is also fairly easy to recognize that it does not deal with a smooth signal. It seems as if little or “fast” waves were put on the large or “slow” waves indicating that the signal contains oscillations of different frequencies. These coexisting frequencies range from very slow ($< 1 Hz$) to ultrafast ($> 200 Hz$) oscillations (see TABLE 2.1 for a classification of frequency bands and FIGURE 2.2) and these different frequency bands are associated with different cognitive processes.

The fundamental of different frequencies or the velocity to pass through peaks and troughs are differences in neurophysiology which allows for different computation of cell assemblies (Kopell et al., 2010). Importantly, the change of oscillations can change the information exchange within cortical circuits. Here, just a few frequencies and their significance are outlined briefly. γ band activity is associated with attention and memory (Burns et al., 2011) and consciousness (Llins et al., 1998) and can be seen as a synchronizing pulse signal, but it is also discussed as a noise filter (Xing et al., 2012). α and especially its phase information predicts visual perception (Busch et al., 2009; Mathewson et al., 2009) and its desynchronization is linked with perception, judgement and memory tasks. Voluntary movements are associated with desynchronization in the upper α and lower β band close to the sensorimotor cortex (Pfurtscheller and da Silva, 1999). Specifying the significance of β rhythms this oscillation might subserve sensorimotor integration and top-down-signaling (Wang, 2010).

⁴the summed electrical potential evoked by neurons

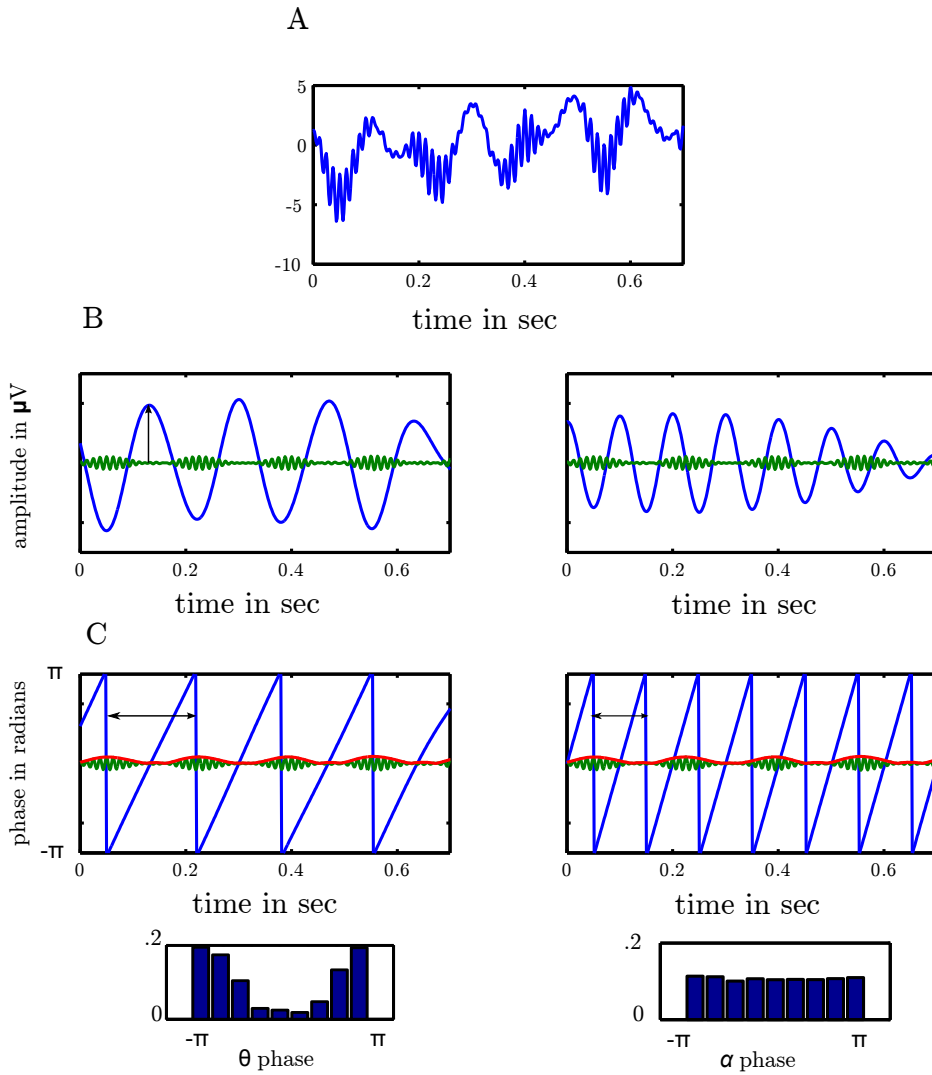


FIGURE 2.1:

Depiction of oscillation characteristics. **A**: shows a simulated time series of data points as the summation of the time series shown in **B**. This time series consists of θ (4-8 Hz), α (8-10 Hz) and high γ (70-90 Hz) time series. The left part of **B** shows the time series of the θ band (blue) and high γ band (green). The arrow depicts the amplitude which differs between low and high frequencies. The green line shows a regular occurrence of “burst” - temporal intervals of increased amplitude co-existing with the trough of the θ band. The left part of figure **C** the phase, frequency, and analytic amplitude are illustrated. The blue line shows the phase ranging from $-\pi$ to π of the θ filtered signal in **B** (cycle duration ≈ 166 ms). The length of the cycle is indicated by the vertical arrows for both low frequency bands. The analytic amplitude, estimated by means of the Hilbert transform, can be seen as a peak-to-peak connection of the signal. A frequency specific phase-amplitude dependency is depicted in lower row of **C**. Both the θ and the α cycle were divided into 9 equally spaced phase bins and within each phase bin the high frequency amplitude was calculated. As it can be seen here the high γ amplitude depends on the phase of the θ activity while there is no dependence on the α phase as indicated by the equal amplitude at different phase.

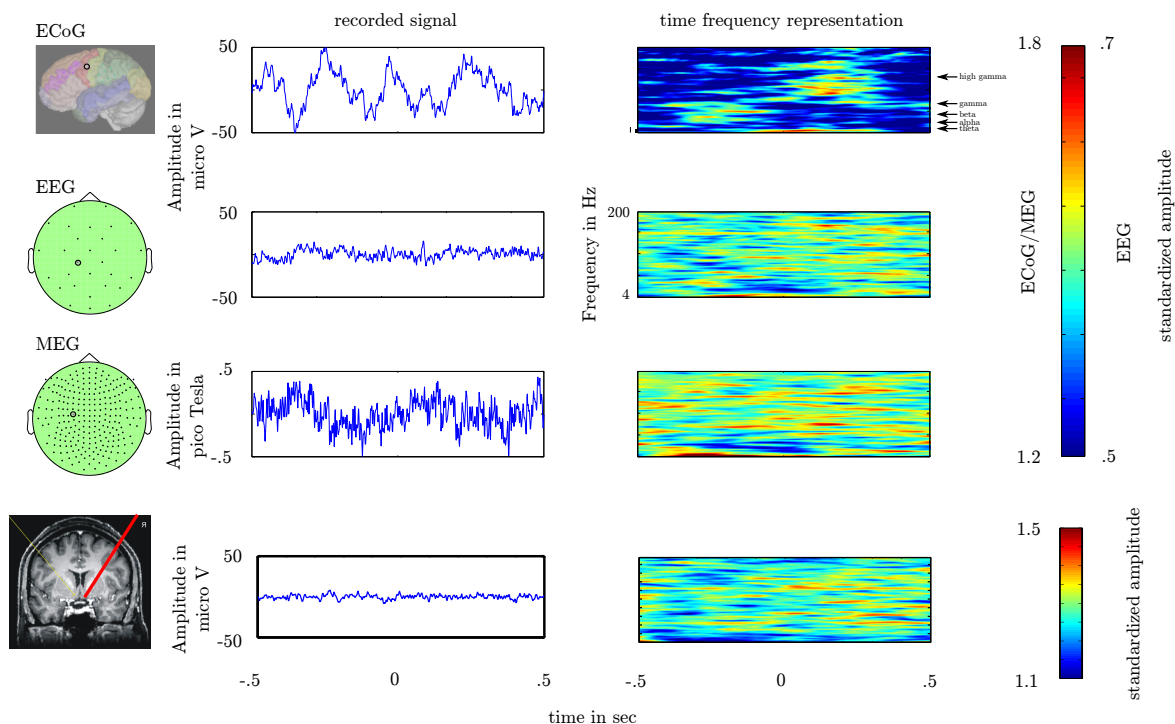


FIGURE 2.2:

Depiction of decomposition of a time series into its frequencies for 3 different recording techniques. In all three examples the subject performed the same finger tapping task and the signal from a channel covering the contralateral motor cortex is shown. Each row represents one subject whereby EEG and MEG were recorded simultaneously. For the time-frequency representation the signal was filtered for center frequencies ranging from 4 to 200 Hz with a bandwidth of 4 Hz and averaged across trials. 0 marks the button press. Please note the high grade of consistency between both non-invasive techniques but also with the invasive technique. In this one temporal changes are readily identifiable. Pseudo colors represent the magnitude of the frequencies which were standardized for a better comparison across bands. The magnitude changes in EEG-recordings are much smaller as compared to ECoG and MEG. Cold colors denote points in time where a given frequency desynchronizes and warm colors where a synchronization takes place.

TABLE 2.1:

Classification of different frequency bands which are related to processing in the human brain

Band name	Frequency range
δ	0-4 Hz
θ	4-8 Hz
α	8-13 Hz
μ	8-13 Hz
β	13-30 Hz
γ	30-60 Hz
high γ	60/80 - 150/200 Hz

2.2 The θ and the high γ band: functions of slow and fast oscillations

The most important fact making different frequencies an increasingly appealing subject to neuroscience are their selective response and co-occurrence with cognitive stages. Since the θ and high γ activity are of special interest in this thesis their roles in the human brain are to be outlined.

In general θ activity is densely associated with learning and memory (Canolty et al., 2006; Jensen and Colgin, 2007) and especially the maintenance of items in working memory (WM) (Axmacher et al., 2010b; Bosma et al., 2009; von Stein and Sarnthein, 2000) or the recollection of personal events (Guderian and Düzel, 2005; Buzsáki, 2005) is linked with θ activity. This low frequency increases especially during active, intentional behavior such as during both exploratory search and goal-seeking behavior (Caplan et al., 2003; Hasselmo et al., 2002), map navigation (Buzsáki, 2005), strategy switches (Cohen et al., 2009b), and spatial navigation (Kahana et al., 1999; Buzsáki et al., 2003). But in the context of learning and memory it seems to show a stronger link with memory than learning which is to say that θ possibly constitutes a mechanism of retrieval of stored information (Kahana et al., 1999). The active retrieval can be mediated by transiently linking the hippocampus with neocortical areas to bind representations (Guderian and Düzel, 2005). Besides the retrieval an important impact in buffering (Jensen et al., 1996) and timing of novel events is attributed to the θ activity. In the context of motor activity it is assumed that θ activity acts to coordinate sensory and motor brain activity (Caplan et al., 2003). All examples implicate that θ activity rather “carries” than represents information. As a carrier which is phase-locked with pyramidal cells activity (Buzsáki et al., 2003) θ activity modulates single-unit activity (Canolty et al., 2006). On the other hand, the locally very discrete γ - high γ activity (Crone et al., 1998a; Fries, 2005) is strongly correlated with average firing rate of single units in the macaque somatosensory cortex (Ray et al., 2008). Furthermore, high γ activity transiently occurs during voluntary movements (Ball et al., 2008) slightly before their initiation and ends before completion (Crone et al., 1998a). Its particular role during formation of motor learning and execution processes is suggested since high γ band dissociates attention/memory from motor intention and furthermore, enables the spatial localization of both functions (Brovelli et al., 2005). However, it is not clear what high γ is (Crone et al., 2011) in terms of its band characteristics. It is difficult to define high γ activity as a “band” due to variable upper and lower boundaries. Moreover, it does not show uniformity since rather narrow bands discriminate different cognitive tasks as speaking and hearing (Gaona et al., 2011). The potential differentiability by high γ activity makes it a good candidate to represent information. This outline should give an overview over the different frequency bands and their characteristics which are picked up by different recording techniques which are compared in the next section.

2.3 Experimental and clinical constraints of invasive and non invasive recordings

In this thesis the neuronal information recorded with different recording techniques is used. Invasive and non-invasive recordings from different groups of subjects were analyzed. In the context of invasive recordings the use of different groups of subjects is pre-defined by the goals of the respective clinical diagnosis or therapies since invasive recordings can only be carried out in a clinical context and hence, are part of a treatment of a certain brain disorder. For example, in epilepsy patients grids of electrodes are implanted to localize foci of pathological activity. This is mostly done to afterwards resect neuronal tissue whose abnormal activity is responsible for the clinical picture exhibited by the patients. Herein, the therapy of drug-resistant epilepsy (Kwan et al., 2010) consists of resection. Another approach is the deep brain stimulation (DBS) procedure which is used in different neurological and psychiatric disorders as epilepsy, Parkinson disease (Cooper et al., 2012) or depression (Bewernick et al., 2010). For example, the stimulation of the Ncl accumbens leads to an antidepressant effect and positive change in clinical symptoms (Bewernick et al., 2010). A therapeutic effect of DBS was also found in the treatment of Parkinson disease (PD). Bradykinesia as one symptom of PD was diminished by means of the stimulation of the Subthalamic Nucleus (STN) (Cooper et al., 2012). As stated above some patients suffering from medically refractory epilepsy can be treated by resection of pathological tissue. However, a group of 4% does not show success of this kind of treatment, since the resectable focus cannot be localized (Ellis and Stevens, 2008). In these patients DBS can be of great importance. Postoperatively, the electrode leads can be externalized to allow electrical test stimulation with different parameters and recording from the depth contacts during different psychological tasks.

In both invasive recordings, ECoG and DBS, collecting data while presenting the patients with an experimental paradigm is a mere subsidiary aim. Hence, the number of subjects is limited and only neuronal activity can be investigated of brain sites of rather clinical interest than experimental considerations. A standardized evaluation of group effects as in EEG-studies is precluded due to the different electrode positions as in ECoG recordings. Additionally, the spatial information is scarce since it is not possible to cover the whole cortex with electrodes or to target all subcortical regions belonging to the motor system. Non-invasive techniques may bridge the gap of knowledge if information of a small set of subdural intracranial recordings are scientifically combined with MEG or EEG recordings of a group of healthy subjects (see for example Ball et al. (2008) on high γ in motor execution). The advantages of non-invasive recordings techniques are the following: first, a greater group of participants can be used and second, EEG and MEG have a high degree of standardization since electrodes and sensors are arranged in a predefined pattern (Jasper, 1958). However, as the experimental benefit owned by non-invasive recording techniques, invasive techniques are superior with respect to the frequency content. In non-invasive recordings lower frequencies dominate whereas the activity of higher frequencies is seldom visible offhandedly (Pfurtscheller and Cooper, 1975). As only the bass line of the music played by the neighbors stereo

system is hearable through the wall the skull filters out higher frequencies such as the walls are doing with the high frequencies of the singer's voice. Therefore, high frequencies as the high γ activity is best investigate with subdural recordings at the expense of smaller groups of subjects. Yet, both non-invasive techniques (EEG and MEG) are not identically limited. While the EEG measures the electrical potential the MEG picks up magnetic signals of the human brain. Okada et al. (1999) reported that at least for shallow sources the MEG is relatively unaffected by the skull pointing to a better recording of even high frequencies with MEG than EEG. Furthermore in EEG errors of localization are much higher than in MEG recordings (Cuffin, 1993). Together, this should demonstrate that all recordings techniques are endowed with different advantages which can be exploited if combined optimally.

One unifying aspect of the recorded signal is that it deals with time series of data representing the brain state at a given time point. These time series are those oscillations described in SECTION 2.1 which pass recurrently through troughs and peaks with a different velocity or frequency. From these signals different information can be extracted which can be done by means of the Hilbert transform explained in the following section.

2.4 The Hilbert Transform: Extracting phase and amplitude information

The characteristics of an ongoing signal - the amplitude and the phase angle of a certain frequency band - are outlined. The amplitude and the phase angle of the signal can be estimated by means of the Hilbert transform

$$\mathcal{H}f(y) = \frac{1}{\pi} \int_{-\infty}^{\infty} \frac{f(x)}{y-x} dx \quad (2.1)$$

which gives the complex valued *analytic signal* of a real-data signal (2008a, The Math-Works). This analytic signal consists of a real part \Re and an imaginary part \Im . The real part is the signal itself and the imaginary part the signal shifted by 90° . The instantaneous amplitude can easily be calculated as $|\mathcal{H}f(y)|$ and can be seen as a function that interpolates from peak to peak in an oscillatory waveform (Canolty and Knight, 2010). The instantaneous phase is calculated as

$$\phi(t) = \arctan \frac{\Re(t)}{\Im(t)} \quad (2.2)$$

(Freeman, 2007). These two time-discrete values of the ongoing signal will be used and related to each other throughout the experiments and are extracted by means of built-in functions of the signal processing toolbox in MATLAB.

2.5 Phase-Amplitude Cross-Frequency Coupling

Cross-frequency coupling describes the dependency of different frequency on one another. In this regard it is important that the dependency is unidirectional. This

means that higher frequency depend on lower frequencies but not the other way around (Buzsáki and Draguhn, 2004). As mentioned above the different frequency bands differ with respect to the number of cycles per second. This cycle can be seen as a continuous and recurrent passing through different phases which comprise a whole circle from $-\pi$ to π (see FIGURE 2.1). From a given phase at a time point the state of the neuronal tissue can be deduced since the phase reflects rhythmic phases of high or low excitability. Temporal fluctuations of perception could be linked to the phasic fluctuations of the signal (Busch et al., 2009; Mathewson et al., 2009). If, for example, a stimulus is presented during a temporal interval of high excitability the probability to reach consciousness increases. Especially the phase of the θ and α oscillation before stimulus onset predicts the perception. These studies show that additionally to different frequency bands there are quantitative different intervals within frequency bands.

Additionally to the frequency content of a recorded signal each frequency is endowed with a “strength” or an amplitude, at which higher frequencies have a much smaller amplitude than lower frequencies. This is not to say that the amplitude of one frequency band is a stable phenomenon. It rather fluctuates. Across one temporal interval one frequency band seems to be regular, followed by a period of a high amplitude which is usually called *burst*. These burst of a higher frequency can occur in a systematic way whenever a lower frequency passes through a certain phase. If there is a systematic dependency of the occurrence of a high frequency burst on the low frequency phase such that for example the probability of a high frequency burst increases at the trough of a low frequency band this is called phase-amplitude cross-frequency coupling (paCFC) since the amplitude depends on the phase. Here, it will be focussed on the explanation of cross-frequency coupling as a within-signal phenomenon. For the sake of completeness it has to be mentioned that a statistical dependency of amplitude and phase can be seen between signals. However, in the experiments presented here the relation between the within-signal coupling and motor learning on the cortical and subcortical level are addressed.

2.6 Testing and parametrization for occurrence of cross-frequency coupling

The definition of paCFC as selective occurrence of high amplitudes of high frequencies at a certain phase cannot be understood as a stair case. It rather shows sluggish changes around the coupling phase. This means that before or after entering the low frequency trough the high frequency amplitude is relatively low and increases while entering and decreases while leaving the trough. Hence, the evolution of the high frequency amplitude across the low frequency cycle resembles the low frequency cycle (see FIGURE 2.1). Therefore, an appropriate model to describe the evolution of the high frequency amplitude is a cosine function. This cosine function predicts the measured high frequency amplitude y at different low frequency phases Φ

$$\hat{y}(\Phi) = \hat{a} * \cos(\omega * y(\Phi) + \phi) \quad (2.3)$$

by simultaneously adjusting three different parameters: \hat{a} defines the amplitude, ω defines the frequency and ϕ the phase angle. If for example $\omega = 1$ then the evolution of the high frequency amplitude follows exactly one low frequency cycle. If $\omega = 2$ than there are two cycles of the high frequency amplitude across one low frequency cycle. The cosine function is optimized such that the squared deviation between $\hat{y}(\Phi)$ and $y(\Phi)$ (the residuals) are minimal. The residuals or the error made by the prediction is defined as

$$SS = \sum_{i=1}^{\Phi} (\hat{y}(i) - y(i))^2 \quad (2.4)$$

The statistical test represents an ANOVA and hence, specifies whether more of the variance in the high frequency amplitude (MS_{cos}) is explained by the variation across the low frequency cycle or by the residuals (MS_{error}). The variance between the low frequency phases is given as

$$MS_{cos} = \frac{SS_{cos}}{df_{cos}} \quad (2.5)$$

with SS_{cos} as the sum of squares of high frequency amplitude between low frequency phases and df_{cos} as the degrees of freedom. The variance within the low frequency phases is given as

$$MS_{error} = \frac{SS_{error}}{df_{error}} \quad (2.6)$$

with SS_{error} as the sum of squares of high frequency amplitude within low frequency phases and df_{error} as the degrees of freedom. The F value is given as the ratio between both as

$$F = \frac{MS_{cos}}{MS_{error}} \quad (2.7)$$

and the significance level of the resulting F -value is defined by the degrees of freedom. The larger F the more of the variance in the high frequency amplitude is explained by the variation across the low frequency cycle than at a low frequency phase (see Tort et al. (2010) for a review of different coupling metrics).

An important part of the approach to relate the strength of coupling to performance is to calculate a time-discrete coupling measure which can be correlated with the time-discrete performance measure. In this context time-discrete means that the strength of coupling is calculated for each trial or additionally for defined consecutive temporal windows within trials. Here, two possibilities to come to a time-discrete coupling measure are presented.

The first is a ratio of the magnitude of low frequency at the coupling phase and the magnitude of the high frequency at the coupling phase. This is tagged *trough-to-peak ratio* or TPR since the test for coupling showed that the coupling phase of the low frequency is close to the trough. The calculation of the TPR is explained in detail in SECTION 4.2.5 for the ECoG-recordings and 5.2.3 for the MEG/EEG-recordings. In general, with this measure one can investigate time-discrete changes at the coupling phase under the assumption of significant coupling. The second measure is directly derived from the test statistic F and can be applied to groups of subjects. The reason why this approach is applied to the subcortical recordings is that each subject has the

General Methods

same number of recording electrodes in a predefined subcortical region. In this case one can investigate whether there is more variance of the high frequency amplitude across the low frequency cycle or between subjects (for details see SECTION 6.2.3). This is not the case in the ECoG recordings since in all patients who participated the grids covered different cortical regions and the amplitude values cannot be averaged in a simple way since otherwise information of diverse cortical regions are merged.

3 Working Hypotheses and Outline of Analyses

The theoretical and methodological background described in CHAPTER 1 and 2 is the basis for the experiments and analysis carried out in the framework of this thesis which are described in the CHAPTERS 4, 5, and 6. Within this chapter a short outline of the experiments and the analysis is given along with the hypotheses which were tested. In general, subjects participating in the experiments were presented with a serial response time paradigm in which they had to track and respond to a sequence of numeric stimuli. In the first study additional paradigms as the Go/No-Go task and an auditory-motor control task were used (see SECTION 4.2.2). In each section of the experiments the reader will find a more detailed description of the hypotheses, the methods, and steps of analysis.

1st study - Chapter 4 As outlined in CHAPTER 1 and 2 paCFC emerges in a wide range of tasks and across a great fraction of recordings sites. Therefore, it is hypothesized that

- **phase-amplitude Cross-Frequency Coupling (paCFC) is observable in the human cortex during motor performance.**

To this end the average amplitude of the high frequency activity was compared across different phases of the underlying low frequency band. Furthermore it is hypothesized that

- **paCFC tracks motor memory formation in the human brain.**

This would show that paCFC is flexible in nature and would establish a link with the process of performance improvement. To test this, in each trial the magnitude of the high frequency amplitude was related to the depth of the trough which was the coupling phase. Combined with the assumption that paCFC is task specific it is expected that

- **task related changes of paCFC emerge in brain sites associated with execution and learning.**

The manuscript of this study is submitted to PLoS One.

2nd study - Chapter 5 Since intracranial recordings do not provide the possibility to cover the whole cortex EEG/MEG-recordings were analyzed under the hypothesis that

- **localization of changes of paCFC can be replicated with non-invasive recordings**

for the motor execution system. The uniqueness of the pattern found in the first study can be a mere result of the spatial limitations of the coverage of electrodes. Hence, whole-head recordings are expected to reveal further brain sites exhibiting changes of paCFC accompanying learning. Especially the frontal cortex, which could not be investigated with the ECoG-recordings, plays an important role during early motor learning since stimulus-response mapping is represented in this brain site. That

- **paCFC accompanies motor learning in the prefrontal cortex**

is the next hypothesis to be tested. If so the question arise how communication and interaction between different cortical sites takes place to mediate motor execution/learning. It is widely assumed that different frequency bands serve as communication channels wherefore, it is expected that

- **brain sites show task specific interaction represented in circumscribed frequency bands.**

This was investigated with a Granger causality approach which resolved the influence of different frequency band.

This study is in preparation.

3rd study - Chapter 6 Study 2 showed that the influence from the prefrontal cortex onto the motor cortex represented by the high γ band discriminates between the tracking of predictable and unpredictable sequences. Therefore, one may ask whether the communication is routed across the cortex or whether subcortical regions can mediate communication via the mechanism of paCFC. Therefore, is is hypothesized that

- **paCFC is task specifically observable in the human Nucleus accumbens.**

Comparable to the 1st study the average amplitude of the high frequency activity was compared across different phases of the underlying low frequency band. Given the role of the Nucleus accumbens in action monitoring and the differences of high frequency information transfer between predictable and unpredictable sequences it is furthermore expect that

- **the NACC shows elevated coupling during phases with a high need for action monitoring**

for example in trials of the tracking of unpredictable events.

The manuscript of this study was published at FRONTIERS IN HUMAN NEUROSCIENCE.

4 Oscillatory Dynamics during Motor Automatization: ECoG Recordings

4.1 Introduction

Phase-amplitude cross-frequency coupling (paCFC) of oscillations in different frequency bands has been proposed as an effective mechanism to form functional networks that recruit local neuronal populations across a global spatial scale (Buzsáki and Draguhn, 2004; Canolty et al., 2006, 2010; Canolty and Knight, 2010). Phase-amplitude CFC between HG (80–150 Hz) amplitude to θ (4–8 Hz) phase was first described by Canolty et al. (2006) and later confirmed by other authors in rats (Tort et al., 2008, 2009a) and humans (Axmacher et al., 2010a). During paCFC amplitudes of higher frequency oscillations, reflecting local cortical processing, are modulated by the phase of low frequency oscillations (Klausberger et al., 2003; Jensen and Colgin, 2007; Cardin et al., 2009; Haider and McCormick, 2009; Voytek et al., 2010). This mechanism has been proposed to engage and coordinate local processing modules across spatially distributed brain areas supporting cognition and motor performance (Grafton et al., 1994; Jueptner et al., 1997b,a; Brovelli et al., 2005; Jensen and Colgin, 2007; Canolty and Knight, 2010; Aron, 2010). Further support for this proposal comes from recent clinical studies linking altered paCFC to debilitating psychiatric and motor disorders (Uhlhaas and Singer, 2010; Allen et al., 2011; Crowell et al., 2012; de Hemptinne et al., 2013). Moreover, paCFC is prominent during language and motor tasks (Canolty et al., 2006; Canolty and Knight, 2010) and the frequency of the slower phase coupling oscillation is task dependent (Voytek et al., 2010). However, beyond clinical studies evidence for a functional role of paCFC in the process of organizing human cognition and behavior is limited predominantly to the memory domain (see (Lisman and Jensen, 2013) for a review). Axmacher et al. (2010b) reported that inter-individual differences in working memory performance correlated with differences in paCFC precision, supporting the functional relevance of CFC for memory processing. Tort and colleagues Tort et al. (2009a) examined the dynamic modification of functional relations between performance and CFC in rat hippocampus and found coupling strength between θ and gamma (γ : 25–100 Hz) correlated with maze learning.

A stronger link between paCFC and behavior in humans would be supported by a correlation between paCFC and trial-by-trial variations in performance. To address this, we examined the relation between paCFC and motor performance during motor automatization. We recorded the electrocorticogram (ECoG) in human patients undergoing epilepsy diagnosis while they learned skilled motor behaviors. To assess the link between paCFC and behavior we compared changes in paCFC to changes in performance over an extended time scale during motor skill acquisition, and correlated

performance and paCFC at the single trial level. We show that paCFC in intracranial subdural recordings between θ (4-8 Hz) and HG (80-180 Hz) in the human cortex tracks level of motor performance across different motor tasks.

4.2 Methods and Materials

4.2.1 Patients

Six epilepsy patients (mean age = 20.5, std = 5.5; 2 female) undergoing pre-surgical monitoring with subdural electrodes participated in the experiments after providing their informed consent. Experimental and clinical recordings were taken in parallel. Recordings took place at the University of California San Francisco (UCSF), CA, USA (4 Patients), Johns Hopkins University, Baltimore, USA (1 Patient) and the Epilepsy Center Bethel (ECB), Bielefeld (1 Patient), Germany and were approved by the local ethics committees (“Committee for the Protection of Human Subjects at UC Berkeley”, “Johns Hopkins Medicine Institutional Review Board” and “Ethical Committee of the University of Magdeburg”).

4.2.2 Experimental Paradigms

We carried out three different motor tasks (serial reaction, go/no-go, temporal coordination) with six different patients (see Figure 4.1). Each patient participated in one of the tasks. All paradigms required coordination of key presses on a computer keyboard to an external stimulus. Patients performed the task sitting upright in their bed using the hand contralateral to the grid.

Serial Reaction Task The serial reaction task (SRT) consisted of a series of visually cued finger taps (Nissen and Bullemer, 1987). The subjects had their fingers placed on different keys of a laptop keyboard (right hand: space bar, “j”, “k”, and “;” - left hand: space bar, “f”, “d”, and “a”). Trials started with one of the numbers 1, 2, 3, or 5 appearing on a laptop-screen cueing the movement of thumb, index finger, middle finger, or little finger, respectively. Numbers were presented until a key was pressed but maximally for 2 seconds. In each subject the four numbers were presented in a fixed sequence (six items long) or random order depending of the block number but only fixed blocks were used. Each block took approximately 10 minutes. Two patients participated in this task (SRT01 - 02). They were instructed to press keys as fast and accurate as possible. One block took approximately six minutes.

Auditory-Motor Coordination Task The second motor-paradigm was an auditory-motor coordination task (AMCT; see Kelso et al. (1998)). One patient participated and was instructed to respond as accurately as possible halfway between successive auditory clicks presented at a constant rate. Seven click sequences, each 60 s long, were presented in a block. The inter-click-interval in a sequence was either 500 ms, 1000 ms or 2000 ms and the participant was informed that the interclick-interval changes. The seven click sequences with the differing interclick-interval were presented randomly within

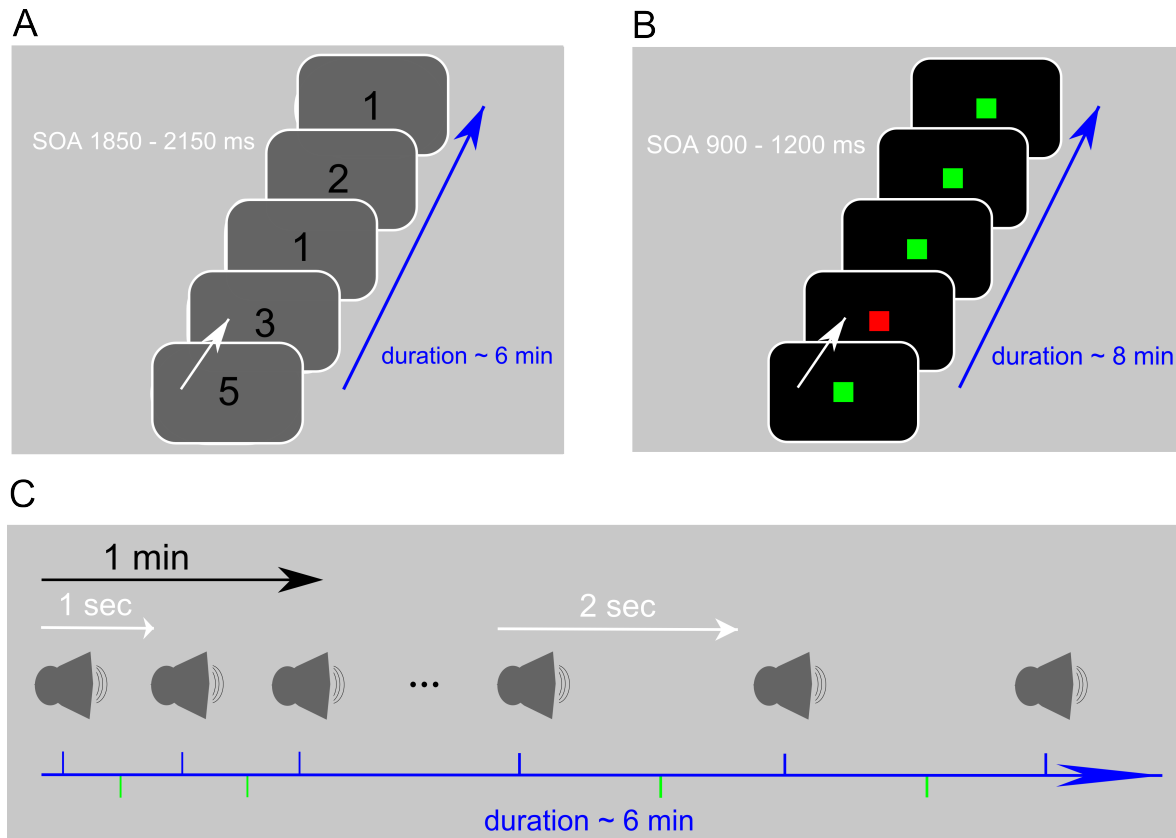


FIGURE 4.1:

Paradigms employed (details described in Methods). A) Serial reaction time task: The numbers on the screen indicate the finger to be used for the key press. B) Go/no-go: Green indicates a go and red indicates a no-go trial. C) Auditory motor coordination: Subjects were instructed to press a key in the middle of the interval between two consecutive tones. The interval length was either one second or two seconds and was held fixed for one minute. Each subject carried out two blocks (see Methods).

each block. Only sequences with a interclick-interval of 1000 and 2000 ms entered the analysis. The clicks were presented with speakers plugged into the laptop's sound card and placed in front of the patient at 1 m distance. One block lasted 7 min.

Go/No-Go task Three patients participated in the go/no-go (GNG; see Aron (2010)) task (GNG01 - 03). In each trial the patients were presented with either a green or red square of 100 ms duration and 900 - 1200 ms stimulus onset asynchrony. The subjects were instructed to respond as quickly as possible to green squares by pressing a key on a laptop keyboard but to withhold responses when a red square was presented (in block 1-3: 20 % of the trials; in block 4: 50% of the trials). The participants were familiarized with the task in an initial short practice session. Only correct Go-trials of the first two blocks entered the analysis. Each block lasted approximately eight minutes.

4.2.3 Data recording

At UCSF the experimental recordings were conducted by members of the Lab of Robert T. Knight. The electrocorticogram (ECoG) was recorded either from 64 platinum-iridium-electrode grids arranged in an 8 x 8 array with 10 mm center-to-center spacing (FTT01, FTT02, GNG01, GNG02 GNG03) or from a 256 electrode grid (both Ad-Tech Medical Instrument Corporation, Racine, Wisconsin) arranged in a 16 x 16 array with 4 mm center-to-center spacing (GNG02). Exposed electrode diameter was 2.3 mm in the 64 electrodes grid and 1.8 mm in the 256 electrodes grid. The electrode signals were recorded with a 256 channel preamplifier (PZ2-256, Tucker-Davis Technologies (TDT), Inc) with the electrode furthest from the motor cortex used as a reference. The data from the pre-amplifier were sampled at 3051.7 Hz on a digital signal processor (RZ2 4 DSP, Tucker-Davis Technologies (TDT), Inc) with 16-bit resolution and stored to hard disk. Trigger signals indicating button presses and stimulus onsets were sent from the stimulus laptop via a USB-1208FS DAQ (Measurement Computing, Norton, MA) plus a photodiode attached to the screen and recorded on the DSP synchronized to the brain data. Trigger timing was additionally recorded on the stimulus laptop by querying the computers performance counter using the Psychophysics Toolbox (www.psychtoolbox.org). In Bielefeld (AMCT) the ECoG signal was recorded at 1000 Hz sampling frequency (16 Bit resolution) with a Nihon Kohden system (Tokyo, Japan) equipped with auxiliary analogue channels for synchronous recording of the trigger signals and the output from the sound card. Here 5 stripes were implanted each equipped with two parallel rows of 5 electrodes each (see Figure 5).

4.2.4 Data pre-processing

We used Matlab 2008a (Mathworks, Natick, USA) for all offline data processing. We first preprocessed the recorded brain data and then we derived measures quantifying adaptation of oscillatory neural dynamics during motor skill learning. All filtering was done using FIR filters. Preprocessing served to remove non-physiological artifacts from the recorded data and to prepare them for further analysis. First we excluded channels exhibiting ictal activity or excessive noise from further analysis. In the remaining “good” channels we then excluded time intervals containing artifactual signal distortions such as steps of pulses by visual inspection. Finally, we re-referenced the remaining electrode time-series by subtracting the common average reference

$$x_{CAR}(t) = \frac{1}{n} \sum_{c=1}^n x_c(t) \quad (4.1)$$

calculated over the n good channels c from each channel time series. The number of rejected channels was small in all patients (mean percentage: 3.7%; SD across participants: 1.4%) that the influence of different re-referencing due to a different number of rejected channels was expected to be marginally. The resulting time series were then used to characterize brain dynamics over the time course of motor behavior automatization in terms of the trough-to-peak ratio (TPR; see Figure 4.2):

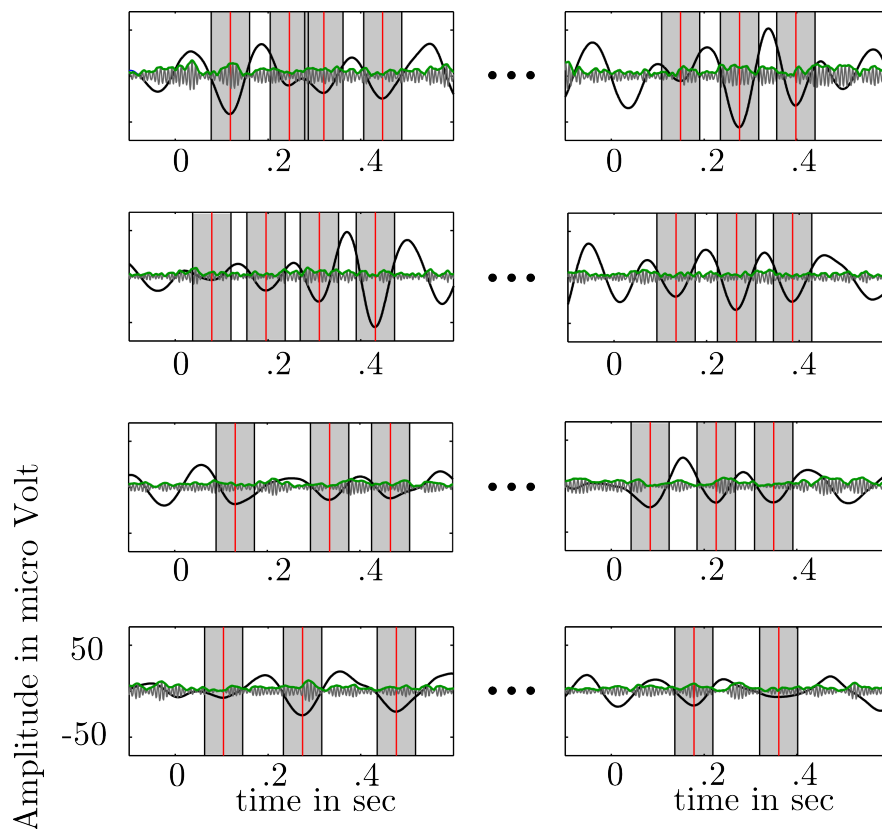


FIGURE 4.2:

Calculation of the trough to peak ratio (TPR). We quantified paCFC as the ratio between θ trough (local minima of the θ time series - red vertical lines) and HG amplitude at the corresponding θ trough. Around each detected trough we spanned a window (half θ cycle - gray bars) in which θ activity (black bold line) and HG amplitude (green line) was averaged.

4.2.5 Calculation of the Trough-to-Peak Ratio

For each trial starting at stimulus onset we calculated the θ -trough to HG peak ratio (TPR) to quantify the evolution of phase-amplitude cross-frequency interactions of cortical oscillations during motor skill learning. Therefore, we band-pass filtered each electrode's time series at two frequency bands, in the θ -range (4 - 8 Hz) and in the HG (80 - 180 Hz) range since coupling was task relevant between these frequencies across a variety of experimental tasks [Canolty et al. \(2006\)](#). We detected θ -troughs, the local minima, in the θ -range filtered time series in the interval between 0 to 500 ms after stimulus onset (Figure 5). We obtained the HG analytic amplitude $A_{HG}(t)$ by Hilbert-transforming the HG filtered time series. For each detected θ -trough we then estimated the depth of the trough D_θ and the simultaneous HG amplitude as the average of the θ -filtered and the A_{HG} time series over an interval of 83 ms (half θ oscillation) centered on the trough. Note that multiple θ troughs fit into the 500 ms analysis leading to multiple estimates per trial. We averaged the individual estimates D_θ and $A_{HG}(t)$ to obtain one measure for θ trough depth \bar{D}_θ and one for HG amplitude

\overline{A}_{HG} for each trial j . From these values we calculated TPR for each trial j as:

$$TPR_j = \log \frac{\overline{D}_{\theta,j}}{\overline{A}_{HG,j}} \quad (4.2)$$

Taking the log of the ratio makes the distribution of TPRs symmetric. Note that the TPR includes both stimulus-locked and non-stimulus-locked brain activity. It summarizes the global cross frequency interaction on the grids.

4.2.6 Phase-Amplitude Coupling

paCFC was tested by splitting the θ oscillations of the 500 ms analysis window into 20 equally spaced phase bins ranging from $-\pi$ to π (18° or 0.314 rad) in each subject and each electrode. In each phase bin we averaged the amplitude envelope of the local HG. A sine wave function

$$\hat{y} = \alpha * \cos(\omega * HG + \phi) \quad (4.3)$$

with α representing the amplitude, ω representing the frequency and ϕ representing the phase angle was fitted to the resulting 20 HG amplitude (y) values. ω close to 1 indicates that HG amplitude variation is accounted for the θ cycle.

4.2.7 ROI analysis

In each patient we grouped electrodes according to the same anatomical landmarks in 6 regions of interest (see Figure 8.2): The anterior (in sum 34 electrodes across subjects) and posterior (44 electrodes) medial frontal gyrus, the anterior (49 electrodes) and the posterior inferior frontal gyrus (81 electrodes), and the superior (48 electrodes) and inferior (46 electrodes) sensorimotor cortex. We averaged the TPR-values within each ROI across electrodes. In each patient we determined the p-value for Pearson's correlation coefficient r and the partial correlation coefficient ρ between the averaged TPR values and behavioral performance across trials. Each ROI in which the mean p-value across subjects fell below the p-value corrected for multiple comparisons ($p_{corr} = \frac{.05}{6}$) was considered statistically significant.

4.2.8 Separating performance from learning effects

We separated performance from learning effects by applying a permutation test statistic. The recorded time series were filtered in the θ (4-8Hz) and in the HG (80-180Hz) frequency. Subsequently, we calculated the HG envelope of the HG time series in each electrode and each trial. We then determined 20 time windows around the stimulus onset each with a width of 500 ms and 400 ms overlap. In order to conduct the TPR permutation test statistic we calculated \overline{D}_θ and \overline{A}_{HG} (see above) around each θ trough in the time window in each electrode and trial which yields 20 \overline{D}_θ and 20 \overline{A}_{HG} values in each trial from which one \overline{D}_θ and one \overline{A}_{HG} value was randomly chosen in each permutation. In each trial the TPR was calculated from the random \overline{D}_θ and \overline{A}_{HG} values and correlated (partial correlation) with behavioral measures. In 500 permutation we

estimated a distribution of partial correlation which served to assess the significance of the observed partial correlation coefficient. Electrodes exceeding the 95% percentile were considered significantly predictive for performance. In a comparable way learning effects were obtained. In general we tried to find the subset of electrodes within the pool of electrodes which are correlated with performance. Specifically we sought to find those electrodes whose Pearson’s correlation coefficient is significantly greater than the partial correlation coefficient (ρ). Therefore we again chose randomly one \overline{D}_θ and one \overline{A}_{HG} value per trial and correlated (Pearson’s correlation – r) the randomly obtained TPR values with behavioral measures. In each permutation we calculated the difference $d_{r-\rho}$ between the randomly obtained r and ρ . In 500 permutations we estimated a distribution of $d_{r-\rho}$ which served to assess the significance of the observed $d_{r-\rho}$. Electrodes exceeding the 95% percentile were considered significantly predictive for automatization. Note that this analysis results in spatial more limited cluster than in the ROI-analysis since in the ROI-analysis Pearson’s r was used and not the difference of $r - \rho$.

4.3 Results

We investigated potential links between paCFC and motor performance in six subjects each performing one of three repetitive motor tasks described next. The three different behavioral tasks (Figure 1) were a serial reaction time task (SRT 2 subjects), a go/no-go task (GNG 3 subjects), and an auditory motor coordination task (AMCT 1 subject). All three tasks required the coordination of finger movements with an external stimulus. We assessed motor performance as reaction time in the SRT and GNG tasks and as the temporal deviation from the target time point in the AMC task. The cognitive requirements for performance improvement are different in all three tasks: learning the motor sequence in the SRT, learning the stimulus-response association in the GNG and improving movement timing in the AMCT. However, the motor automatization component is performance improvement with practice. The dynamics of the different performance measures were assessed in a group statistic, by comparing the average behavioral outcomes between fixed trial bins (see Figure 4.3). We recorded the ECoG while subjects performed two blocks of one of each task with the hand contralateral to the electrode grid. The ECoG-time series was filtered in the θ -band (4-8 Hz) and in the HG-band (80-180 Hz) yielding two separate filtered signals (see Methods). We calculated the analytic amplitude of the HG-band time series by taking the absolute value of the Hilbert transform of the filtered time series. The analytic amplitude is a new time series representing the amplitude envelope of the HG-oscillations at any moment in time. We performed the analysis on the 500 ms interval immediately following the stimulus onset. This interval includes the preparation of the responses indicated by the stimulus and includes approximately three θ -cycles.

4.3.1 Phase amplitude cross frequency coupling

We first asked whether the amplitude envelope of the local HG oscillations is phase coupled to the local θ -band oscillations. Figure 4.4A shows the time course of sine waves

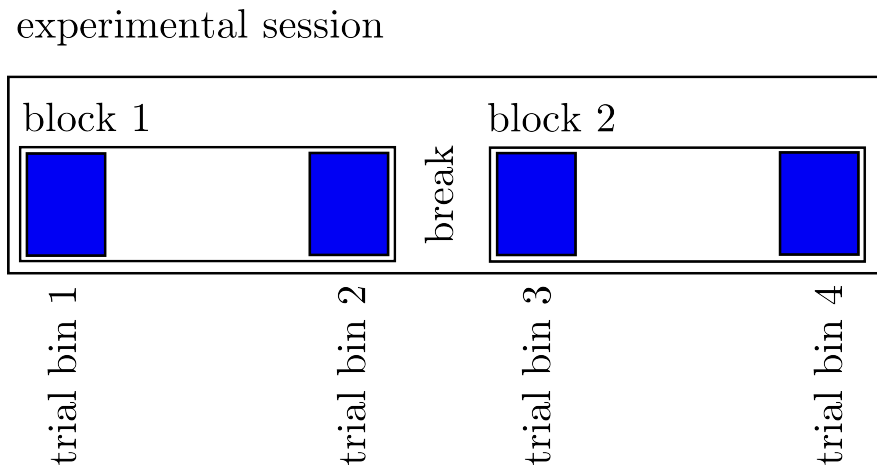


FIGURE 4.3:

Here we depict the separation of the whole experimental session into trial bins. The experimental session in each patient consisted of 2 blocks separated by a short break. In each block we defined two trial bins each containing 30 trials (blue). We compared the PLV across the four trial bins to assess the evolution of connectivity length of α and HG activity during motor behavior automatization.

fitted to the single trial variations of HG analytic amplitude pooled across all electrodes in one subject. **As predicted, HG analytic amplitude varied systematically over the θ -cycle.** Figure 4.4B shows single subject sine wave fits to the HG analytic amplitude averaged over trials and electrodes. Each fit was significant ($p < 0.001$) and the HG amplitude variations were consistent over subjects with only a slight deviation of subject 1 (see Figure 4.4B). The frequencies of the fitted sine waves are in the θ band (.95 Hz, SE: .02 Hz) and the phase angle is .6 rad (SE: .23 rad, see Methods for an explanation of the sine wave parameters frequency and phase angle). The maximum of the HG-analytic amplitude centers around the trough in the θ -cycle (mean = 2.56 rad, std = .56 rad, skewness = -.16).

4.3.2 Covariation of paCFC with automatization

To investigate if cross frequency coupling (paCFC) covaries with motor performance variations during automatization, we first calculated the trough to peak ratio (θ -trough to HG peak ratio TPR; see Methods) over all electrodes on the grids as a metric for paCFC and related it to behavioral performance. Figure 4.5A shows the development of TPR and motor performance over the time course of the two experimental blocks each subject completed. **Both TPR and performance increased during the experiment, as indicated by the fitted exponential functions.** A statistical test confirmed this finding. In this test, we first compared average motor performance in the initial 30 trials of the first block with performance in the final 30 trials and found a significant improvement (Wilcoxon rank sum test across all subjects: $p < .05$, Figure 4.5B, See Figure 4.3 for the structure of the experimental session). However, performance plateaued in the second block as indicated by no significant difference

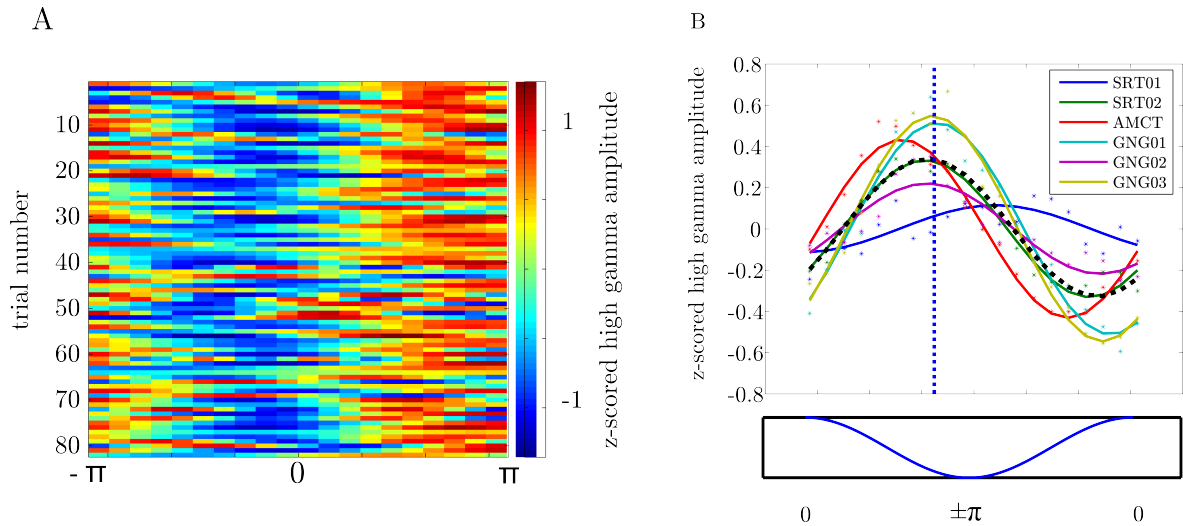


FIGURE 4.4:

The amplitude of the HG oscillations is phase coupled to the θ -band (4-8 Hz) oscillations in all subjects across paradigms. A) Time courses of sine wave functions fitted to the single trial amplitude envelopes of the HG oscillations of one subjects collapsed over electrodes. B) Sine wave functions fitted to the trial-averaged HG oscillation amplitudes envelopes of each subject. Each solid line represents the fit for one subject. Each dot represents the individual trial average of the HG oscillation in one of 20 intervals equally spaced over a θ cycle. The black dashed line shows the averaged sine waves across subjects. The vertical blue dashed line denotes the averaged phase angle the HG amplitude peaks across subjects. The maximum of the θ cycle is at phase 0 and the minimum at $\pm\pi$.

($p=0.18$). The difference between the first and the second block is indicated by a significant block-by-trial-bin interaction in a two way ANOVA across subjects ($F(1,20) = 5.95$; $p = .03$, $df_{error} = (N_{subj} - 1) * N_{trialbin}$). See TABLE 4.1 for a summary of the individual motor performance. The next question was whether TPR exhibits the same behavior (Figure 4.5C). **In concordance with behavioral performance we found, that the TPR increased between the first and the last 30 trials of the first block (Wilcoxon rank sum test across all subjects: $p < .05$) but did not change between the first and the last 30 trials of the second block ($p=0.3$).** A significant block-by-trial-bin interaction in a two way ANOVA ($F(1,20) = 5.95$; $p = .03$) confirmed that TPR changed during the first block and plateaued during the second block. This suggests that, on average, paCFC covaries with motor performance with paCFC and motor performance increasing early in the first experimental block and both plateauing in the second block.

Support for a functional relation between paCFC and motor performance would be provided by a trial-by-trial TPR with performance correlation. In order (i) to test for this correlation and (ii) to disentangle cortical regions showing varying paCFC with performance, we pooled the data in six anterior and frontal regions of interest (ROIs; the anterior and posterior medial frontal gyrus, the anterior and the posterior inferior frontal gyrus, and the superior and inferior sensorimotor cortex (see Figure 4.6) for all

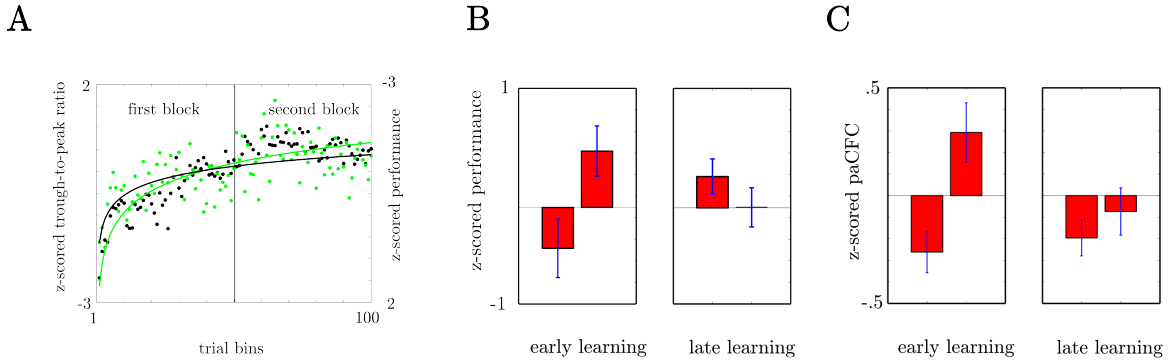


FIGURE 4.5:

Covariation of average paCFC with performance over the time course of the experiment. A) The development of TPR and motor performance during the time course of the experiment. Results are collapsed across all six subjects/three experiments. Data for the first block and second block are shown in the left and second half of the plot. Each point represents the average in one of 100 time bins. Exponential functions fitted to the data z-scored over both blocks indicate a similar time course for performance and TPR. B) Subject averaged motor performance during the first and last sets of 30 trials in the first (early learning) and the second (late learning) experimental block. C) Subject averaged TPR. Data was z-scored within blocks and TPR was averaged over all electrodes.

Paradigm		trial bin			
	Patient	1	2	3	4
SRT					
	SRT01	917 (271)	767 (227)	748 (219)	707 (161)
	SRT02	1472 (300)	1017 (284)	859 (207)	966 (232)
AMCT					
	AMCT01	117 (66)	98 (65)	147 (197)	142 (129)
Go/No-Go					
	GNG01	343 (46)	323 (117)	331 (109)	302 (128)
	GNG02	426 (185)	301 (42)	260 (28)	301 (66)
	GNG03	433 (168)	379 (178)	286 (40)	393 (89)

TABLE 4.1: contains behavioral data. For SRT (serial reaction time task) and GNG (Go/No-Go) task reaction time is shown (standard deviation) in msec. For AMCT (auditory-motor coordination task) the absolute deviation from precision is shown also in msec. Each trialbin encompasses 30 trials.

five subjects with a square 8x8 (N=4) /16x16 (N=1) grid implantation. In each ROI we pooled the TPR values across electrodes and determined the p-values of the trial-by-trial correlation with performance of each ROI (Figure 4.6; for details see Methods and Figure 8.2). **Significant correlation of TPR with motor performance (corrected for multiple comparisons) was observed in pre-/motor cortex and in anterior and posterior inferior frontal sulcus.** We predicted two sources of

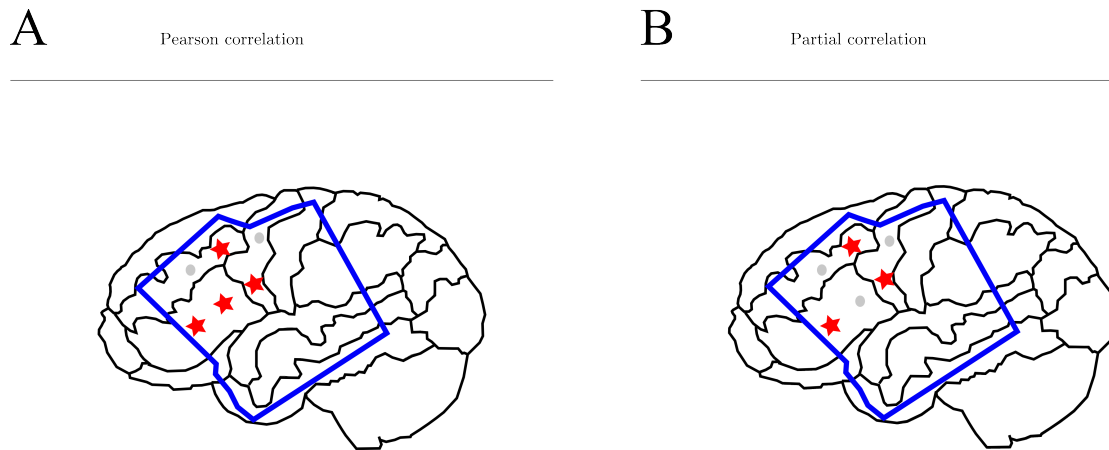


FIGURE 4.6:

Depiction of the results from the ROI-analysis. A) ROIs with significant automatization unrelated TPR/performance correlations. B) ROIs with significant automatization related TPR/performance correlations. ROIs with significant correlations (Bonferroni correct for six comparisons) are marked with an asterisk. The 6 ROIs are the anterior and posterior medial frontal gyrus, the anterior and the posterior inferior frontal gyrus, and the superior and posterior sensorimotor cortex. The blue margin shows the grid coverage across all subjects with a square grid implanted.

variability in single trial correlation between TPR and motor paCFC: one that is automatization related and varies systematically over time and another one that is not related to automatization and varies randomly from trial to trial. The first analysis supported automatization related trial-by-trial correlations reflecting the co-evolution of coordination between brain networks and improvements of motor performance during motor behavior automatization. We then calculated in the same ROIs the partial correlation of TPR with performance. This analysis factored out the fraction of correlation between TPR and performance which can be attributed to random trial-by-trial covariations and is automatization unrelated. **This automatization unrelated correlation of TPR with motor performance was observed in sensorimotor cortex and in premotor cortex, in the posterior middle temporal sulcus (corrected for multiple comparisons) and overlaps with the automatization related correlation.**

4.3.3 Discrimination of automatization from Random Performance Fluctuations.

To disentangle these two potential and functionally distinct causes of paCFC-performance covariations and disentangle the spatially wide ROIs we performed two different correlation analyses separately for each recording electrode. First, we calculated the partial

correlation of TPR with performance. Second, we calculated the standard Pearson correlation between TPR and motor performance. Pearson correlation captured the automatization related plus the automatization unrelated correlation. Combined with partial correlation this was used to distinguish between the two effects. Electrodes that capture automatization related TPR with performance correlations should show a partial correlation different from zero and a Pearson correlation different from the partial correlation (see Methods). Importantly, we reasoned that if we observed a significant Pearson correlation in an electrode that significantly changes if we discount time related correlations (in partial correlation), then the TPR performance correlation in this electrode is partly due to automatization related TPR performance correlations. Figure 4.7A shows the electrodes where random trial-by-trial fluctuations of TPR correlated with motor performance (significant partial correlation - uncorrected for multiple comparisons). Clusters of electrodes showing high correlations are located in sensorimotor cortex, in premotor cortex, in lateral prefrontal cortex and in ventral anterior temporal cortex. Figure 4.7B shows the distribution of electrodes with automatization related trial-by-trial correlations between TPR and motor performance. **Clusters of automatization related electrodes were apparent in premotor cortex, in lateral prefrontal cortex and in ventral anterior temporal cortex.** Importantly, the variation of TPR with automatization was not a result of a shift of the HG amplitude peak relative to the θ trough and hence the coupling phase remained stable during automatization .

4.4 Discussion of ECoG Results

Phase-amplitude cross-frequency coupling has been proposed to support interaction within functional networks (Canolty and Knight, 2010). Here we show that fluctuations of θ and HG paCFC are tightly linked to motor behavior automatization at the single-trial level and show robust automatization clusters over pre-motor and motor cortices.

4.4.1 Automatization and theta and high gamma activity

During motor behavior automatization θ and HG activity show a clear development of coupling that asymptotes in strength as motor behavior automatization plateaus. paCFC is highly dynamic and task-specific (Yanagisawa et al., 2012; Canolty and Knight, 2010) and it has been proposed that paCFC enables adaptive behavior (Canolty et al., 2006). Here we report data from three different motor behavior automatization experiments showing that paCFC dynamics reflect adaptive behavior supporting a relationship between paCFC and motor behavior automatization on a trial-to-trial level. Notably, despite the differences in tasks similar cortical regions associated with automatization or random trial-to-trial performance are identified by paCFC evolution. The dynamic nature of paCFC and the task-specific coupling patterns have been shown in a variety of studies with task dependent differences in coupling frequencies and coupling phase (Scheffer-Teixeira et al., 2013; Voytek et al., 2010; Yanagisawa et al., 2012; Miller et al., 2012; Belluscio et al., 2012). Here, we add an important paCFC characteristic. We show that even though the preferred phase as indicated by coupling

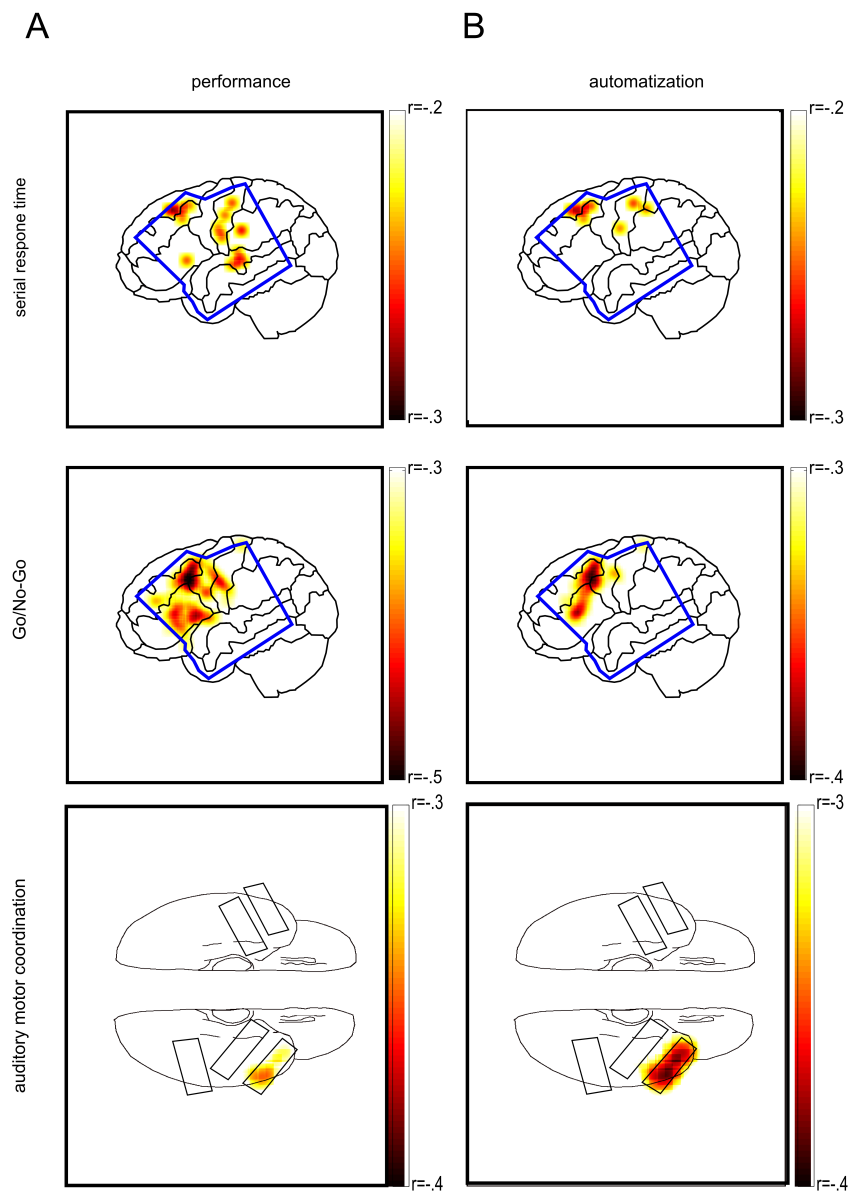


FIGURE 4.7: Electrodes with significant trial-by-trial correlations of TPR with performance. The significance threshold was determined in a permutation procedure (see Methods) A) Learning unrelated correlations of TPR with performance. B) Learning related correlations of TPR with performance. Darker colors indicate stronger correlations. See Methods for calculations on separating performance and learning related effects. The blue shape in the first and second row show the outline of all superimposed square grids. The black shapes in the third row denotes the grid locations for the participant in the AMCT. Spatial distortions result from the projection onto the cortex (for details see Figure 8.2)

phase stability does not change the activity pattern of both frequencies varies with behavioral changes.

4.4.2 Biological mechanism

Oscillatory dynamics are proposed Buzsáki and Draguhn (2004) to be inherent to the interplay of brain regions for cognitive control in memory and learning (de Hemptinne et al., 2013). For example θ activity observed in hippocampal and neocortical regions varies as a function of the state of the subjects (Cantero et al., 2003). The neocortex exhibited more prominent θ activity during wakefulness compared to REM sleep. automatization during practice can be achieved by distributed θ networks which are up-regulated during wakefulness by integrating or coordinating local activity. Here, the concept of information integration means that θ oscillations accumulates and integrates the results of local processing as reflected in HG activity in the premotor/motor region. HG activity, either an indication of spiking activity or very fast network oscillations (Ray and Maunsell, 2011; Scheffer-Teixeira et al., 2013), may be involved in planning and initiation of motor responses (Crone et al., 1998b). This frequency possibly reflects the activation of cortico-subcortical networks involved in the feedback control of discrete movements (Cheyne et al., 2008). Taken together we speculate that information on planning of motor responses is integrated into memory by paCFC which results in performance improvement during the process of automatization.

4.4.3 Conclusion

We identified cross-frequency coupling in the human cortex which is associated with motor performance variability per se. In this network a smaller area is integrated whose oscillatory dynamics reflect the progress in automatization. This learning related network suggests the establishment of a memory trace which is accumulated during practice and which is represented in a mutually adapted level of activity of θ and HG activity (Brashers-Krug et al., 1996; Brovelli et al., 2005; Muellbacher et al., 2002; Simon et al., 2002). In this respect paCFC provides a mechanism subserving motor memory formation Canolty et al. (2006).

5 Oscillatory Dynamics during Motor Learning: MEG Recordings

5.1 Introduction

As outlined in CHAPTER 4 it was long hypothesized that frequency interactions enables effective information processing and hence learning in humans. The first direct evidence supporting this hypothesis was shown in SECTION 4.3. Completing the significance the temporal changes co-occurring with behavioral changes could be localized in contralateral premotor and motor areas which are assumed to play a crucial role during motor learning and execution. However, evidence for the notion that local information is exchanged between dispersed brain sites by the mechanism of paCFC in a functional relevant manner does not exist. Therefore, it is unknown whether temporal changes of paCFC observed in the (pre-) motor area represent integration of information stemming from different cortical sites to enable coordinated behavior. This problem is inherent to ECoG recordings where electrophysiological processes can be registered across a wide frequency range but only with spatial limitations. These can be circumvented by whole-head recordings, however, non-invasively which bears the constraint of a poorer signal-to-noise ratio in higher frequencies (Ball et al., 2008; Whitham et al., 2007). Consequently, we approach the following questions. First, it was asked, whether changes of paCFC specifically between θ and high γ oscillations can be observed during early motor learning and whether those changes exclusively can be ascribed to cortical regions which point to a functional significance. The hypothesis here is, that changes can be seen in the (pre-) motor cortex as in SECTION 4.3 and in prefrontal regions since this region is associated with the transduction of higher level behavioral goals into actions (Grafton et al., 1998). If indeed there are different spatially circumscribed regions, our second question is whether interaction between those regions in the sense of information exchange can be quantified (Korzeniewska et al., 2008; Kamiński and Blinowska, 1991; Kamiński et al., 2001). Until now it was found that contralaterally to the performing hand changes can be seen in the premotor/motor cortex. However, it is not known whether this information processed is generated also in the motor cortex or whether behaviorally relevant information stems from other cortical sites. In this study three different aspects of paCFC mediating motor skill learning were shown. First, paCFC changes during motor learning can also be picked up with non-invasive recordings. Importantly, the finding of changes in the contralateral premotor/motor cortex in intracranial recordings can be replicated. Second, whole head recordings identify additionally the right prefrontal cortex where paCFC changes and inter-individual performance levels can be predicted by paCFC. Third, with a granger causality approach it will be shown that the right prefrontal cor-

tex processes and transfers information to the premotor/motor cortex in a functional significant manner.

5.2 Methods and Material

5.2.1 Recording and Participants

MEG and EEG were recorded simultaneously in an electromagnetically shielded room at the Otto-von-Guericke University in Magdeburg. The data was sampled at 1017.25 Hz , using a whole-head BTi Magnes system with 248-sensors (4D-Neuroimaging, San Diego, CA, USA). A total of eleven right-handed healthy subjects participated in the experiment (mean age: 24.1, std age: 1.5) all of whom gave written informed consent. The study was approved by the local ethics committee.

5.2.2 Paradigm

Subjects carried out the serial reaction time task as explained in SECTION 4.2.2 in which they were presented with a number on a screen (visual cue) that indicated which finger to move (1: thumb, 2: index, 3: middle and 5: little finger) (see upper left quadrant of FIGURE 4.1). The visual cue was presented every two seconds and the participants were instructed to press immediately a button with the finger indicated by the visual cue using their dominant hand. Moving the ring finger individually appeared to be difficult and was therefore, excluded from the experiment. The subjects were seated comfortably in an upright position, the elbow was rested on a pillow and the hand was held in a prone-position. The whole experiment consisted of five blocks. Each block in turn consisted of four sessions. Within the first three sessions the subjects were presented with a fixed sequence of six numbers they had to respond to with the corresponding finger. In the last session the four numbers were presented in an unpredictable order. In total each of the four sessions within each block contained 48 trials. Each session within a block were separated by a break of 15 seconds in which the subjects were instructed to relax.

5.2.3 Calculation of the theta-phase high gamma-amplitude Cross-Frequency Coupling.

In SECTION 4.3 we reported about the finding that ECoG electrodes covering the premotor/motor cortex contralateral to the hand performing showed a covariation between the paCFC and performance measures (reaction time, precision). As for the ECoG recordings the θ trough to high γ peak ratio (TPR) was calculated to quantify the evolution of phase-amplitude cross-frequency interactions of cortical oscillations during motor skill learning. To this end θ troughs as the local minima within the ongoing signal were detected. The high γ analytic amplitude was obtained by Hilbert-transforming the high γ filtered time series. For each detected θ -trough the depth of the through was estimated as the average of the θ -filtered time series over an interval of 83 ms (half θ oscillation) centered on the trough. Further, for each detected θ -trough

the magnitude of the simultaneous high γ amplitude was estimated as the average of the over the same interval of 83 ms centered on the trough (see APPENDIX 9.1.1 for details on the selected interval and frequency bands).

5.2.4 Calculation of trial-by-trial paCFC

The first approach was chosen to separate between the sensors and find the patterns of channels which show maximal changes during early learning. However, for the comparison between the experimental conditions the mean changes are of interest since it is less probable that condition differences are reflected by the extremes of the paCFC distribution. The trial-by-trial paCFC was calculated as outlined above for all MEG sensors and for all subjects. However, first, the combination matrix was calculated for all trials in the first block of training. Second, the mean of the combination matrix of each trial was calculated separately for all MEG sensors. The trial-by-trial paCFC was calculated in the fixed and the random condition in the same way.

5.2.5 Granger causality

Between clusters of sensors we quantified the information transfer to determine the direction of information flow and to make a statement about the hierarchical order of the cortical areas covered by the sensors. We used a granger causality (Granger, 1969) measures which fosters the definition of the frequency band carrying information. The causality measure is based on a multivariate autoregressive model (MVAR) (Korzeniewska et al., 2008). The rationale behind this approach is that if the prediction of future events or points in time of one time series x is improved by taking past events of another time series y into account than most likely y is causal for x . This MVAR is fitted to the MEG data with the aim to predict time series of interest from time series recorded at all other sensors of interest (see APPENDIX 9.1.2 for details of Granger Causality estimation and prove of robustness). Since the flow of information from a given region A to B may be different from the flow from B to A this measure is also called directed informational transfer (DIT).

5.3 Results of MEG Recordings

5.3.1 Behavioral Results

We analyzed the behavioral data under the premise to see whether our subjects learned only in the fixed sequence and not in the random condition within our interleaved design. **The subjects improved only in the fixed sequence** (see FIGURE 5.1) which was approved by a two-way ANOVA with the factors sequence type and number of blocks. We found a significant effect of sequence type indicating that subjects responded faster in the fixed condition ($F_{(1,100)} = 13.12; p < .001$) and a significant effect of block number ($F_{(4,100)} = 2.93; p < .05$). The learning gain was assessed with separate ANOVA of reaction times. In the fixed condition the subjects were getting faster during blocks ($F_{(4,50)} = 4.51; p = .003$) whereas there was no such improvement

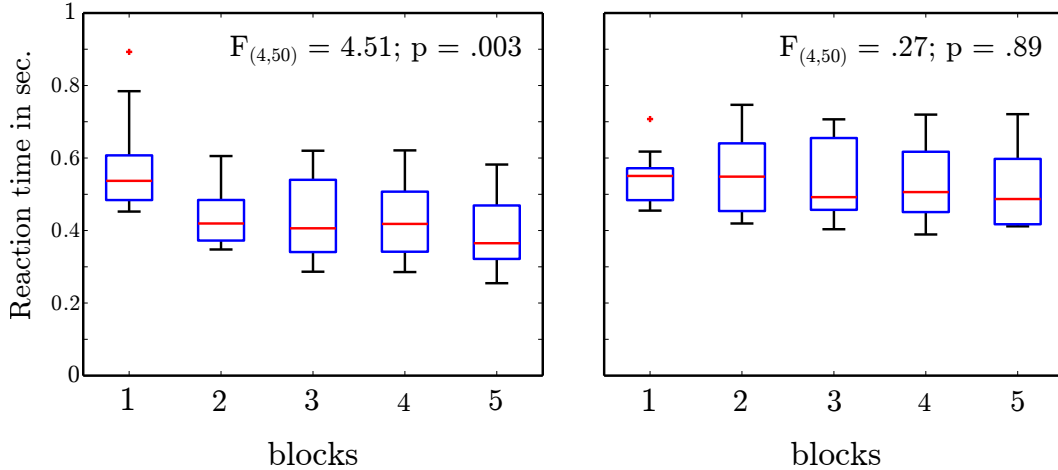


FIGURE 5.1: Depiction of behavioral results. In the left quadrant the change of reaction times (y-axis) across blocks of training (x-axis) are shown as boxplots in the fixed sequence condition. Red lines indicate the median. The right quadrant shows the same for the random sequence condition. We see in both upper quadrants that the mean lies under 600 ms. Therefore, we opt to use the interval of 600 ms after stimulus onset for the analysis of both the paCFC and Granger causality.

in the random condition ($F_{(4,50)} = .27$). For each block we calculated the median reaction time to define this time range which was used in each trial to calculate the paCFC. In each block across both sequence types the median fell below 600 ms after stimulus onset (see FIGURE 5.1) wherefore we used the time range of 600 ms following stimulus onset for the analysis of paCFC.

5.3.2 Increase of paCFC in the contralateral (pre-)motor cortex

In intracranial recording electrodes covering the contralateral premotor and motor cortex showed a strong change of the paCFC indicated by the theta-trough to high gamma analytic amplitude ratio (TPR). Since invasive recording techniques provide distinct signal content than non-invasive recordings it was asked whether TPR does exist and whether brain sites where TPR changes forms spatial patterns, which indicate a functional relevance. For each sensor Δ paCFC was calculated across trials of the first block containing the fixed sequence. Δ paCFC was calculated as the increase of the paCFC since an increase during learning in ECoG recordings (see Calculation of the theta-phase high gamma-amplitude Cross-Frequency Coupling) was observed. This yields a vector of 248 slope values each representing the Δ paCFC in each sensor across trials. This vector was z-scored and 9 sensors exceeded a z-score of 2 ($p = .02$). On the scalp these **sensors generate a spatial pattern with one cluster of 6 sensors restricted to the contralateral PMC/MC** and 3 single sensors. The latter ones were excluded. One can argue that this is a random result and has nothing to do with task specific processing. Specifically one can assume that this result can be achieved either by a complete random process or is just a result in this group of subjects since the sensor according to the group mean was chosen. (see APPENDIX 9.2 for details of

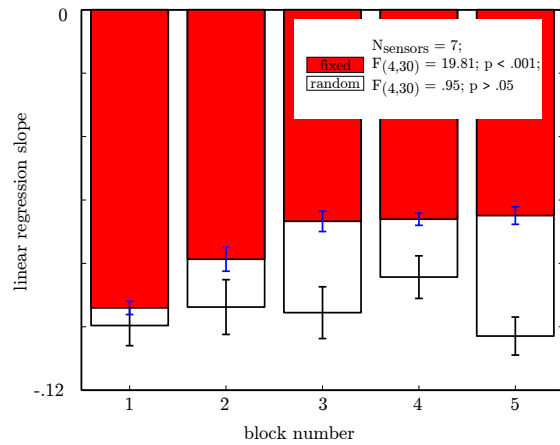


FIGURE 5.2: We extracted in the first training session 7 sensors covering the right prefrontal cortex where the slopes derived from the linear regression equations were maximal. We hypothesized that the dorsolateral prefrontal cortex is engaged in stimulus-response-mapping and this is important during early training or when rules characterizing external stimulus sequences cannot be extracted and hence, in during the random sequence. This is indeed the case. During the training of the fixed sequence (red bars) the slopes of the paCFC recorded at the sensors covering the DLPFC decrease. This indicates that in later blocks the activity associated with the stimulus-response-mapping is less important than at the beginning. However in the random sequence condition the slopes did not change.

control analysis.)

5.3.3 paCFC pattern in the right prefrontal cortex

Due to the whole-head recording it is possible to identify with the same analysis as explained above one region where the paCFC decreases significantly. This is the ipsilateral and hence, right prefrontal cortex (rPFC; $N = 7$; 4 sensors with significant theta modulation and 5 single sensors were excluded), where maximal slopes of the paCFC are greater compared to all other sensors. This region is associated with stimulus-response-mapping (SRM) (Miller and Cohen, 2001). In these 7 sensors the magnitude of the maximal slopes over blocks were compared with an ANOVA with the factors sequence type and number of blocks. We found a significant effect of the sequence ($F_{(1,60)} = 36.8; p < .0001$), the number of the block ($F_{(4,60)} = 4.16; p < .005$). Importantly, a significant interaction between the sequence type and the number of blocks ($F_{(4,60)} = 2.6; p < .05$) was found. This was further approved by two separated ANOVAs for the fixed and the random condition. In the rPFC sensors the Δ paCFC varied over blocks ($F_{(4,30)} = 19.81, p < .001$). Specifically, the absolute slope of paCFC was elevated in the first blocks ($1 > 2, 3, 4, 5; 2 > 4; t_{(6)} < -5; p < .0009$). However, this was not the case for the random sequence ($F_{(4,30)} = .95$; see FIGURE 5.2).

In both regions those sensors were extracted which had the greatest change of paCFC.

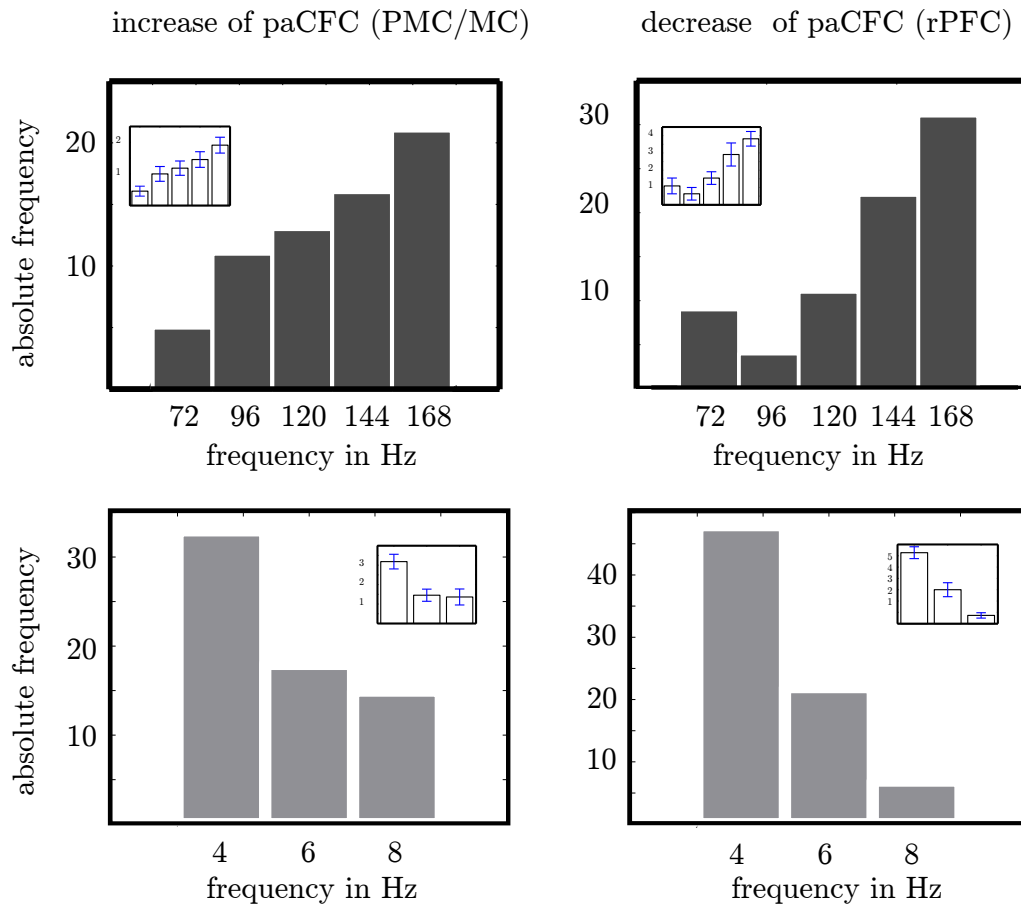


FIGURE 5.3:

Depiction of the probability to chose a low frequency in the θ range ($4Hz$) and a high frequency in the high γ range $\approx 170 Hz$.

In this analysis we did not predefined the interacting low and high frequencies but rather looked in each sensor individual for the frequency combination which showed the greatest change. This implies that each low and each high frequency should have the same probability to be selected. However, the probability to chose a low frequency in the θ range ($4Hz$) and a high frequency in the high γ range $\approx 170 Hz$ was elevated (see FIGURE 5.3).

So far, two spatial patterns can be seen, which are dispersed across the human cortex and show an elevated change of paCFC during early learning compared to all other cortical regions. This puts the question whether both regions are hierarchically ordered. Hierarchy can be defined as a system of functional inferior and superior elements each entrusted with a different task. We speculated that superiority is given if two prerequisites are fulfilled. First, a superior element can be that element which shows a great deal of specialization (for example to discriminate between high and low performance). Second superiority of one element is given if this very element governs another element. We tackle both questions in the following two analyses.

5.3.4 paCFC/performance prediction in the right prefrontal cortex

A higher level in the hierarchy and hence, dominance is assumable if activity in a given region predicts inter-individual differences of performance, since this points to sensitivity of the neuronal activity in this region. Therefore, here we studied whether individual performance differences can be explained by different paCFC levels. This analysis was conducted separately for each sensor covering the PMC/MC and the rPFC. Again it is important that sensors whose paCFC predicts individual performance levels form clusters and are not randomly arranged. Only if adjacent sensors are located either in the PMC/MC or the rPFC one of both regions can be seen as directive. We tested whether individual reaction times (average of first half of trials of each block) correlate with individual paCFC (average of first half of trials of each block) levels in individual sensors. **Only the paCFC level of the sensors rpfc_6 and rpfc_7 covaried with inter-individual differences of performance in the last block at a significance threshold corrected for number of channels and blocks** ($r < -.86; p < .05/(N_{channel} - x - N_{blocks})$: see FIGURE 5.4). Additionally, rpfc_3 and rpfc_5 covaried if significance threshold is corrected for number of channels only. This effect arises only after the passage of 2 complete iterations of the fixed sequence trials (see FIGURE 9.4) and is not visible in sensors covering the PMC/MC even at an uncorrected significance threshold and for the random sequence. Central to this finding is that covariance of paCFC and response time is neither a result of an increase of variance in response time nor paCFC variability. (see SECTION 9.3).

5.3.5 Granger causality reveals different roles for rPFC and PMC/MC

The exclusive covariation in the rPFC only allows concluding that both cortical sites show differences in processing and hence, the rPFC assumes functional dominance in processing the SRM. But this does not offer a valuable conclusion of the hierarchical interaction of both cortical sites. As outlined above it is supposed that a hierarchy is recognizable if activity in one site drives activity in another site. This was tested with an analysis of causality. Since we are especially interested in frequency resolved information transfer the directed information transfer rate (DIT) (Korzeniewska et al., 2008; Kamiński and Blinowska, 1991; Kamiński et al., 2001) was calculated both within the cortical regions PMC/MC and rPFC and between both regions (mc2rpf, rpf2mc). We tested whether a difference in information transfer exists for the fixed compared to the random sequence. Furthermore, it was investigated which frequency band discriminates between the sequence type. This was done for all frequencies ranging from θ to high γ including the α , β and γ range. In each region (mc, rpf, mc2rpf, rpf2mc) the 5 DIT values each representing one of the 5 blocks of the random with the fixed sequence were compared. The significance level was corrected for multiple comparisons by releveling the threshold to 95 % of the maximal absolute t -value of all p -values $< .05$ (see FIGURE 5.5). This adjusted significance level corresponds with $t_{(4)} > 4.1(p < .012)$ for the inrpf and with $t_{(4)} < -4.2(p < .011)$. **This shows that the DIT from the rPFC to the PMC/MC is greater during the fixed sequence and this effect arises only in a subband of the high gamma range (≈ 172 -180 Hz). Further-**

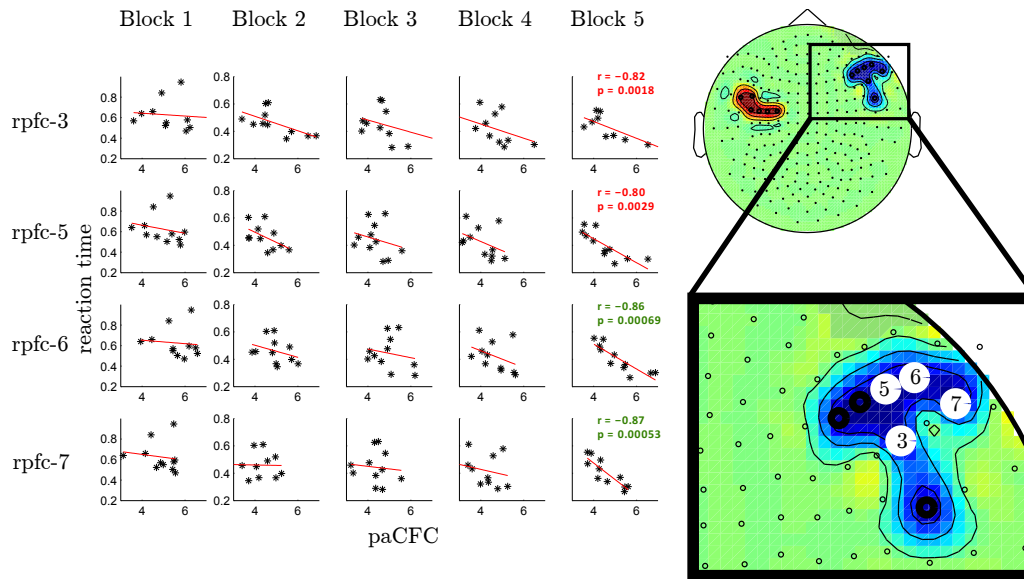


FIGURE 5.4: Here, for each block the covariation of paCFC and performance is depicted for those sensors whose paCFC varied significantly with reaction times across subjects. In the first block the reaction time was greater than in late blocks. The y-axis in Block 2 is valid for the three last blocks, also. Apparently only in the last block the reaction times vary as a function of the paCFC across subjects. This effect is not visible in the PMC/MC and hence only in the DLPFC where paCFC activity is associated with . For the four MEG sensor whose paCFC predicts inter-individual performance differences in the last block the covariation for the first blocks is shown, too, where there was no such significant correlation. Importantly the regression lines tend to become steeper with training. In the column of the fifth block in red Pearson's r and the corresponding p -value are shown since those sensors only pass a significance level corrected for the number of sensors ($p = .05/13$). Only the covariation of the paCFC of sensor 6 and 7 pass the significance level corrected for the number of sensors and blocks ($p = .05/(13*5)$).

more, the DIT within the rPFC is elevated in the random compared to the fixed sequence in another subband of the high gamma range (≈ 68 -88 Hz, see Figure 5.5).

5.4 Discussion of MEG Results

Summary of Results The observation that paCFC of theta and high gamma activity changes during motor learning is consistent with evidence from invasive studies. In this whole-head recording first, we replicated the finding that only sensors covering the PMC/MC showed significant changes and second, showed that the rPFC also shows significant changes during learning even though we did not restrict our analysis to a subset of sensors. We precluded the possibility that this result can be achieved by trialshuffled and frequency scrambled data or is a mere result of this group of subjects.

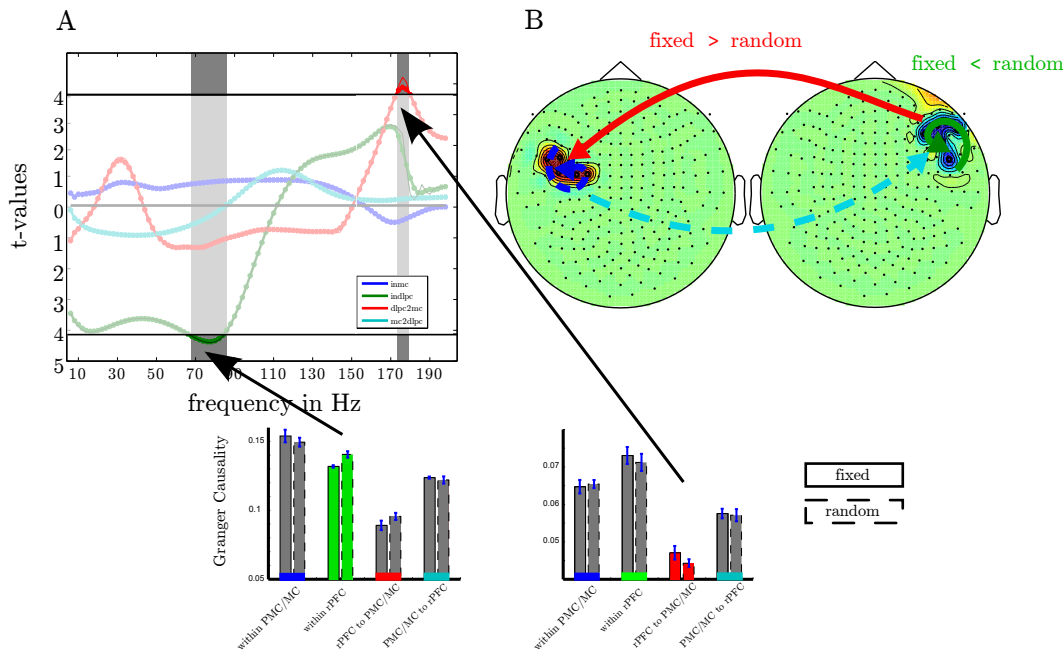


FIGURE 5.5: we depict the directed informational transfer (DIT) between the PMC/MC and the rPFC. **A** shows the t-values for the comparison of the DIT between the fixed and random sequence condition as a function of frequency. Each of the colored lines shows this for the DIT within the PMC/MC (inmc: dark blue), within the DLPFC (indlpfc: green), from the DLPFC to the PMC/MC (dlpfc2mc: red) and from the PMC/MC to the DLPFC (mc2dlpfc: light blue). The black lines show the corrected significance level for multiple comparisons. The uncorrected level for 4 degrees of freedom is at 2.16. Yet, the corrected level was determined as 95% of the maximal absolute t-value corresponding to an uncorrected level. This refers only to the red and green line, since the light and dark blue line never exceeded not even the uncorrected level. **B**: The comparison of DIT between the fixed and the random sequence condition yields very low negative t-values indicating a strong differences within the DLPFC in DIT for both conditions. This difference is represented in a subband of the high gamma range. On the other hand there is also a subband in the high gamma range which transfers different information from the DLPFC to the PMC/MC in both experimental conditions. Note, that the DIT from the PMC/MC to the DLPFC is greater than the DIT from the DLPFC to the PMC/MC. But this DIT does not discriminate between experimental conditions. Hence, a feedback route is assumed.

Importantly both regions interact in a hierarchical manner. This can be seen since the right prefrontal cortex showed changes of paCFC which matched the differences of progress of learning in the both conditions. Most strikingly, our data indicate that the rPFC directs the PMC/MC exclusively in the high gamma range. This is evidence for the hypothesis that cortical activity is transferred on a large-scale between cortical areas to enable effective human behavior. Most probably this frequency specific transfer

is mediated by theta activity (Buzsáki et al., 2004).

We propose that in this cortical system paCFC serves as a process of information integration. Technically spoken integration can be defined as functional entity constructed of different interacting groups which gear into each other to achieve efficiency. The alternative hypothesis could be that theta and high gamma activity are engaged in a process of cooperation. The strongest arguments to favor the idea of integration are that (1) we observe two distinct spatial regions showing changes of paCFC, (2) functional relevant information transfer is clearly directed and all the more important that (3) information discriminates our experimental conditions and (4) information content is clearly defined. The first argument means that for a process of cooperation there would be no need for more than one cortical region mediating motor learning. If there are more than one region the probability is high that they interact by exchanging information. Second, due to the granger analysis a clear distinction can be made how the exchange takes places. In fact the rPFC directs task relevant information which is integrated in the PMC/MC for an optimal task execution. We found evidence that information to be integrated discriminates our experimental conditions (3rd argument). If no distinction could be made no behavioral differences could be explained by the process of paCFC. To support the notion of integration not only the way of information flow should be clear (2nd argument) but also the content to be integrated should be clarified (4th argument). It turned out that only the high gamma band codes information to be integrated. According to recent studies Ray et al. (2008) this high gamma activity is tightly correlated with spikes of cortical neurons. Importantly only the high gamma band is engaged in task relevant coupling with theta which is seen as the frequency range mediating the information flow between spatially dispersed cortical areas (Buzsáki et al., 2004; Guderian and Düzel, 2005). Comparing the information transfer in higher with lower frequencies it is obvious that higher frequencies show only reduced transfer but apparently the absolute level of information transfer gives no clue about the effectiveness of the information transferred. Korzeniewska et al. (2011) found connections which were directed from motor related areas. We also found such connections which are greater than the information transfer from the rPFC to the PMC/MC. Apparently signal contents transporting information about rules are visible in the reversed direction and not from the motor to the prefrontal cortex. We assume that the information from the PMC/MC to the rPFC is a feedback loop. But this remains to be an issue for future investigations. Furthermore we do not know whether other for example subcortical brain sites like the basal ganglia show paCFC relevant for behavior. If this is the case paCFC in the theta and high gamma range can be a general motor control and learning mechanism.

This integration of information results from the cooperation of two hierarchical interconnected areas where the rPFC is identified as the leading unit. The right anterior prefrontal cortex is associated with episodic retrieval (Allan et al., 2000; Henson et al., 1999; Pierrot-Deseilligny et al., 2003), self-recognition (Keenan et al., 2000), decision-making (van 't Wout et al., 2005) or attended emotional judgement (Grimm et al., 2008). In sum top-down control is attributed to the rPFC. This proposal is well in line with our results since task relevant information is forwarded to the PMC/MC where

information are integrated. However, until now individual differences are not taking into account in this organizational unit of the rPFC (Blumenfeld and Ranganath, 2007). This can be the result of the insensitivity of measures applied. More strikingly paCFC calculated as the theta-trough to high gamma peak ratio (TPR) predicts inter-individual capability of motor memory. It is important that anatomically the subjects show differential activity where rules of the occurrence of external stimuli are represented and not in the executive brain site (PMC/MC). It seems as if fast subjects show less SMR activity in the rPFC than slow subjects. In fast learners the SMR rule is well established and this is represented in high degree of higher paCFC compared to slow learners. Therefore, we have to conclude that a higher degree of autonomous behavior is linked to higher paCFC in the rPFC.

Please note that we identified two different high gamma frequency bands one which codes the stimulus response mapping. less interaction within the rPFC during fixed condition We identified a complex interplay between the PMC/MC and the rPFC. During the execution of the fixed sequence there is less informational transfer within the rPFC and this unit has therefore, more capacity for more transfer to the PMC/MC where in turn more information can be integrated which leads to a rapid increase of the paCFC. In the random condition the informational transfer within the rPFC is elevated and hence less information is transported to the PMC/MC which leads to a more slowly increase of paCFC. Importantly, information transfer took place exclusively in the high gamma range. This is consistent with our previous results, that especially the paCFC between theta and high gamma is predictive for motor performance (Dürschmid, 2013).

6 Oscillatory Dynamics track Cognitive Control: Subcortical Recordings from the Nucleus Accumbens

6.1 Introduction

The nucleus accumbens (NAcc) is part of the ventral striatum and plays a pivotal role in integration of information (Goto and Grace, 2008) from the limbic system, particularly between the prefrontal cortex (PFC) and the hippocampus (HC). The NAcc is considered the interface by which the HC gates input from the prefrontal cortex (French and Totterdell, 2002). In rats the PFC and HC converge onto single NAcc-neurons (Goto and Grace, 2008; Finch, 1996) and the PFC-NAcc and HC-NAcc connections are mutually dependent. For instance long term potentiation of the HC-NAcc association entails a long term depression of the PFC-NAcc association (Grace et al., 2007). It is assumed that this selective strengthening of the HC-NAcc connection is important for the rapid facilitation of goal-directed behaviors and for supporting automatized actions (Goto and Grace, 2005; Belujon and Grace, 2008). Such automatized actions are especially evident in motor learning tasks in which the NAcc integrates information for the planning of movements (Mogenson et al., 1980; Grace, 2000). Münte et al. (2007) speculated that the human NAcc evaluates the information used for the adjustment of response strategies. Accordingly, lesions in the NAcc limit the flexibility required for changes in behavior during learning (Grace et al., 2007). However, knowledge about the specific neural mechanisms utilized to integrate information from the PFC and the HC in the human brain is still limited.

Phase-amplitude cross-frequency coupling (PAC) of oscillations has been suggested as an effective mechanism for recruiting local networks to form functional global networks and to gate information (Buzsáki and Draguhn, 2004; Canolty et al., 2006, 2010; Staudigl et al., 2012; Cohen et al., 2009a). PAC describes the dependency of the amplitude of a high frequency on the phase of a low frequency. In rats and mice there is a tight connection between the phase of the "theta" band (θ) of local field potentials (LFP) and single unit activity (SUA) (Chrobak and Buzsáki, 1998; Sirota et al., 2003; Siapas et al., 2005) presumably allowing neurons to form a larger assembly of neurons by means of transient coupling (Chrobak and Buzsáki, 1998). These studies suggest that the interaction between PFC and HC may occur via PAC. O'Donnell and Grace (1995) showed that hippocampal hyper- and depolarization leads to hyper- and depolarization in the NAcc. In the state of depolarization neurons in the NAcc are more

likely to fire action potentials in response to stimulation of the PFC (French and Totterdell, 2002; Goto and Grace, 2008) providing evidence for PAC with an enhancement of high frequency amplitudes during troughs in θ activity. Tort et al. (2008) showed transient θ phase - high gamma (γ) coupling in the rat's striatum during movement through a maze. Furthermore Tort et al. (2009b) demonstrated a function link between performance improvement and the strength of theta-gamma coupling during the course of learning. However, until now it has not been established whether NAcc shows PAC between θ and high γ activity in a functionally specific manner in humans. This would indicate that integration of information within the NAcc could rely on transient coupling between frequencies.

In the previous studies recording techniques were used which either could not pick up activity from subcortical structures or can pick up activity with only a very limited sensitivity wherefore, we studied the NAcc activity in three human subjects directly by means of subcortical electrodes. In a serial reaction time task (Nissen and Bullemer, 1987) the participants had to track and respond to a sequence of numeric stimuli in a fixed and a random order condition which modulated different cognitive control demands. From Tort et al. (2009b) one can hypothesized that PAC transiently occurs in the NAcc and is modulated by the level of cognitive control. We tested the following hypotheses: PAC emerges in the NAcc. Second, PAC discriminates between phases of high and low cognitive control. Third, PAC varies systematically with behavioral performance measures across experimental conditions (high and low cognitive control - HCC and LCC) .

6.2 Methods and Material

6.2.1 Participants

3 patients (mean age 38.3 years (SD 12.34), 2 female, all right handed) with a history of intractable epilepsy participated in this study. We directly recorded from the bilateral NAcc and the anterior Thalamus (ANT). For details on surgery and deep brain stimulation approach please see SECTION 10 and TABLE 10.1 summarizing clinical background of the patients. The study was approved by the local ethics committee.

6.2.2 Paradigm

We carried out a serial reaction time task (see FIGURE 6.1) which required a single finger movement that was specified by a numeric stimulus presented on a monitor screen. Stimulus presentations were controlled by MATLAB. Patients were instructed to respond with their right thumb, index finger, middle finger, or little finger, which rested respectively on the spacebar, “j”, “k” and “;” keys of a computer keyboard. Four different numbers (1, 2, 3, 5) were presented on the screen (height 2 cm, .15° visual angle). These numbers indicated the finger they had to use to press the key. Six blocks of 60 trials, each comprising the presented number and the corresponding finger movement, were conducted with each patient. The four numbers were presented in a fixed or random order depending on the block number, with 3 fixed order blocks

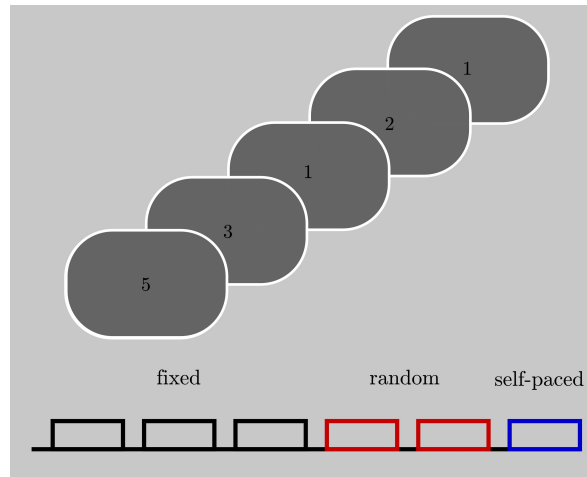


FIGURE 6.1:

Subjects were presented with stimuli indicating which finger to move. Each block contained 60 trials (presentation of a single number). Colors denote the type of the sequence. Together, the subjects were presented with 3 blocks of a fixed sequence, 2 blocks of a random sequence, and one block in which they could choose a sequence on their own.

followed by 2 random sequence blocks and a final block of self-paced finger movements. In the fixed order blocks a repetitive sequence of 6 numbers was presented in all 3 blocks. In sum, the participant performed 30 repetitions of the 6-number-sequence. In the random blocks the four numbers were presented randomly. In the self-paced block a fixation cross was presented instead of the numbers. The participants were not informed about the type of sequence. The interstimulus interval (ISI) was variable and depended on the reaction time of the participants, with a fixed time between response and next stimulus of 700 ms plus a jitter of ± 110 ms. In this interval the stimulus remained presented. Thus, block and trial length depended on the participant reaction time (mean block length per participant: Pat01: 117 sec (std: 18.4), Pat02: 93 sec (std: 25.6), Pat03: 96 sec (std: 26.03); mean trial length per participant: Pat01: 1.6 sec (std: .52), Pat02: 1.01 sec (std: .31), Pat03: 1.03 sec (std: .21). Blocks were separated by a 1 min rest. During this resting period an X was presented on the screen. A + presented for 5 sec informed the participant about the beginning of a new block.

6.2.3 Cognitive Control

These 3 types of sequences (fixed, random and self-paced) differed with respect to the need for ongoing monitoring of actions and performance outcomes and subsequently, adjustments of behavior and learning which we tagged cognitive control in accordance to MacDonald et al. (2000) and Ridderinkhof et al. (2004).

fixed sequence The fixed sequence allowed the participant to learn the sequence. During the early phase (cognitive phase (Fitts and Posner, 1973a)) of learning, when

the fixed sequence is unknown, a high level of cognitive control is necessary to establish a strategy to complete the task (Fitts and Posner, 1973a) namely to associate the stimulus with the response. The longer the training the less necessary cognitive control is since the stimulus-response association was learned and that the participants knows which finger to move before the actual stimulus is presented on the screen.

random sequence The sudden onset of a novel or unpredictable event captures attention and disrupts ongoing performance (Barcelo et al., 2006). In our experiment switching from the fixed to the random sequence marks such onset of several unpredictable events. This interruption of stimulus predictability signals the need for a change in strategy from a learned and hence, automatic to an unlearned mode. The occurrence of errors makes cognitive control necessary which leads to post-error slowing in healthy participants and more careful responses after errors (Notebaert et al., 2009). Hence less errors are expected during phases of high cognitive control. In healthy participants, differences in cognitive control are reflected by a reduction of initially long reaction times after the completion of several repetitions of the 6-item sequence of the same fixed sequence (Nissen and Bullemer, 1987; Knopman and Nissen, 1991). The presentation of random sequences after the fixed sequences will force the participant to abandon a learning strategy and elevate reaction times to a plateau value.

self-paced sequence During the last block the participants could chose the sequence on their own with no obligation. Since the selected movement had not to be adjusted according to an external stimulus we expected short reaction times which would indicate less action monitoring or cognitive control. In sum, we classified trials of high cognitive control (HCC - initial tracking of the fixed sequence and tracking the random sequence) and low cognitive control (LCC - tracking the learned fixed sequence and during the self-paced sequence).

6.2.4 Data Collection

Intracranial recordings were obtained using a Walter Graphtek (Walter Graphtek GmbH, Lübeck, Germany) system, with a sampling rate of 512 Hz, a resolution of $.25 \mu\text{V}$, and analog bandwidth of 200 Hz. We referenced online to the right earlobe. The ground electrode was placed at P8. During recording a highpass filter of 0.19Hz and a lowpass filter of 240 Hz was used. In the left and right NAcc and ANT (a total of 16 recording electrodes), adjacent electrodes were combined with each electrode referenced to the neighboring contact (i.e. 1–2, 2–3, 3–4, with “1” representing the most ventral and “4” representing the most dorsal electrode contact). This resulted in a bipolar montage with each NAcc/ANT monitored by three electrode positions. This montage was used to enhance the spatial resolution of the intracranial recordings and to ensure that the recorded activity originated from nearby tissue.

6.2.5 General Data Analysis

We used Matlab 2008a (Mathworks, Natick, USA) for all offline data processing. The resulting time series for the electrodes located in the NAcc were segmented in epochs of -1 to 2 sec relative to the event (stimulus and response). In separate analyses these epochs were aligned to the motor response or onset of the instructive stimulus. These time series were used to characterize event-related brain dynamics in terms of phase-amplitude cross-frequency coupling (PAC). We inspected the signal visually for artifacts and decided not to reject any epochs. Since we focused on single frequency bands we avoided signal drifts by applying bandpass filters for the frequency bands of interest (see below). All filtering was done using a 4th order butterworth filters (IIR-filters). All steps of data analysis were applied also to the recordings from the anterior Thalamus.

6.2.6 Behavioral Data

Two behavioral parameters - reaction times (RT) and error rate (p_e) - were assessed as indicators of cognitive control. The DBS procedure allows for the recording of only a limited pool of subjects (here $N = 3$). This limited number of subjects may influence strongly statistical test results so that effects can be missed even though potentially observable in a larger set of subjects. An ANOVA comparing RT differences across blocks - which may indicate differences in cognitive control - therefore, used RT of each trial in each subjects as the random variable ($n=180$) and blocks as factors ($p=6$). Reaction times of each subjects were z-scored across trials. Individual reaction times are summarized in TABLE 6.2. The summed number of errors in each participant was used to calculate p_e for each block except the self-paced block (errors cannot be made since the sequence was generated by the participant itself) we calculated

$$p_e = \frac{N_{errors}}{N_{trials}} \quad (6.1)$$

with N_{errors} designating the set of trials with false responses and N_{trials} as the total number of trials in a given block. A χ^2 test statistically compared the blockwise p_e . These values were related to Phase-Amplitude Cross-Frequency Coupling (PAC) in a correlation analysis to test the specific hypothesis of a functional relationship between PAC and behavioral performance (see **Section 2.7**).

6.2.7 Frequency analysis

In the first step we analysed whether oscillations show significant amplitude variations following the stimulus or the motor response. The rationale was to exclude the possibility that expected effects of phase-amplitude Cross-Frequency Coupling could be the result of the variation of only one frequency. We filtered the epochs in each trial in a broad range of frequencies ranging from 4 to 150Hz (center frequencies) with a step of 2Hz (band width of 4Hz). By means of the absolute Hilbert transform we estimated the envelope of the oscillatory activity for each filtered time series in each trial. We then grouped the trials according to the HCC and LCC condition (see Section: Cognitive

Control). In each frequency band and at each time point we compared the amplitude values across subjects and trials with a t-test. To assess statistical significance we corrected the significance threshold with a false discovery rate (FDR). Therefore, we fitted a cumulative normal distribution function to all p-values $<$ the uncorrected significance threshold ($p < .05$ see FIGURE 6.2. All comparisons between HCC and LCC whose p-values $< .05$ in this new distribution were considered statistically significant. We furthermore, asked whether the amplitude in experimental conditions evolves differently with respect to their baseline. In each trial we calculated the differences between the baseline (average of 500 ms before motor response) and the averaged activity in the temporal interval of 500 ms following the motor response. We then tested by means of a t-test for differences between the experimental conditions (HCC-LCC).

6.2.8 Phase-Amplitude Cross-Frequency Coupling (PAC)

Calculation of PAC To define whether frequencies interact and whether this interaction shows a temporal pattern, we quantified the relationship between the phase of the θ frequency band and the amplitude of a high frequency band in a manner comparable to the approach of Tort et al. (2009b). Specifically, for a given electrode e we used the temporal interval i around the button press in the fixed and random sequence trials ($N_{trials} = 300$) since in both the subject had to respond according to an external stimulus. In this interval i we separated the θ oscillation into 30 phase bins ($-\pi$ to π ; $N_{bins} = 30$) and calculated the averaged high frequency amplitude within each phase bin (see FIGURE 6.3A). We filtered the raw signal in the θ (4-8 Hz (Axmacher et al., 2010b)) band and a high frequency band covering the γ and high γ bands. The high frequency band was divided into narrow sub-bands with center frequencies ranging from 25 - 175 Hz, a bandwidth of 30 Hz, and a step size of 2 Hz. We used the Hilbert transform to estimate the high frequency amplitude time series and the θ phase time series. From this the amplitude-phase-histograms were derived with the 2π - θ -cycle split into 30 phase bins of equal width (.21 rad or 12°) in consecutive temporal intervals. We first calculated the cross-frequency spectrogram (amplitude variation of a high frequency oscillations as a function of the phase of a low frequency oscillation) within each subject. This means that the θ -phase values over the temporal interval (166ms) were sorted into 30 equally spaced phase bins. The window size of each temporal interval was set such that a full cycle of the centerfrequency (6Hz) of the θ range (4-8Hz) was covered (166 ms). Next the HG amplitudes observed at the various time points were separately averaged for each phase bin. As the last step in each subject we fitted a cosine function to the resulting HG amplitude values over phase bins. To prove the dependency of the HG amplitude on a same θ phase across subjects we averaged the resulting fit functions (see FIGURE 6.3). As the final step in our analysis we statistically compared whether more variance is explained by the variance across subjects or more variance is explained by the averaged fit functions (see next paragraph). If the latter was the case than all subjects HG amplitude depended on the same θ phase and the MI was high. For example, if coupling did not rely on the same θ phase than the variance across subjects would be higher compared to the variance across the θ cycle. In sum, first the subject specific electrophysiology was evaluated followed by the statis-

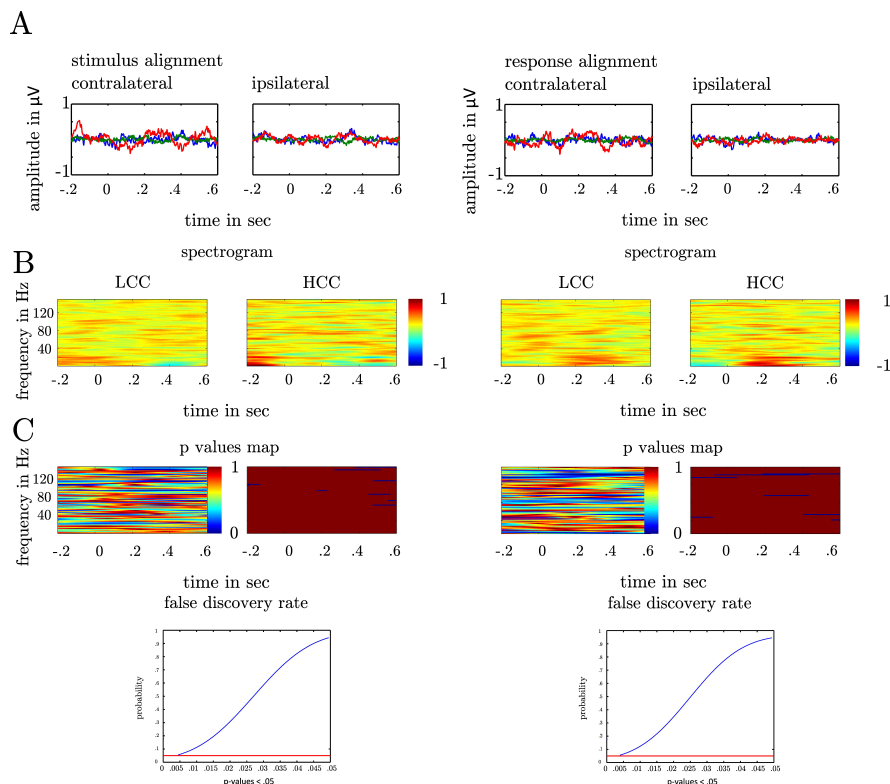


FIGURE 6.2: Depiction of local field potentials locked to the response and the stimulus presentation both for the contra- and ipsilateral recording sites. The LFP in each trial was filtered between 3 and 200 Hz. Each colored line represents one subject. **B**: Depiction of spectrograms for the low cognitive control condition (left-LCC) and the high cognitive control condition (right-HCC). In each subject we estimated the spectrogram by means of the Hilbert transform. In each trial aligned to the motor response/stimulus, we calculated the envelope of the bandpass filtered time series (4-150 Hz, bandwidth: 4Hz, step: 2Hz). The upper plots show the average across subjects and trials both aligned to the response and the stimulus in the HCC and LCC. For a better comparison of the amplitude across frequencies the spectrogram was z-scored for depiction only. All analysis were conducted on the non-standardized time series. The colorbar denotes the strength of amplitude in μV (z-score). **C**: depicts the statistical evaluation by means of a t-test. At each time point in each frequency we calculated the p-value for the difference between LCC and HCC across subjects and trials (left plot). The right plot shows the time points and frequencies with a p-values < .05 (blue) on an uncorrected significance threshold. We corrected for multiple comparisons by taking the distribution of p-values < .05 into account. The .05% confidence interval of this new distribution (last row) served as a new significance threshold. Note that no p-value fell below this threshold indicating that between the HCC and the LCC condition no significant difference in amplitude modulation was found.

tic within the entire group of subjects. We tested whether – despite averaging the fit function – more variance is explained by the fit function than by the variability across

subjects. The same analysis was also conducted with 2 underlying θ cycles. These analyses yielded roughly the same results, but with a poorer temporal resolution. The window of analysis was shifted in time by 10 ms between -600 and 600 ms around both the stimulus and the motor responses. This led to 121 temporal intervals ($N_{interval}$). Subsequently, in each interval the phase-amplitude distribution (distribution of high gamma amplitude values across theta phase-bins) was averaged across the electrodes separately for each hemisphere (contra- and ipsilateral to the performing hand) and for stimulus and response alignment.

Quantification of PAC To quantify PAC we used the variance σ_{PAC}^2 of the mean high frequency amplitude and the Modulation Index (MI; see FIGURE 6.3B and 6.3C). σ_{PAC}^2 is suited to be an exploratory measure since no specific model is assumed. In contrast the MI assumes a specific form of dependency of high frequency amplitude on the θ cycle and is defined by the strength of coupling and the phase to which the high frequency amplitude is coupled. In each temporal interval i we calculated the high γ amplitude distribution across the θ cycle per subject. We then averaged the high frequency amplitude across participants. This averaged high frequency amplitude is shown in FIGURE 6.3B as a dashed line. We calculated the variance σ^2 of the averaged high frequency amplitude as a function of the θ phase

$$\sigma_{(H\gamma/\theta)}^2 = \frac{1}{N_{bins}} \sum_{i=1}^{N_{bins}} (a_i - \bar{a})^2 \quad (6.2)$$

with a_i representing the mean high γ amplitude for a given phase bin across participants and \bar{a} representing the averaged amplitude of a_i over θ phases. The larger σ^2 the larger are the differences of the high frequency amplitude at different θ phases. A high value of variance indicates a high concordance of PAC across participants. In FIGURE 6.3B we show this for two cases. The left plot shows a high variance of the averaged high frequency amplitude. The right plot shows that individual fluctuations of the high frequency amplitude are cancelled out in the average. This leads to a small variance indicating a lack of coupling. To compare across different high frequency bands we normalized the amplitude values by z-scoring. We used the variance to compare the modulation of high frequencies by θ phase across all anatomical regions. Note that a high σ^2 only indicates that at different θ phases the high frequencies differ in amplitude: it does not explain whether the variance of the high frequency amplitudes is accounted for the θ cycle. Therefore, in each high frequency showing a significant variance level we determined the goodness of a cosine fit (F-value). The cosine function (representing the θ cycle) was fitted to the z-scored high frequency amplitude values in each subject. The best cosine fit function minimizes the sum of squares of errors. We termed the test statistic *modulation index* according to (Tort et al., 2009b). However, in our analysis the modulation index (MI) represents an ANOVA and hence, specifies whether more of the variance in the high frequency amplitude (MS_{cos} - explained by the θ cycle) is explained by the variation across the θ cycle or across the participants (MS_{error} - unexplained by the θ cycle). Therefore, we averaged the cosine fit functions across subjects and assessed whether despite averaging more variance of the high frequency amplitude is explained by the θ cycle than the variance across subjects.

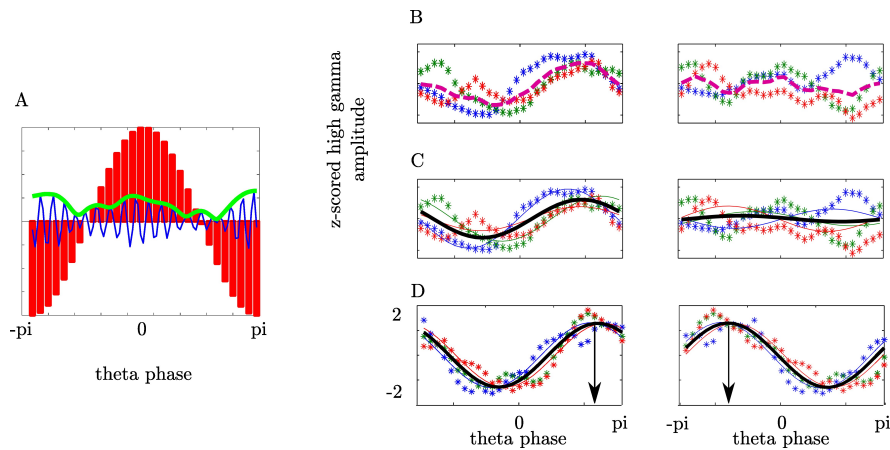


FIGURE 6.3: Phase-amplitude Cross-frequency coupling describes the dependency of high frequency amplitude on phase of low frequency oscillation. A: θ oscillation was separated into 30 phase bins covering the entire cycle ($-\pi$ to π ; red bars). In each bin the magnitude of the high γ analytic amplitude (green line) of the ongoing high γ band (blue line) was calculated. B: Depiction of high γ amplitude as a function of θ phase for three subjects (colored asterisks) in one temporal interval. For each subject the mean high γ amplitude corresponding to each of the θ phase bins was calculated across trials. Afterwards the variance across the mean over subjects (dashed line) was calculated. In the left plot (contralateral NAcc) the variance of the high frequency amplitude across the θ bins is bigger as compared to the variance across subjects for a given bin resulting in an enhanced averaged variance as compared to the ipsilateral NAcc (right plot). C: The variation of high γ amplitude as a function of θ phase was predicted by a cosine function assuming a unimodal dependency of high γ amplitude on the θ phase. A cosine function was fitted to individual high γ amplitudes (solid lines) and pooled across subjects (bold black line). In the left plot a high modulation index results from higher variation across the θ cycle than amplitude differences between subjects. D: PAC defines the θ phase the high γ amplitude is coupled to. Both plots show the same coupling strength however, with different coupling phases. In the left plot the high γ amplitude is coupled to the descending part of the θ cycle whereas in the right plot the coupling phase is the ascending part of the θ cycle.

The variance between the θ phases is given as

$$MS_{cos} = \frac{SS_{cos}}{df_{cos}} \quad (6.3)$$

with SS_{cos} as the sum of squares of high frequency amplitude between θ phases and df_{cos} as the degrees of freedom. The variance within the θ phases is given as

$$MS_{error} = \frac{SS_{error}}{df_{error}} \quad (6.4)$$

with SS_{error} as the sum of squares of high frequency amplitude within θ phases and df_{error} as the degrees of freedom. MS_{error} takes the variability across subjects into account. The MI is given as the ratio between both as

$$MI = \frac{MS_{cos}}{MS_{error}} \quad (6.5)$$

The larger the MI more of the variance in the high frequency amplitude is explained by the variation across the θ cycle than across the participants. In fact this MI is comparable to an ANOVA which directly compares an effect of a condition (here θ cycle) in relation to a random variable (here individual high γ amplitude values) in each factor of the condition (here each single phase bin of the θ cycle). If each subject would show coupling however, with a strong coupling phase angle shift this would result in a low MI. Also strong gamma bursts in one subject and hence not a smooth variation of the HG amplitude across the θ cycle would result in a low MI since the variation across subjects increases compared to the variation across the θ cycle.

Furthermore, PAC is defined not only by the coupling strength but also by the phase of the θ cycle at which the HG amplitude reaches its maximum. In FIGURE 6.3D we show differences in coupling phase with the same coupling strength. Here all subjects show strong coupling since the variation of HG amplitude values in each subject is accounted for the θ cycle. The bold line shows the average of the individual cosine fit functions. Despite averaging across subjects more variance is accounted for the θ cycle than for variance across subjects at each phase. In the left plot HG amplitude is coupled to the descending part of the θ cycle whereas in the right plot the HG amplitude is coupled to the ascending part of the cycle. The coupling phase was estimated by determining the θ phase where the averaged cosine fit function reaches its maximum.

Statistical Test of PAC To estimate the empirical distribution of σ^2 in each temporal interval we calculated the variance of original time series filtered in the high γ range but randomly shifted in time as a function of the original θ phase in 500 randomizations. The 97.5th percentile of this distribution was used as the critical value when appraising the significance of our results. To estimate the empirical distribution of MI in each temporal interval we calculated the MI on the same set of randomizations as used for σ^2 . The 97.5th percentile of this distribution was used as the critical value when appraising the significance of our results.

Functional Relation between PAC and behavioral performance We tested the specific hypothesis that a functional relationship between PAC and cognitive control exists. To this end we assessed the correlation between both RTs and p_e with PAC. In sliding windows of 50 consecutive trials with a step of 2 trials we calculated the grand average of reaction times (1. average of RT over trials, 2. average across subjects) and the p_e . In separate analyses we tested both behavioral measures p_e and RTs for possible correlations with MI and coupling phase.

6.2.9 Preclusion of θ Phase Resetting

In each subject we investigated whether the coupling can be attributed to a resetting of the θ phase. At each time point across trials in each subject we calculated the phase concentration κ of circular data which is the reciprocal to the variance in a normal distribution to exclude the possibility that PAC results from phase realignment of the θ oscillation across trials. A high κ -value indicates a preferred θ phase across trials at a given time point. Statistical significance was assessed by a permutation procedure. In 500 runs the trial-wise time series were shifted in time separately. In each run κ was calculated. The confidence intervals for phase concentration κ were derived from the resulting 500 κ time series.

6.2.10 Specificity of θ -high γ Coupling

We furthermore sought to preclude the possibility that the high frequency amplitude was coupled to the phase of frequencies other than θ . In the 200 ms following the motor response we calculated the variance of amplitude of all high frequency bands in the γ /high γ range (center frequencies: 55-165 Hz, bandwidth: 30 Hz, step size: 2 Hz) as a function of the phase of low frequencies ranging from 3 to 16 Hz (bandwidth: 4 Hz, step size: 1 Hz). Here, we first calculated the high frequency amplitude distribution across the cycle of each low frequency and then averaged the across the subjects as shown in FIGURE 6.3. We then calculated the variance of the averaged high frequency amplitude distribution. The variance would be high if all participants would show a comparable distribution of the high frequency amplitude across the cycle of a given low frequency cycle. In contrast the variance would be low if participants would not show a comparable dependency of the high frequency amplitude on the low frequency cycle.

6.3 Results

6.3.1 Behavioral Results

First, we tested whether the participants performed differently throughout the task (see Methods) indicating differences in cognitive control. We assumed that tracking and responding to an unknown (i.e. block 1), a well-learned (i.e. block 2-3) or an unpredictable sequence (i.e. block 4-5) call for different cognitive control demands. Unknown

and unpredictable sequences demand a high cognitive control since recent patterns cannot be extracted. **Differences in reaction times across blocks (see Table 6.2) were confirmed with an ANOVA ($F_{(5,1074)} = 87.11, p < .0001$; see Figure 6.4A).** Post-hoc paired t-tests confirmed changes in reaction time between blocks. These results were summarized in TABLE 6.3. The relative comparison between blocks show that blocks 2 and 4 show more similar mean RTs than blocks 1 and 4. However, it is of note that blocks 1 and 2 are statistically different as well and even though not statistically significant there is a trend from block 2 to 3 and all the more important from 3 to 4. Therefore, the overall trend across the experiments suggests that there is a course from HCC to LCC during the second and third block to HCC in both random sequence blocks and again to LCC in the self-paced block in terms of reaction times. In sum, we interpret the results in an absolute way (global course across the experiment) given that we recorded behavioral data from (i) non-healthy subjects which participated in (ii) only one block due to the limited recording time. **Furthermore blocks differed with respect to the error frequency p_e which was confirmed with a χ_2 test** (mean p_e per block: .044, .050, .056, .050, .022, $p < .005$, please see TABLE 10.2 for the pairwise comparisons.). FIGURE 6.4B shows the continuous increase of p_e from block 1 (HCC) to block 3 (LCC) and a decrease of p_e from LCC to HCC in block 4 and 5. Note, in the self-paced block 6 no errors could be made and hence p_e could not be calculated.

6.3.2 Amplitude variation

To exclude the possibility that PAC results can solely result from significant amplitude variations in one frequency we compared amplitude variations in a broad range of frequencies ranging from θ to high γ (see Methods) recorded in the contralateral NAcc of epochs aligned to the motor response. **No single t-tests neither for the amplitude variation at each time point nor the test for different evolution with respect to the baseline passed the significance threshold FDR-corrected for multiple comparisons (see FIGURE 6.2).**

6.3.3 High γ amplitude varies as a function of θ phase in the contralateral NAcc

Increase of Variance of High γ amplitude Our general hypothesis was that the high γ amplitude varies as a function of θ phase in the NAcc. We tested the statistical significance of σ_{PAC}^2 in the bilateral NAcc and the bilateral ANT associated both with the numeric stimulus and the response. **We found an increase in σ_{PAC}^2 shortly after the motor response solely in the contralateral NAcc (see Figure 6.5) but not in the ipsilateral NAcc nor in the ANT.** FIGURE 6.6 specifically shows σ_{PAC}^2 and MI for the contralateral NAcc. The increase in the contralateral NAcc was statistically significant, exceeding the 97.5th percentile of our computed distribution of gamma variances σ_{PAC}^2 ($CI_{97.5} = .57$). FIGURE 6.6A).

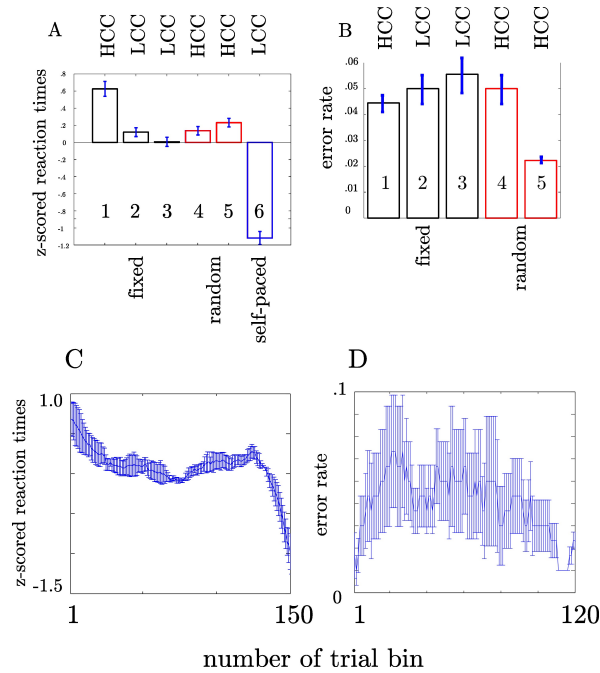


FIGURE 6.4: Depiction of behavioral results. x-axis: sequence type. Numbers within the bars show the number of the block. HCC and LCC above the bars indicate the level of cognitive control necessary to perform the task (HCC - high cognitive control and LCC - low cognitive control) A: Reaction times were pooled across subjects and trials. Each bar encompasses reaction times of 180 trials (1 block). Error bars represent the standard error across trials. The color of the bar indicates the sequence type as in FIGURE 6.1. Trialwise reaction times vary in accordance with sequence type. For more clarity post-hoc differences are summarized in **Table 2**. Participant show increasingly faster response with training the fixed sequence. Following the fixed sequence reaction times are slower during the random sequence. B: Error rates per block pooled across subjects. Error rates are only shown for fixed and random blocks since no error can be calculated for self-paced blocks. C: Depiction of the evolution of RT across the trial bins. The error bars in both plots denote the standard error of the mean. D: Depiction of the evolution of error rate across the trial bins. The error bars in both plots denote the standard error of the mean

High γ amplitude is accounted for the θ cycle By calculating the modulation index (MI) we then tested whether the variance of the high frequency amplitude is accounted for the θ cycle (see FIGURE 6.6A). **As for σ_{PAC}^2 we found an increased MI following the motor response.** The increase in the contralateral NAcc was statistically significant, exceeding the 97.5th percentile of our computed distribution of MI_{random} ($CI_{97.5} = 18$, see FIGURE 6.6A). The increased σ_{PAC}^2 of high γ (100-140 Hz) amplitude in the contralateral NAcc could be accounted for by the θ phase. This coupling was absent for the ipsilateral NAcc and following the stimulus, as well. We assumed that this is a result of different reaction times between subjects ($F_{(2,1077)} = 136.54$, $p < .0001$). We furthermore confirmed that coupling was restricted to the θ -

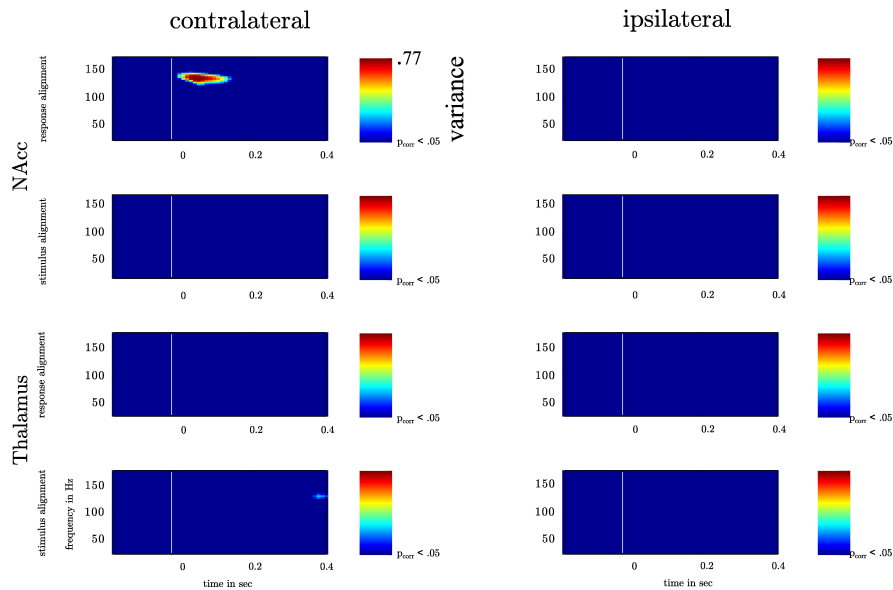


FIGURE 6.5: Depiction of the variation of high γ amplitude across θ cycle for bilateral NAcc and bilateral anterior Thalamus. The recorded time series in the contra- and ipsilateral NAcc and Thalamus were aligned to the motor response or the instructive stimulus. In each frequency band ranging from 25-175 Hz (centerfrequencies) we calculated the variance of high frequency amplitudes across the θ cycle (4-8 Hz) as a function of time. Variance increased significantly solely following the motor response in the contralateral NAcc (p-value corrected for the number of recording sites). Variance values corresponding with a p-value smaller than p_{corr} are depicted color-coded ranging from blue (small variance) to red (high variance).

high γ interaction (see FIGURE 6.10) and that an increase of coupling could be found in each subject (see FIGURE 6.7). The individual coupling patterns all show a different temporal layout following the coupling on the population level. However, only in the temporal interval of coupling on the population level in all subjects the MI tends to increase.

6.3.4 Coupling strength reflects cognitive control

Our second question was whether the MI changes as a function of cognitive control. We tested this for the MI between θ (4-8 Hz) and high γ band (112-142 Hz) since both bands showed the strongest coupling increase collapsed across all trials. **An initial comparison of the MI in HCC versus LCC trialbins (each containing 10 nonoverlapping trials) revealed that MI is significantly greater in HCC trial bins** ($t_{16} = -2.54$; $p = .016$, see FIGURE 6.8). In the next step we tested whether the MI shows a systematic variation as a function of the experimental condition (HCC: block 1, 4 and 5 and LCC: block 2,3 and 6). Therefore, we calculated the MI for the contralateral NAcc for each temporal interval across trial bins. Trial bins contained 50 trials with a step size of 2. Thus, we calculated the MI first for the trials 1 to 50, then for trials 3 to 53, and continued until trial 300 to 349 (see FIGURE 6.9A). Between 0 and

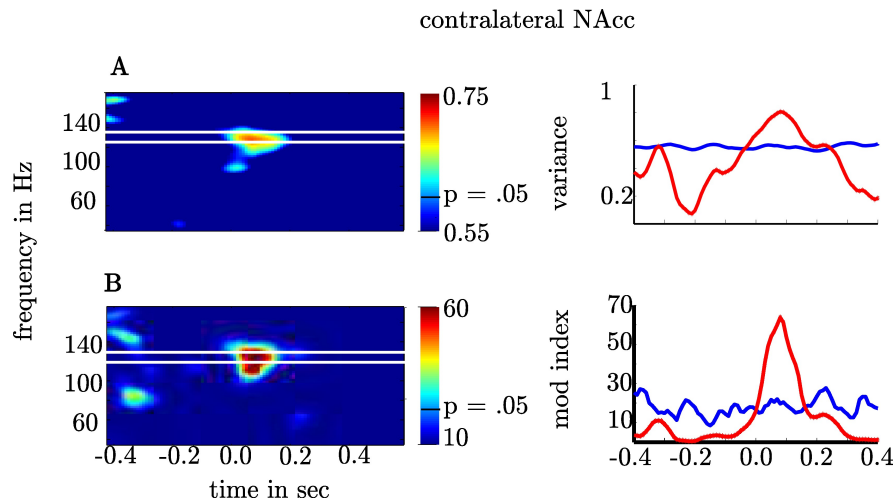


FIGURE 6.6: Depiction of θ -high γ PAC for the contralateral NAcc. A: The first row gives the $\sigma^2_{(H\gamma/\theta)}$ as a function of time (x-axis) and frequency (y-axis). The second row shows the modulation index. The second column shows the frequency band (≈ 100 - 140 Hz; red line) with significant increase of $\sigma^2_{(H\gamma/\theta)}$ and PAC. The blue lines denote 97.5th percentile used as confidence interval of the normal distribution for σ^2 and F-distribution for MI. Note that the variance and the Modulation index exceeded the significance threshold for more than 200 ms and each point is the result of a temporal interval of 166 ms. This means that coupling is present in non-overlapping temporal intervals and hence, extends across several cycles.

200 ms we determined when the maximal MI occurred. **In periods of high cognitive control (HCC) the MI exceeded the statistical significance threshold (see Figure 6.9B). Coupling decreased in the low cognitive control condition (late fixed trial bins and final self-paced movement block).** Importantly, coupling peaks earlier during the LCC sequences (mean coupling time = 90 msec) compared to HCC sequences (mean coupling time = 140 msec, see FIGURE 6.9C; $t_{99} = -8.27$, $p < .1$ - $.12$). The point in time of maximal coupling and MI covaried significantly ($r = .7$; $p < .0001$ see FIGURE 6.9D). Note, that differences in MI cannot be explained by longer RTs since trials were aligned to the motor response.

6.3.5 Functional Relation between PAC and Behavior

MI correlates with error rate A further strong indication for functional relation between PAC and behavior would be provided by a covariation of MI with performance. It is assumed that the NAcc is engaged in action monitoring. We assume that high cognitive control allows for high action monitoring which should result in a low probability of making an error. In contrast low cognitive control should result in a comparatively high probability of making an error. We therefore tested whether the PAC represented by the MI (coupling strength) or the coupling phase predicts the probability of making an error p_e or reaction times. To achieve a continuous measure in the consecutive trial bins containing 50 trials as described above we calculated p_e . Subjects showed on aver-

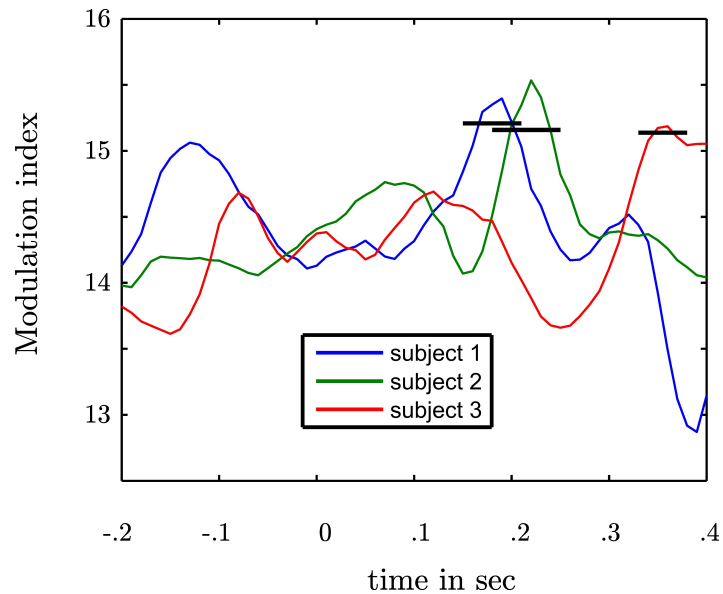


FIGURE 6.7: Depiction of subject specific MIs in the contralateral NAcc following the motor response. Each line represents the modulation index as a function of time of one subject. 0 marks the response time. Following the motor response in each subject an increase of modulation strength is observable. The black bars represent the upper confidence intervals derived from a permutation procedure in each subject. Following the motor response in each subject a statistically significant coupling was found.

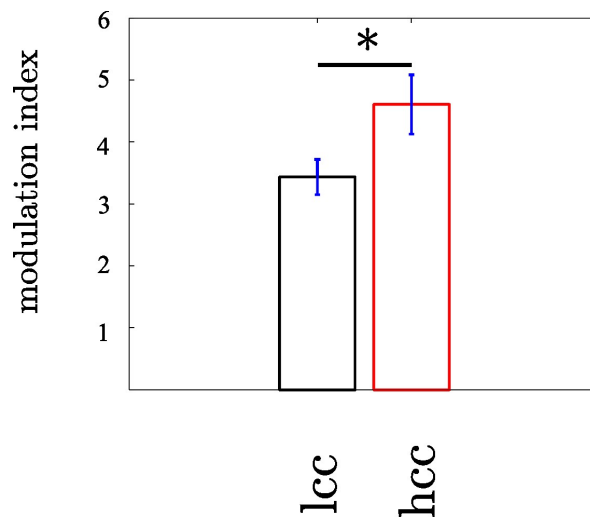


FIGURE 6.8: The modulation of the high γ frequency by the θ phase differs between trials with low (LCC) versus high (HCC) cognitive control ($p < .05$). The modulation index (MI) was calculated in nonoverlapping trial bins of 10 trials. In trial bins containing only trials from the HCC condition the modulation was enhanced compared to trial bins of LCC trials. Error bars denote the standard error across trial bins.

age a reduced p_e at the beginning of the experiment and while performing the random trials where the modulation index was high, which accords with the view that action monitoring is high when subjects first begin to track the fixed sequences and during the random sequences (HCC). **The MI was significantly correlated with p_e ($r = -.21$; $p < .05$).** Additionally, since the trial bins were not statistically independent we determined the significance of Pearson's correlation coefficient r against the distribution of r values calculated from 500 shuffles of trials. We found that the observed r value could not have been derived from a chance distribution ($p = .01$). This indicates a statistical significance. In FIGURE 6.11 we depict this probability p_e averaged across our three subjects (gray curve) together with the MI (blue curve). **In contrast MI did not vary with reaction times in the same trial bins ($r = -.15$; $p > .05$).**

Coupling Phase correlates with Reaction Times. Hasselmo et al. (2002) proposed a model of the functional relevance of the rat hippocampal θ rhythm in which the encoding and retrieval of memory information occur in different phases. He argues that this mechanism is important for the reversal of prior learning. Furthermore, we tested whether the coupling phase varies as a function of cognitive control. In each trial bin we determined the point in time of maximal MI, and evaluated the cosine function which served as the basis for the MI. The θ phase that corresponded with the maximal value of the cosine function representing the peak of the high γ amplitude was taken to be the coupling phase. **We found the coupling phase discriminates between trial bins of HCC and LCC (see Figure 6.11). In trial bins containing fixed trials the mean θ phase is 1.72, while for random trials it is 2.29. A Watson-Williams test for circular data confirmed the significance of this coupling phase difference ($F_{1,99} = 23.6$; $p < .0001$).** Again, since the phase scores of the each trial bins are not statistically independent, we calculated the significance of phase differences against the distribution of F values calculated from 500 shuffles of trials. We found that the observed p value could not have been derived from a chance distribution ($p < .0001$). As for the MI we tested whether the change of phase as a function of cognitive control has a significance for the observed behavior. We used ρ as the correlation coefficient between one circular and one linear random variable. **In contrast to the MI we found the coupling phase is significantly correlated with the reaction times ($\rho = .55$, $p < .001$).** ρ could not have been found within the set of 500 trial shuffles ($p < .001$). **However, the coupling phase did not predict p_e ($\rho = .15$, $p > .05$).**

Note that there is a slight phase angle shift between the subjects. However as revealed by the MI, this phase shift does not influence that more variance is explained by the variation across the theta cycle than between subjects. This is explicitly considered in our MI measure. In trial bins (see paragraph on Functional Relation between PAC and behavioral performance) of high cognitive load (long reaction times and a low error rate as at the beginning of the experiment and during random sequence trials) subjects coupling phase is the same, namely around the trough of the θ oscillation (see FIGURE 6.12B) . In contrast, during phases of low cognitive control (during late trials of the fixed sequence and during self-paced sequence trials) subjects show a great variation of the coupling phase. This is indicated by the greater errorbars during trialbins of

low cognitive control (LCC; see FIGURE 6.12B) In each trial bin we grouped the HG amplitude according to the 30 θ bins for the temporal interval ranging from 0 to 200 ms. We fitted a cosine function to the resulting 30 HG amplitude values. The coupling phase of the θ oscillation was defined as the phase at which the HG amplitude was maximal. This leads to 3 coupling phases one per each subject in each trial bin. To better illustrate the in-phase coupling we collapsed the rising and the falling part of the θ cycle. Therefore, the y-axis in 10B ranges from 0 (θ peak) to $\pm\pi$ (θ trough). The x-axis gives the number of trial bins. The upper plot in 9B shows the average and the standard error (error bar) of coupling phases across subjects for each trial bin. The red line shows the standard error. This line demonstrates that the standard error across subjects is low in trial bins of HCC and high in trial bins of LCC.

6.3.6 θ phase re-alignment

We tested for each subject whether PAC results can be a mere result of theta phase re-alignment. Here, we compared the phase concentration of the θ oscillation with an empirical distribution (see Methods). We did not find a statistically significant phase re-alignment in none of the subjects neither following the stimulus or motor response (see FIGURE 6.13).

6.3.7 Specificity of θ -high γ Coupling

We tested whether coupling between θ and high γ activity exclusively show coupling or whether other frequency combinations also show coupling. **We found the variance of the high frequency bands (≈ 100 -140 Hz) across the phase of the θ (4-8Hz) band was higher than any other frequency combination** (see FIGURE 6.10). This yields a comparable narrow frequency interaction as found by (Tort et al., 2008).

6.4 Discussion of DBS Results

6.4.1 Summary of Results

We investigated the dynamics of phase-amplitude cross-frequency coupling in the human Nucleus accumbens and show, that in the NAcc contralateral to a movement the θ phase modulates the high γ amplitude (≈ 100 -140 Hz) following a motor response. Importantly, this previously undescribed oscillatory pattern in the human NAcc increases with cognitive control and predicts behavioral adaptation as reflected in the reduction in error rates. Compared to reaction times the error rates show a more sluggish change which may explain the resemblance of the error rate if averaged across blocks. This means that changes in terms of RTs are more closely confined to the definition of blocks while the error rate changes with a greater time lag. However, the temporally resolved course revealed strong changes during the course of the experiment. We observed the

strongest PAC in the first part of a task in which subjects responded to an unfamiliar fixed order stimulus sequence, and during responses to stimuli presented in a random order that required high load of cognitive control. In contrast, in periods with low cognitive control demands, i.e. when subjects responded to already learned stimulus sequences and during self-paced sequences, PAC was reduced. This pattern of response locked PAC cannot be accounted for reaction time differences since analyzed epochs were locked to the subject's responses, and no PAC was observed when epochs were locked the stimulus presentations. Hence, coupling takes place in the temporal interval following a decision. This pattern is consistent with coupling patterns observed in rats by Tort et al. (2008). These investigators found enhanced coupling between θ and high γ (80-120 Hz) within and between the striatum and the hippocampus. Coupling was strongest in epochs where a decision had to be made and thus were related to cognitive demands. Tort et al. (2008) hypothesized that PAC is a mechanism coordinating striatal and hippocampal learning circuits. As mentioned above, the hippocampus is strongly connected with the NAcc and a selective strengthening of this connection is assumed to be important for rapid facilitation of goal-directed behavior (Goto and Grace, 2005). The result that PAC decreases with learning indicates that PAC is related with the facilitated goal-directed behavior as proposed by Goto and Grace (2005). That PAC occurs whenever a high level of cognitive control has to be applied supports the notion that PAC qualifies for facilitation. Thus, our data indicate that PAC can be a mechanism of information integration since it occurs during high cognitive control supporting the hypothesis that PAC provides an effective mechanism to recruit local networks from functional related global networks to gate information (Buzsáki and Draguhn, 2004; Canolty et al., 2006).

6.4.2 Interplay of Frequencies for integration of information

It is assumed that the control of motor behavior in NAcc is accompanied by release of dopamine (Wilson, 1983). Münte et al. (2007) found the human NAcc involved in error-related modulation which preceded scalp error-related negativity (ERN). On a behavioral level NAcc activity inhibits specific conditioned motor behavior (Wilson, 1983). In the present study the patients probability of making errors systematically varies during the course of the experiment. This variation matches with the course from HCC to LCC to HCC and again to LCC. We hypothesize that the variation of making errors signals a change in motor behavior and hence points to adaptation to the external demands as a result of learning. The error probability was especially low at the start of the experiment and during the random sequence task. The PAC in the contralateral human NAcc correlates with this change, which suggests that theta/high gamma coupling strength might be related with adaptation of behavior in later trials. This gains support by the PAC modulation occurring in early trials followed by behavioral adaptation. Once adapted in terms of reaction times and error rate no PAC modulation takes place. Thus, we speculate that the control for a specific action or motor routine as during an unknown or random sequence can be provided by enhanced coupling of θ -high γ oscillations in the NAcc. This increased coupling becomes important when a subject has to switch from a previously established and automatized motor

routine to an unpredictable motor sequence. In contrast, a reduction in coupling, as observed during the tracking of the learned sequence, might facilitate automatization. In our study enhanced action monitoring is especially important during learning of the fixed sequence and during the random sequence, since automatic behavior has to be interrupted. To achieve this, the NAcc has to integrate information between different cerebral units. This could be the information necessary to control the gating into the motor system from the limbic system and the prefrontal cortex (Mogenson et al., 1980). The NAcc neuronal activity is mutual depend on hippocampal input (O'Donnell and Grace, 1995) as well as PFC activity (French and Totterdell, 2002). Thus, the complex connections with limbic, prefrontal and motor structures make the NAcc an ideal site for the integration of information which is supported by the phase-amplitude cross-frequency coupling mechanism.

6.4.3 PAC is strongest following a decision

Tort et al. (2008) reports that in the rat's striatum and hippocampus PAC was strongest during the decision phase while rats navigated through a maze. In contrast, in our experiment the period of movement was short because there was only a single button press. This can explain differences in the timing of PAC patterns. In the present study, PAC shortly after the decision was made and correlated with the probability of making an error, suggesting that changes in response selection based relative to past experiences calls for the coordination of information carried by different frequencies. Based on our results, we propose that the human NAcc signals the unpredictability of a future external event to which a response will have to be given, thereby indicating the necessity of stopping an automated response. This is accomplished by integrating information in the θ and high γ band. In support of this contention (Berns et al., 2001) found the reward system and especially the human NAcc is responsive to different levels of predictability. In particular, the NAcc was more active during an unpredictable sequence, in line with our finding that PAC was elevated at the beginning of learning and during the tracking of the random sequence. Further, Poldrack et al. (2005) found differences in activity in the striatum, especially in the putamen and the nucleus caudatus adjacent to the NAcc, for automated vs. unfamiliar motor behaviors. The increased coupling following a decision under a condition of high cognitive control might represent a type of associative memory which combines information about events (button press) and the context (stimulus presentation) (Tort et al., 2009b). Here one can imagine that the association which is acquired more easily under higher cognitive control provides the subject with the possibility to respond faster. Furthermore, we observed two patterns of the course of coupling. In the first coupling decreased during fixed trials and in the second coupling increased during random trials and both differ with respect to the predictability of the upcoming event and hence which finger to move. This says that during fixed trials the subjects are informed based on the memory of past trials which finger is to move and hence the finger movement options are limited to one finger. In contrast in the random trials the subject has to hold up three finger movement options (3 since 4 different stimuli are presented with the constraint that no stimulus was consecutively repeated twice). This might also explain why PAC

increases constantly during random trials. Alternatively, this pattern can be a result of the monitoring of the recent action which is underscored by the temporal relation. This interpretation is supported by the involvement of the human NAcc in action monitoring – the error detection and correction (Münte et al., 2007). The correlation of the modulation strength with the error rate indicates that NAcc activity is involved in action monitoring. Action monitoring in turn involves a comparison between the representations of an appropriate response and the response actually made (Scheffers and Coles, 2000). These diverge if a response error was committed. Error monitoring is accompanied by prominent scalp potentials (Nieuwenhuis et al., 2001) and the activity in the NAcc is involved in error-related modulations (Münte et al., 2007). The authors have shown that the early surface potential which indicated the error detection was preceded by NAcc activity. Accordingly, activity in the NAcc should contribute to ERN when the error rate is high. Moreover, the NAcc activity involved in error detection should occur earlier than the PAC modulation since the error signal on the scalp level is evoked around 100 ms and is delayed by the NAcc by about 40ms (Münte2007). Importantly, PAC modulation occurs when the error rate is small. This makes the PAC a complementary event to the error-related modulation. We speculate that PAC modulation occurs when the comparison process between the appropriate and the actual response revealed that no error was made. Therefore, PAC could be the signal involved in confirmation of the correct response which facilitates goal-directed behavior in later trials. Due to the vicinity to the motor response one could argue that PAC is a mere mechanical artifact, however coupling is observed only in one region and shows a tight functional correlation with behavioral measures. Furthermore, in case of an artificial result we expected coupling to be represented across a broad band of low coupling and high coupled frequencies. However, coupling was restricted to the θ – high γ range. Hence, we precluded PAC to be a result of an artifact as a possible explanation. Based on this, we speculate that PAC in the NAcc signals a deviation from expectancy: a negative reinforcement that implies the need to stop an automated motor routine in which learned responses are pre-activated to reduce reaction times.

6.4.4 Differences in coupling phase

During the course of the experiment the coupling phase of θ oscillations varied systematically, with coupling close to the θ trough during early learning and tracking the random sequence (high cognitive control), and coupling to the descending part of the θ cycle during tracking a well-learned fixed sequence (low cognitive control). A comparable result was found in a study conducted by Belluscio et al. (2012). In this study high γ activity (90-150 Hz) peaked near the θ trough during running but was coupled to the peak of the θ oscillations during REM-sleep. The authors hypothesized that modulation of the high γ band by the θ band is state dependent. Here, we show that coupling in the human NAcc is also state dependent. The average coupling phase varies as a function of cognitive control applied by the subjects and parallels the results of Belluscio et al. (2012). This strengthens our hypothesis that PAC might provides a mechanism to integrate information. Hasselmo et al. (2002) highlight the functional importance of different phases in the θ cycle for memory with the descending phase nec-

essary for retrieval of memory and the trough for encoding of new information. They state that encoding of new information is facilitated if θ activity shifts in phase to accelerate the process of encoding. In our study when new information has to be encoded and the motor response has to be adjusted due to the new environmental requirements we observe strong coupling of the high γ activity to the θ trough. This epochs in which new information has to be encoded are the trials in the early part of the fixed sequence and the random sequence which differ from the trials late in the fixed sequence with respect to the possibility of memory retrieval. Retrieval is only possible when the fixed sequence has been learned distinguishing between the two distinct cognitive states.

6.4.5 Conclusion

Together these results show that motor learning is accompanied by a complex interplay of θ and high γ activity. In the NAcc contralateral to the performing hand the coupling of these frequencies varies systematically with the experimental conditions which allowed the participants to perform differently.

Patient	block # 1	block # 2	block # 3	block # 4	block # 5	block # 6
1	1,027 (301)	1,090 (261)	1,077 (255)	1,108 (284)	1,057 (212)	645 (395)
z-score	.079 (.934)	.268 (.786)	.229 (.769)	.323 (.858)	.170 (.640)	-1.071 (1.191)
2	881 (214)	658 (106)	628 (146)	639 (122)	721 (180)	210 (182)
z-score	.991 (.823)	.135 (.407)	.022 (.562)	.063 (.469)	.377 (.692)	-1.588 (.700)
3	814 (290)	642 (158)	604 (148)	655 (116)	680 (135)	510 (191)
z-score	.804 (1.431)	-.045 (.782)	-.230 (.733)	.022 (.574)	.143 (.667)	-.695 (.943)

TABLE 6.1: shows the mean reaction times and standard deviations of reaction times for each subject and block. Each value encompasses 60 trials. Since subjects differ in their reaction times (see Results) we z-scored the reaction times across all trials for each subject. This means that individual RTs were transferred into standard values by z-transformation individually for each subject. The second row of each patient shows the mean (std) of the z-scored reaction times. The subjects showed a different evolution of RTs across the experiment. But this concomitant in each group analysis – that individual subjects show only a trend which resembles the result of the group analysis or may slightly deviate from the trend in the group – does not challenge the statement resulting from the ANOVA for a group of participants. Even though we could only dispose of a very small group the trend of behavioral changes in terms of RTs remains.

Patient	block # 1	block # 2	block # 3	block # 4	block # 5
1	4	6	7	5	1
2	1	1	2	4	1
3	3	2	1	0	2

TABLE 6.2: shows the number of errors for each subject and block.

comparison	t-value	p-value
1-2	5.03	< .0001
1-3	6.09	<.0001
1-4	4.91	<.0001
1-5	3.96	<.0001
1-6	15.09	<.0001
2-3	1.52	.13
2-4	-.22	.82
2-5	-1.54	.12
2-6	13.41	<.0001
3-4	-1.8	.06
3-5	-3.05	.002
3-6	12.04	<.0001
4-5	-1.33	.19
4-6	13.73	<.0001
5-6	14.72	<.0001

TABLE 6.3: The left column shows which blocks were tested. The middle column gives the t-value for significance of mean differences and the right column the corresponding p-value.

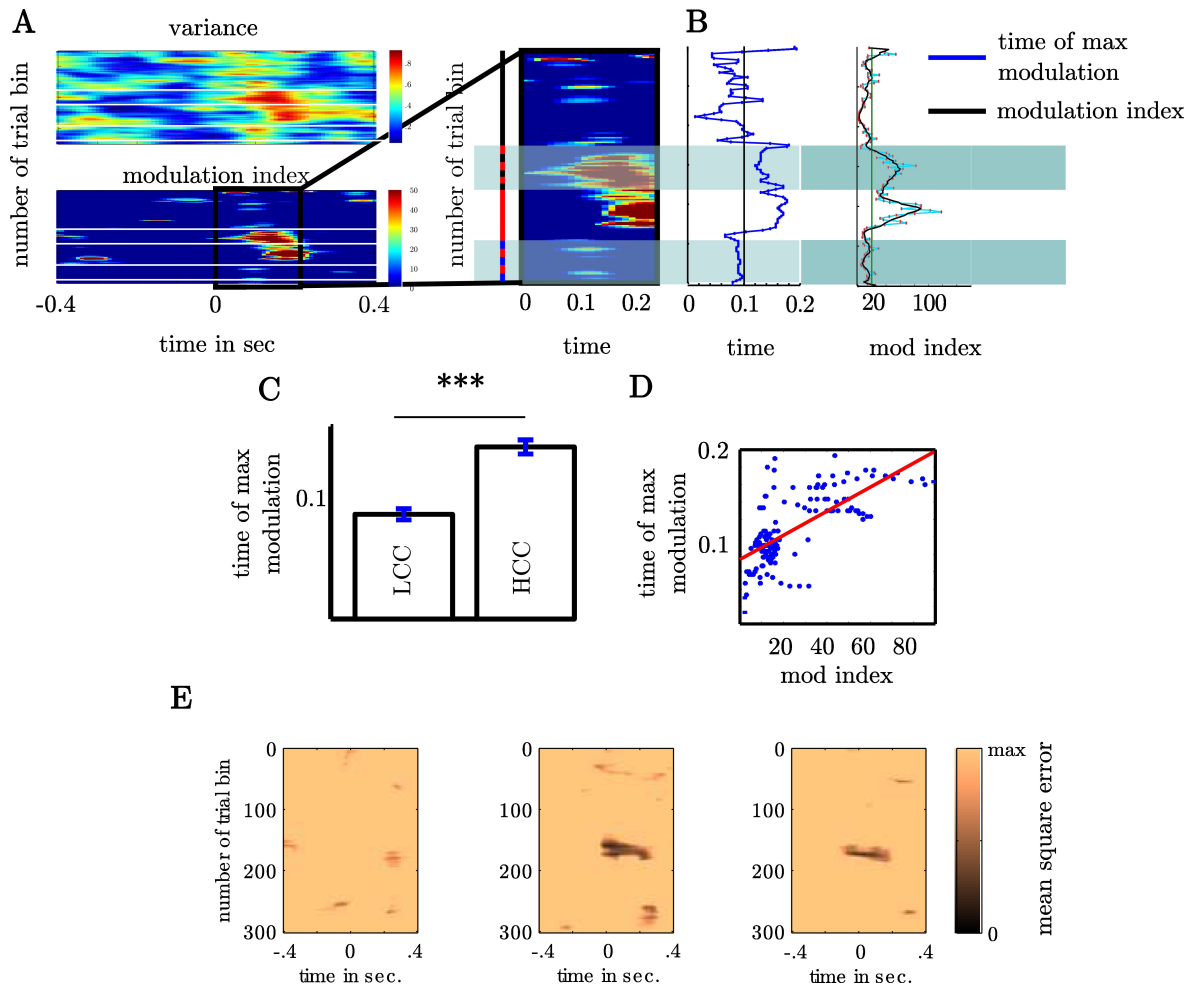


FIGURE 6.9: Coupling strength varies with sequence type A: Variance of high γ as a function of θ phase (upper plot) and modulation of high γ by θ phase (lower plot). Both plots show the variance and the modulation as a function of time (x-axis) and trial bin (y-axis). Trial bins are arranged from top to bottom. Both show that across subjects coupling is elevated at the beginning of the fixed and during the random trials. For consecutive trialbins each containing 50 trials we calculated the modulation index. Following the motor response the MI varied with sequence type. The sequence type is indicated by the colored bar left to the magnification: black corresponds to fixed, red to random and blue to self paced trials. The alternating red-black bar denotes those trialbins containing both fixed and random trials. Note that including only a small proportion of random trials elevates the modulation index. Alternating blue-black bar denotes those trialbins containing both random and self-paced trials. B: Depiction of points in time at which modulation peaks for trialbins. The right panel shows the dependency of maximal modulation index on trial bin in the 0 to 200 ms interval (see Figure 6.5 right column) following the motor response. C: In fixed trials coupling is earlier then in random trials. Only trial bins containing either fixed or random trials were used in this analysis. D: Time of coupling between θ and high γ depends on coupling strength. E: shows the individual summed square errors of each subject from the mutual cosine fit function as a function of trial bin. The greater error of subject 1 does not mean that this subject does not exhibit a sine shaped dependency of the high gamma activity as shown in FIGURE 6.3C. As the blue line deviates more strongly from the black bold line compared to the red and green line the summed mean error is greater than for subjects 2 and 3. However, it shows a clear sine shaped dependency. This means that subject 1 either contributes less to the strength of the MI or probably attenuates the MI but this does not challenge the visual impression that the high gamma amplitude is coupled to a resembling phase as subject 2 and 3.

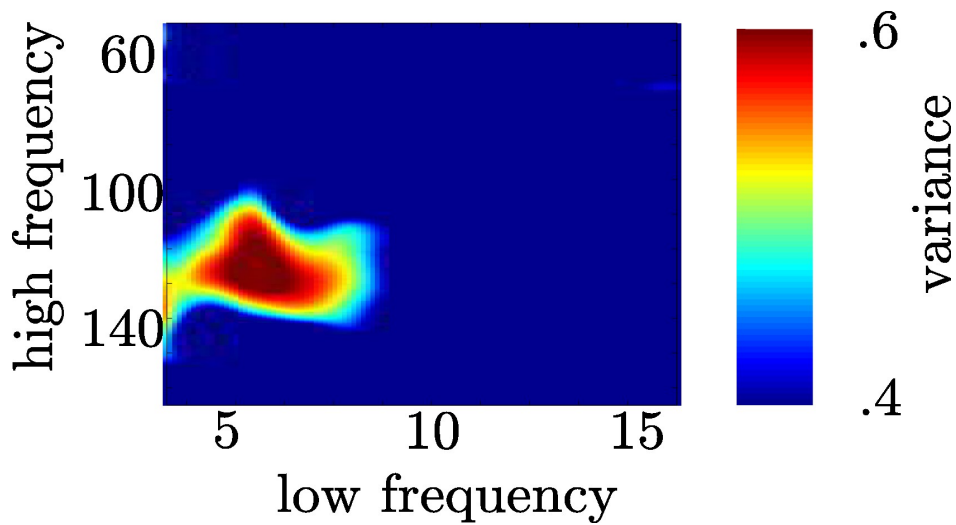


FIGURE 6.10: Coupling following the motor response is restricted to the θ and high γ range. In the time range between 0 and 200 ms (see A right column) we calculated coupling strength between narrow high frequency bands (centerfrequencies: 50 to 180 Hz, bandwidth: 30Hz, step size: 2Hz) and narrow low frequency bands (centerfrequencies: 3 to 16 Hz, bandwidth: 4Hz, step size: 1Hz)

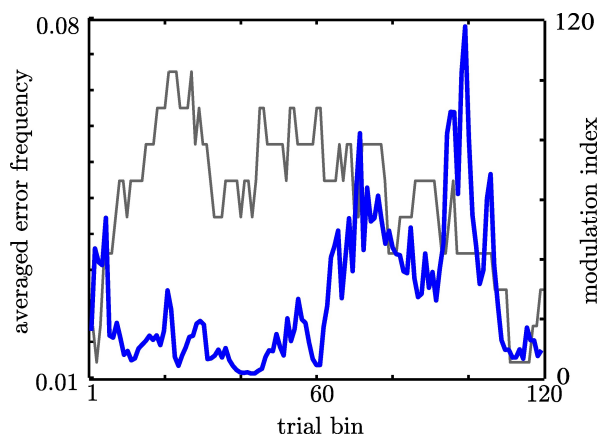


FIGURE 6.11: Coupling strength predicts the probability to make an error as indicated by the correlation analysis. Here we depict both correlated measures to illustrate the resembling course over time. The gray line gives the probability to make an error across subjects. The blue line shows the Modulation Index.

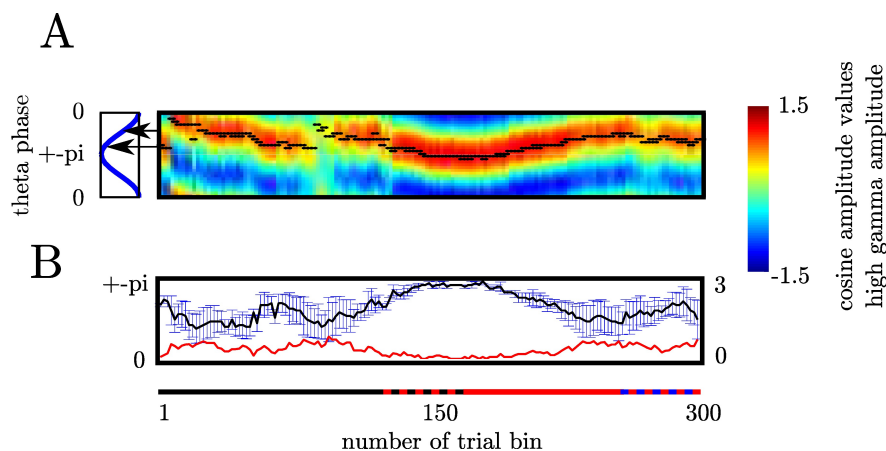


FIGURE 6.12: A: Cognitive demands in different sequence types are reflected by difference in coupling phase. In each trialbin we determined the modulating phase of the θ cycle. Black dots denote the phase the high γ amplitude is coupled to for each trial bin. The sequence type is indicated by the colored line: black corresponds to fixed, red to random and blue to self paced trials. The alternating red-black line denotes those trial-bins containing both fixed and random trials. Alternating blue-black line denotes those trial-bins containing both random and self-paced trials. Phase differences were investigated comparing trials bins containing exclusively fixed and random trials, respectively (solid black and solid red intervals). Black arrows mark the mean θ phase. Coupling phases differ significantly between fixed and random trial bins. Please note that at the beginning of the entire experiment, when the sequence to be learned is unknown high γ amplitude peaks at the same frequency as during the unpredictable random sequence. B: During high cognitive load HG amplitude is coupled to the θ trough across subjects while during low cognitive load the coupling phase is different across subjects as indicated by the greater errorbars during trialbins of low cognitive control (LCC). In each trial bin we grouped the HG amplitude according to the 30 θ bins for the temporal interval ranging from 0 to 200 ms. We fitted a cosine function to the resulting 30 HG amplitude values. The coupling phase of the θ oscillation was defined as the phase at which the HG amplitude was maximal. This leads to 3 coupling phases one per each subject in each trial bin. To better illustrate the in-phase coupling we collapsed the rising and the falling part of the θ cycle. Therefore, the y-axis ranges from 0 (θ peak) to $\pm\pi$ (θ trough). The x-axis gives the number of trial bins. The upper plot in 9B shows the average and the standard error (error bar) of coupling phases across subjects for each trial bin. To better visualize this dependency of the SEM on the cognitive control we inserted the course of SEM over trial bins (red line) shows the standard error. This line demonstrates that the standard error across subjects is low in trial bins of HCC and high in trial bins of LCC.

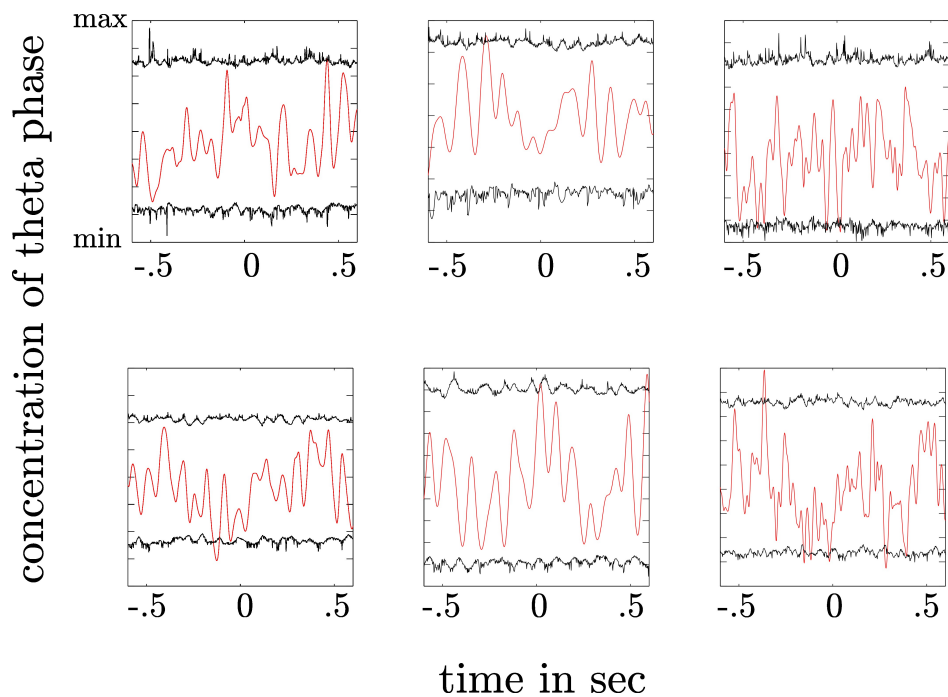


FIGURE 6.13: Depiction of theta phase concentration as a function of time (red line) together with the confidence intervals derived from a permutation procedure (black lines). The upper plot shows the concentration parameter κ as a function of time for trials aligned to the stimulus. The lower plot shows the same for trials aligned to the response. High concentration values would indicate a preferred θ phase across trials at a given time point. Concentration values exceeding the upper confidence interval would indicate a statistically significant alignment of the θ phase across trials. In both plots no significant θ phase alignment can be observed.

7 Summary and General Discussion

This thesis encompasses three different parts all dealing with behavioral improvement of performance in finger movement tasks in human subjects. Across a set of recording techniques (ECoG, MEG and DBS) and cortical and subcortical structures the role of paCFC in the human brain during the process of motor learning and adaptation was investigated. Even though a great deal of research gathered evidence that paCFC exists in the rodent, primates and also the human brain and this might be associated with the formation of memory, a direct link has not been established yet. Hence, the phenomenon of paCFC in the human cortex is still under debate also due to implications derived from the report of Canolty et al. (2006). With a wide range of tasks investigated and a huge fraction of covered cortical areas, paCFC did not appear to occur in specific brain areas (Jensen and Colgin, 2007). Overall, within this thesis it was aimed at finding specific effects of paCFC under the hypothesis that the occurrence of paCFC indeed is linked to the process of improvement of motor performance. Motor learning experiments appeared to be a uniquely interesting tool since behavioral improvement occurs gradually during an early learning phase. Finding a comparable rapid change of paCFC with time-discrete recordings would underscore the link with human behavior and the flexibility necessary to form memory. Cortical sites linked with motor learning and execution are known making it easy to test whether changes of paCFC can be first, localized at all and second, localized in the known motor learning/execution framework (Grafton et al., 1992).

7.1 Summary of the experimental results

In the first experimental CHAPTER 4 it was investigated whether paCFC and performance measures show similar temporal patterns of evolution during early learning. The motivation for this study was twofold. The intention was to establish an experimentally supported link between the phenomenon of phase-amplitude Cross-Frequency Coupling and the process of performance improvement. Since especially in motor learning subjects show a very fast and continuous change of improving performance temporal fluctuations of paCFC can be related via correlation measure.

paCFC occurred in each subject which underscores the assumption of a general phenomenon in the human brain. Relying on this result whether paCFC indeed tracks the formation of motor memory was investigated. In the first analysis robust effects were found which were clearly visible if the coupling measure was averaged across the entire grid neglecting spatial information. Interestingly, paCFC evolution across time showed an almost identical course over time as the improvement of performance. This effect remained stable if temporal and spatial information – trial-by-trial analysis in

anatomical defined regions of interest – was taken into account. Methodologically this means that the effect obtained in the grand average is not only due to extensive noise reduction, but deals with a process accompanying motor learning. Functionally, this indicates that execution and learning related networks (Grafton et al., 1992) show changes of paCFC tightly associated with learning on a fast temporal scale. The fact that significant channels were determined by a permutation test by shifting the time series shows that the temporal structure of both frequency bands to one another is important in motor execution/learning related brain sites. The prediction is not possible if the temporal dependency is distorted and hence, coupling is dissolved. Furthermore, this analysis extended the term cross-frequency coupling by another important aspect. Across the low frequency θ cycle the high γ amplitude varies and additionally and most importantly, the prediction of behavioral changes varies. This could indicate that different phase carry discriminative information as claimed by model data in study of Hasselmo et al. (2002) and could imply direct evidence for the functional relevance of cross-frequency coupling.

In the second experimental CHAPTER 5 the question was tackled whether such fine-grained and systematic changes of paCFC can be found with a non-invasive recording technique. The answer strongly depended on the type of measure the non-invasive recording technique uses. With EEG-recordings the findings could not be replicated whereas MEG-recordings, less prone to the filtering due to the skull, showed a comparable localization of learning related changes of paCFC. At this point one has to say that the difference of results between EEG and MEG can be also a mere result of the difference in density of electrode/sensor coverage. The disadvantageous possibility of localizing cortical sources in EEG can be deteriorated by scarce number of electrodes. Hence, a general statement about the detectability of paCFC changes with EEG cannot be made.

On the other hand systematic changes of paCFC in the (pre-)motor and the right prefrontal cortex are manifested in the MEG-recordings. Even though, a source localization approach was not carried out it is assumed that both clusters are a result of the activity in the (pre-)motor and the right prefrontal cortex since the activity picked up by the MEG reflects underlying cortical activity. When contrasting the information transfer as formalized by the Granger Causality approach it was shown that the prefrontal cortex mainly sends information to the (pre-)motor cortex. This directionality could imply that indeed the prefrontal cortex drives the motor cortex or at least sends information about the stimulus-response mapping which is necessary for the execution of the task. This information is preferentially transported in the high γ range. Importantly, this indicates that the mechanism paCFC operates to integrate information across a wide spatial scale.

Hence, it was assumed that routing of information can be realized not exclusively across the cortex. Most probably, information transfer can be mediated by subcortical structures as shown in CHAPTER 6. As hypothesized the NAcc shows paCFC. This coupling effect is strongly limited in three dimensions. First, coupling is elicited by the motor response (temporal dimension). Second, coupling frequencies are located in

the θ and high γ range (frequency dimension). Third, only the contralateral NAcc – not the ipsilateral nor the bilateral parts of the anterior thalamus – is the anatomical region where coupling takes place (anatomical dimension). In this region the paCFC shows systematic nonstationarities since fluctuations predict the cognitive load applied by the subject. All these results classify the mechanism of paCFC as a necessary phenomenon in the human brain and contradicts a notion that paCFC might be a pure epiphenomenon.

The results gathered in the experiments demonstrate that paCFC is strongly involved in the process of motor performance improvement. Here, a temporally resolved course of paCFC was characterized which resembles strongly the improving performance. Other studies also pointed to the importance of cross-frequency coupling for memory processes. Axmacher et al. (2010b) showed that the hippocampus, a key structure for the formation of memory, shows that paCFC accompanies the maintenance of multiple items in working memory. The fact that the coupling frequency changes systematically with the number of items to be hold in working memory suggests that paCFC shows a flexible adaptation to the environmental demands. As mentioned in SECTION 2.2 studies show that both seem to assume different tasks in the process of motor learning and memory formation.

7.2 Perspectives for future research

In this project the intention was to disentangle the role of paCFC as a mechanism underlying the processes of learning and memory formation in the human brain. However, since these studies cannot depict all aspects of paCFC exhaustively there remain questions important to be answered in future research projects.

Event-related paCFC The first question is a more analytic question about the temporal evolution of paCFC on a fast scale. It can be asked whether paCFC is indeed a transient phenomenon and locked to an experimental event. The preliminar results in a new study show a strong event-related coupling in the subdural recordings with a strong increase of coupling following both the instructive stimulus and the motor response eliciting coupling in adjacent prefrontal and motor areas, respectively.

θ phase locking In the field of Cross-Frequency Coupling the temporal layout of the occurrence of coupling between different frequency bands is investigated. However, it should be kept in mind that the functional role of single frequency bands is still a matter of debate. For example, research on oscillatory dynamics in the mammalian brain attributes a crucial role in the organization of neuronal ensembles to θ oscillation (Kahana et al., 1999; Canolty et al., 2006; Lisman, 2010; Jensen and Colgin, 2007). Theta oscillations are specifically related to the temporal firing patterns of single units (Siapas et al., 2005) and it is assumed that θ provides a reference frame for a neuronal code in which different spatial information is represented at different phases of the θ cycle. These studies suggest that the phase of θ activity is important for controlling the neuronal dynamics necessary to accomplish specific cognitive tasks. However, most

of the studies on task-dependent θ oscillations focus on the power changes during cognitive tasks (Raghavachari et al., 2001, 2006; Kahana et al., 1999). Only a few studies (Sarnthein et al., 1998; Raghavachari et al., 2006) relate human memory function to macroscopic connections via shared phase information. These studies made use of signal coherence between topographically dispersed brain areas. However, this measure makes it difficult to distinguish between phase from amplitude information. Hence, the direct test that human cortical theta phase information changes task-specifically as the basis for organizing neuronal ensembles remains to be tested. Since, theta activity has been associated with motor performance (Caplan et al., 2003; Tombini et al., 2009; Gentili et al., 2011) and memory processes (Klimesch et al., 1994, 1996, 1997; Klimesch, 1999; Klimesch et al., 2001; Kahana et al., 2001; Raghavachari et al., 2001, 2006; Jensen and Tesche, 2002; Caplan et al., 2003; Osipova et al., 2006) we investigated theta phase and amplitude variation in a motor learning task. In this study we used the same serial response time task as explained in the CHAPTERS 4, 5 and 6 in which the participants had to track and respond to a sequence of numeric stimuli. Our results show that θ phaselocking between MEG sensors decreases following unpredictable stimuli as compared to predictable stimuli.

Multisensory Integration In the experiments presented here we used motor learning tasks to test the hypothesis of involved paCFC changes during motor performance improvement. But as outlined in the INTRODUCTION human beings are potentially adept in acquiring very complex tasks as playing piano. Here, the piano player is required to integrate motor and auditory information to successfully perform a concerto in a complex way which requires the timing of several hierarchically organized actions (Zatorre et al., 2007). This makes tasks as the auditory-motor task (see CHAPTER 4) an ideal tool to investigate paCFC in the context of multisensory integration. In a larger group of healthy subjects psychometric functions can be estimated which show the capability of subjects to press a button precisely in between two auditory stimuli as a function of the temporal interval of two auditory stimuli. The behavioral performance represented by the psychometric function can then be related to paCFC which could show whether coupling between oscillations of different frequency bands supports multisensory integration.

Bibliography

- Allan, K., Dolan, R. J., Fletcher, P. C., and Rugg, M. D. (2000). The role of the right anterior prefrontal cortex in episodic retrieval. *Neuroimage*, 11(3):217–227.
- Allen, E. A., Liu, J., Kiehl, K. A., Gelernter, J., Pearlson, G. D., Perrone-Bizzozero, N. I., and Calhoun, V. D. (2011). Components of cross-frequency modulation in health and disease. *Front Syst Neurosci*, 5:59.
- Aron, A. R. (2010). From Reactive to Proactive and Selective Control: Developing a Richer Model for Stopping Inappropriate Responses. *Biol Psychiatry*.
- Axmacher, N., Cohen, M. X., Fell, J., Haupt, S., Dimpelmann, M., Elger, C. E., Schlaepfer, T. E., Lenartz, D., Sturm, V., and Ranganath, C. (2010a). Intracranial EEG correlates of expectancy and memory formation in the human hippocampus and nucleus accumbens. *Neuron*, 65(4):541–549.
- Axmacher, N., Henseler, M. M., Jensen, O., Weinreich, I., Elger, C. E., and Fell, J. (2010b). Cross-frequency coupling supports multi-item working memory in the human hippocampus. *Proc Natl Acad Sci U S A*, 107(7):3228–3233.
- Ball, T., Demandt, E., Mutschler, I., Neitzel, E., Mehring, C., Vogt, K., Aertsen, A., and Schulze-Bonhage, A. (2008). Movement related activity in the high gamma range of the human EEG. *Neuroimage*, 41(2):302–310.
- Bangert, M., Peschel, T., Schlaug, G., Rotte, M., Drescher, D., Hinrichs, H., Heinze, H.-J., and Altenmüller, E. (2006). Shared networks for auditory and motor processing in professional pianists: evidence from fMRI conjunction. *Neuroimage*, 30(3):917–926.
- Barcelo, F., Escera, C., Corral, M. J., and Periez, J. A. (2006). Task switching and novelty processing activate a common neural network for cognitive control. *J Cogn Neurosci*, 18(10):1734–1748.
- Belluscio, M. A., Mizuseki, K., Schmidt, R., Kempster, R., and Buzsáki, G. (2012). Cross-frequency phase-phase coupling between θ and γ oscillations in the hippocampus. *J Neurosci*, 32(2):423–435.
- Belujon, P. and Grace, A. A. (2008). Critical role of the prefrontal cortex in the regulation of hippocampus-accumbens information flow. *J Neurosci*, 28(39):9797–9805.
- Berger, H. (1929). Über das Elektrenkephalogramm des Menschen. *Archiv fr Psychiatrie*, 87:527–570.

Bibliography

- Berns, G. S., McClure, S. M., Pagnoni, G., and Montague, P. R. (2001). Predictability modulates human brain response to reward. *J Neurosci*, 21(8):2793–2798.
- Bewernick, B. H., Hurlmann, R., Matusch, A., Kayser, S., Grubert, C., Hadrysiewicz, B., Axmacher, N., Lemke, M., Cooper-Mahkorn, D., Cohen, M. X., Brockmann, H., Lenartz, D., Sturm, V., and Schlaepfer, T. E. (2010). Nucleus accumbens deep brain stimulation decreases ratings of depression and anxiety in treatment-resistant depression. *Biol Psychiatry*, 67(2):110–116.
- Blakemore, S. J., Frith, C. D., and Wolpert, D. M. (2001). The cerebellum is involved in predicting the sensory consequences of action. *Neuroreport*, 12(9):1879–1884.
- Blumenfeld, R. S. and Ranganath, C. (2007). Prefrontal cortex and long-term memory encoding: an integrative review of findings from neuropsychology and neuroimaging. *Neuroscientist*, 13(3):280–291.
- Bosma, I., Reijneveld, J. C., Klein, M., Douw, L., van Dijk, B. W., Heimans, J. J., and Stam, C. J. (2009). Disturbed functional brain networks and neurocognitive function in low-grade glioma patients: a graph theoretical analysis of resting-state MEG. *Nonlinear Biomed Phys*, 3(1):9.
- Brashers-Krug, T., Shadmehr, R., and Bizzi, E. (1996). Consolidation in human motor memory. *Nature*, 382(6588):252–255.
- Brovelli, A., Lachaux, J.-P., Kahane, P., and Boussaoud, D. (2005). High gamma frequency oscillatory activity dissociates attention from intention in the human pre-motor cortex. *Neuroimage*, 28(1):154–164.
- Burns, S. P., Xing, D., and Shapley, R. M. (2011). Is gamma-band activity in the local field potential of V1 cortex a "clock" or filtered noise? *J Neurosci*, 31(26):9658–9664.
- Busch, N. A. (2005). *Interaction of bottom-up and top-down processes in human evoked gamma-band activity*. PhD thesis, Otto-von-Guericke University Magdeburg.
- Busch, N. A., Dubois, J., and VanRullen, R. (2009). The phase of ongoing EEG oscillations predicts visual perception. *J Neurosci*, 29(24):7869–7876.
- Buzsáki, G. (2005). Theta rhythm of navigation: link between path integration and landmark navigation, episodic and semantic memory. *Hippocampus*, 15(7):827–840.
- Buzsáki, G., Buhl, D. L., Harris, K. D., Csicsvari, J., Czéh, B., and Morozov, A. (2003). Hippocampal network patterns of activity in the mouse. *Neuroscience*, 116(1):201–211.
- Buzsáki, G. and Draguhn, A. (2004). Neuronal oscillations in cortical networks. *Science*, 304(5679):1926–1929.
- Buzsáki, G., Geisler, C., Henze, D. A., and Wang, X.-J. (2004). Interneuron Diversity series: Circuit complexity and axon wiring economy of cortical interneurons. *Trends Neurosci*, 27(4):186–193.

- Canolty, R. T., Edwards, E., Dalal, S. S., Soltani, M., Nagarajan, S. S., Kirsch, H. E., Berger, M. S., Barbaro, N. M., and Knight, R. T. (2006). High gamma power is phase-locked to theta oscillations in human neocortex. *Science*, 313(5793):1626–1628.
- Canolty, R. T., Ganguly, K., Kennerley, S. W., Cadieu, C. F., Koepsell, K., Wallis, J. D., and Carmena, J. M. (2010). Oscillatory phase coupling coordinates anatomically dispersed functional cell assemblies. *Proc Natl Acad Sci U S A*, 107(40):17356–17361.
- Canolty, R. T. and Knight, R. T. (2010). The functional role of cross-frequency coupling. *Trends Cogn Sci*, 14(11):506–515.
- Cantero, J. L., Atienza, M., Stickgold, R., Kahana, M. J., Madsen, J. R., and Kocsis, B. (2003). Sleep-dependent theta oscillations in the human hippocampus and neocortex. *J Neurosci*, 23(34):10897–10903.
- Caplan, J. B., Madsen, J. R., Schulze-Bonhage, A., Aschenbrenner-Scheibe, R., Newman, E. L., and Kahana, M. J. (2003). Human theta oscillations related to sensorimotor integration and spatial learning. *J Neurosci*, 23(11):4726–4736.
- Cardin, J. A., Carlén, M., Meletis, K., Knoblich, U., Zhang, F., Deisseroth, K., Tsai, L.-H., and Moore, C. I. (2009). Driving fast-spiking cells induces gamma rhythm and controls sensory responses. *Nature*, 459(7247):663–667.
- Cheyne, D., Bells, S., Ferrari, P., Gaetz, W., and Bostan, A. C. (2008). Self-paced movements induce high-frequency gamma oscillations in primary motor cortex. *Neuroimage*, 42(1):332–342.
- Chrobak, J. J. and Buzsáki, G. (1998). Gamma oscillations in the entorhinal cortex of the freely behaving rat. *J Neurosci*, 18(1):388–398.
- Cohen, M. X., Axmacher, N., Lenartz, D., Elger, C. E., Sturm, V., and Schlaepfer, T. E. (2009a). Good vibrations: cross-frequency coupling in the human nucleus accumbens during reward processing. *J Cogn Neurosci*, 21(5):875–889.
- Cohen, M. X., Axmacher, N., Lenartz, D., Elger, C. E., Sturm, V., and Schlaepfer, T. E. (2009b). Nuclei accumbens phase synchrony predicts decision-making reversals following negative feedback. *J Neurosci*, 29(23):7591–7598.
- Cooper, S. E., McIntyre, C. C., Fernandez, H. H., and Vitek, J. L. (2012). Association of Deep Brain Stimulation Washout Effects With Parkinson Disease Duration. *Arch Neurol*, pages 1–5.
- Crone, N. E., Korzeniewska, A., and Franaszczuk, P. J. (2011). Cortical gamma responses: searching high and low. *Int J Psychophysiol*, 79(1):9–15.
- Crone, N. E., Miglioretti, D. L., Gordon, B., and Lesser, R. P. (1998a). Functional mapping of human sensorimotor cortex with electrocorticographic spectral analysis. II. Event-related synchronization in the gamma band. *Brain*, 121 (Pt 12):2301–2315.

Bibliography

- Crone, N. E., Miglioretti, D. L., Gordon, B., Sieracki, J. M., Wilson, M. T., Uematsu, S., and Lesser, R. P. (1998b). Functional mapping of human sensorimotor cortex with electrocorticographic spectral analysis. I. Alpha and beta event-related desynchronization. *Brain*, 121 (Pt 12):2271–2299.
- Crowell, A. L., Ryapolova-Webb, E. S., Ostrem, J. L., Galifianakis, N. B., Shimamoto, S., Lim, D. A., and Starr, P. A. (2012). Oscillations in sensorimotor cortex in movement disorders: an electrocorticography study. *Brain*, 135(Pt 2):615–630.
- Cuffin, B. N. (1993). Effects of local variations in skull and scalp thickness on EEG’s and MEG’s. *IEEE Trans Biomed Eng*, 40(1):42–48.
- de Hemptinne, C., Ryapolova-Webb, E. S., Air, E. L., Garcia, P. A., Miller, K. J., Ojemann, J. G., Ostrem, J. L., Galifianakis, N. B., and Starr, P. A. (2013). Exaggerated phase-amplitude coupling in the primary motor cortex in Parkinson disease. *Proc Natl Acad Sci U S A*, 110(12):4780–4785.
- Donner, T. H., Siegel, M., Fries, P., and Engel, A. K. (2009). Buildup of choice-predictive activity in human motor cortex during perceptual decision making. *Curr Biol*, 19(18):1581–1585.
- Dürschmid, S. (2013). Oscillatory Dynamics Track Motor Performance Improvement in Human Cortex. *submitted to PLoS One*, 1:1–1000.
- Ellis, T. L. and Stevens, A. (2008). Deep brain stimulation for medically refractory epilepsy. *Neurosurg Focus*, 25(3):E11.
- Finch, D. M. (1996). Neurophysiology of Converging Synaptic Inputs From the Rat Prefrontal Cortex, Amygdala, Midline Thalamus, and Hippocampal Formation Onto Single Neurons of the Caudate/Putamen and Nucleus Accumbens. *Hippocampus*, 6:495–512.
- Fitts, P. M. and Posner, M. I. (1973a). *Human Performance*, chapter 2, pages 8–25. Learning and Skilled Performance. Wadsworth Publishing Company.
- Fitts, P. M. and Posner, M. I. (1973b). *Learning and Skilled Performance*. Number 2. Prentice-Hall International, Human Performance.
- Freeman, W. (2007). Hilbert transform for brain waves. scholarpedia. doi:10.4249/scholarpedia.1338.
- French, S. J. and Totterdell, S. (2002). Hippocampal and prefrontal cortical inputs monosynaptically converge with individual projection neurons of the nucleus accumbens. *J Comp Neurol*, 446(2):151–165.
- Fries, P. (2005). A mechanism for cognitive dynamics: neuronal communication through neuronal coherence. *Trends Cogn Sci*, 9(10):474–480.

- Gaona, C. M., Sharma, M., Freudenburg, Z. V., Breshears, J. D., Bundy, D. T., Roland, J., Barbour, D. L., Schalk, G., and Leuthardt, E. C. (2011). Nonuniform high-gamma (60-500 Hz) power changes dissociate cognitive task and anatomy in human cortex. *J Neurosci*, 31(6):2091–2100.
- Gentili, R. J., Bradberry, T. J., Oh, H., Hatfield, B. D., Contreras-Vidal, J. L., and Vidal, J. L. C. (2011). Cerebral cortical dynamics during visuomotor transformation: adaptation to a cognitive-motor executive challenge. *Psychophysiology*, 48(6):813–824.
- Goto, Y. and Grace, A. A. (2005). Dopamine-dependent interactions between limbic and prefrontal cortical plasticity in the nucleus accumbens: disruption by cocaine sensitization. *Neuron*, 47(2):255–266.
- Goto, Y. and Grace, A. A. (2008). Limbic and cortical information processing in the nucleus accumbens. *Trends Neurosci*, 31(11):552–558.
- Grace, A. A. (2000). Gating of information flow within the limbic system and the pathophysiology of schizophrenia. *Brain Res Brain Res Rev*, 31(2-3):330–341.
- Grace, A. A., Floresco, S. B., Goto, Y., and Lodge, D. J. (2007). Regulation of firing of dopaminergic neurons and control of goal-directed behaviors. *Trends Neurosci*, 30(5):220–227.
- Grafton, S. T., Hazeltine, E., and Ivry, R. B. (1998). Abstract and effector-specific representations of motor sequences identified with PET. *J Neurosci*, 18(22):9420–9428.
- Grafton, S. T., Mazziotta, J. C., Presty, S., Friston, K. J., Frackowiak, R. S., and Phelps, M. E. (1992). Functional anatomy of human procedural learning determined with regional cerebral blood flow and PET. *J Neurosci*, 12(7):2542–2548.
- Grafton, S. T., Woods, R. P., and Tyszka, M. (1994). Functional Imaging of Procedural Motor Learning: Relating Cerebral Blood Flow With Individual Subject Performance. *Human Brain Mapping*, 1:221–234.
- Granger, C. (1969). Investigating Causal Relations by Econometric Models and Cross-spectral Methods. *Econometrica*, 37:424–438.
- Grimm, S., Beck, J., Schuepbach, D., Hell, D., Boesiger, P., Bermpohl, F., Niehaus, L., Boeker, H., and Northoff, G. (2008). Imbalance between left and right dorsolateral prefrontal cortex in major depression is linked to negative emotional judgment: an fMRI study in severe major depressive disorder. *Biol Psychiatry*, 63(4):369–376.
- Guderian, S. and Düzel, E. (2005). Induced theta oscillations mediate large-scale synchrony with mediotemporal areas during recollection in humans. *Hippocampus*, 15(7):901–912.
- Haggard, P. (2008). Human volition: towards a neuroscience of will. *Nat Rev Neurosci*, 9(12):934–946.

Bibliography

- Haider, B. and McCormick, D. A. (2009). Rapid neocortical dynamics: cellular and network mechanisms. *Neuron*, 62(2):171–189.
- Hasselmo, M. E., Bodeln, C., and Wyble, B. P. (2002). A proposed function for hippocampal theta rhythm: separate phases of encoding and retrieval enhance reversal of prior learning. *Neural Comput*, 14(4):793–817.
- Henson, R. N., Shallice, T., and Dolan, R. J. (1999). Right prefrontal cortex and episodic memory retrieval: a functional MRI test of the monitoring hypothesis. *Brain*, 122 (Pt 7):1367–1381.
- Jasper, H. H. (1958). The ten-twenty electrode system of the International Federation. *Electroencephalogr Clin Neurophysiol*, 10:371–375.
- Jensen, O. and Colgin, L. L. (2007). Cross-frequency coupling between neuronal oscillations. *Trends Cogn Sci*, 11(7):267–269.
- Jensen, O., Idiart, M. A., and Lisman, J. E. (1996). Physiologically realistic formation of autoassociative memory in networks with theta/gamma oscillations: role of fast NMDA channels. *Learn Mem*, 3(2-3):243–256.
- Jensen, O. and Tesche, C. D. (2002). Frontal theta activity in humans increases with memory load in a working memory task. *Eur J Neurosci*, 15(8):1395–1399.
- Jueptner, M., Frith, C. D., Brooks, D. J., Frackowiak, R. S., and Passingham, R. E. (1997a). Anatomy of motor learning. II. Subcortical structures and learning by trial and error. *J Neurophysiol*, 77(3):1325–1337.
- Jueptner, M., Stephan, K. M., Frith, C. D., Brooks, D. J., Frackowiak, R. S., and Passingham, R. E. (1997b). Anatomy of motor learning. I. Frontal cortex and attention to action. *J Neurophysiol*, 77(3):1313–1324.
- Kahana, M. J., Seelig, D., and Madsen, J. R. (2001). Theta returns. *Curr Opin Neurobiol*, 11(6):739–744.
- Kahana, M. J., Sekuler, R., Caplan, J. B., Kirschen, M., and Madsen, J. R. (1999). Human theta oscillations exhibit task dependence during virtual maze navigation. *Nature*, 399(6738):781–784.
- Kamiński, M., Ding, M., Truccolo, W. A., and Bressler, S. L. (2001). Evaluating causal relations in neural systems: granger causality, directed transfer function and statistical assessment of significance. *Biol Cybern*, 85(2):145–157.
- Kamiński, M. J. and Blinowska, K. J. (1991). A new method of the description of the information flow in the brain structures. *Biol Cybern*, 65(3):203–210.
- Keenan, Wheeler, Gallup, and Pascual-Leone (2000). Self-recognition and the right prefrontal cortex. *Trends Cogn Sci*, 4(9):338–344.

- Kelso, J. A., Fuchs, A., Lancaster, R., Holroyd, T., Cheyne, D., and Weinberg, H. (1998). Dynamic cortical activity in the human brain reveals motor equivalence. *Nature*, 392(6678):814–818.
- Klausberger, T., Magill, P. J., Mrton, L. F., Roberts, J. D. B., Cobden, P. M., Buzski, G., and Somogyi, P. (2003). Brain-state- and cell-type-specific firing of hippocampal interneurons in vivo. *Nature*, 421(6925):844–848.
- Klimesch, W. (1999). EEG alpha and theta oscillations reflect cognitive and memory performance: a review and analysis. *Brain Res Brain Res Rev*, 29(2-3):169–195.
- Klimesch, W., Doppelmayr, M., Pachinger, T., and Ripper, B. (1997). Brain oscillations and human memory: EEG correlates in the upper alpha and theta band. *Neurosci Lett*, 238(1-2):9–12.
- Klimesch, W., Doppelmayr, M., Russegger, H., and Pachinger, T. (1996). Theta band power in the human scalp EEG and the encoding of new information. *Neuroreport*, 7(7):1235–1240.
- Klimesch, W., Doppelmayr, M., Yonelinas, A., Kroll, N. E., Lazzara, M., Rlm, D., and Gruber, W. (2001). Theta synchronization during episodic retrieval: neural correlates of conscious awareness. *Brain Res Cogn Brain Res*, 12(1):33–38.
- Klimesch, W., Schimke, H., and Schwaiger, J. (1994). Episodic and semantic memory: an analysis in the EEG theta and alpha band. *Electroencephalogr Clin Neurophysiol*, 91(6):428–441.
- Knopman, D. and Nissen, M. J. (1991). Procedural learning is impaired in Huntington’s disease: evidence from the serial reaction time task. *Neuropsychologia*, 29(3):245–254.
- Kopell, N., Kramer, M. A., Malerba, P., and Whittington, M. A. (2010). Are different rhythms good for different functions? *Front Hum Neurosci*, 4:187.
- Korzeniewska, A., Crainiceanu, C. M., Kuś, R., Franaszczuk, P. J., and Crone, N. E. (2008). Dynamics of event-related causality in brain electrical activity. *Hum Brain Mapp*, 29(10):1170–1192.
- Korzeniewska, A., Franaszczuk, P. J., Crainiceanu, C. M., Kuś, R., and Crone, N. E. (2011). Dynamics of large-scale cortical interactions at high gamma frequencies during word production: event related causality (ERC) analysis of human electrocorticography (ECoG). *Neuroimage*, 56(4):2218–2237.
- Kwan, P., Arzimanoglou, A., Berg, A. T., Brodie, M. J., Hauser, W. A., Mathern, G., Mosh, S. L., Perucca, E., Wiebe, S., and French, J. (2010). Definition of drug resistant epilepsy: consensus proposal by the ad hoc Task Force of the ILAE Commission on Therapeutic Strategies. *Epilepsia*, 51(6):1069–1077.
- Lisman, J. (2010). Working memory: the importance of theta and gamma oscillations. *Curr Biol*, 20(11):R490–R492.

Bibliography

- Lisman, J. E. and Jensen, O. (2013). The - neural code. *Neuron*, 77(6):1002–1016.
- Llins, R., Ribary, U., Contreras, D., and Pedroarena, C. (1998). The neuronal basis for consciousness. *Philos Trans R Soc Lond B Biol Sci*, 353(1377):1841–1849.
- Lordahl, D. S. and Archer, E. J. (1958). Transfer effects on a rotary pursuit task as a function of first-task difficulty. *J Exp Psychol*, 56(5):421–426.
- MacDonald, A. W., Cohen, J. D., Stenger, V. A., and Carter, C. S. (2000). Dissociating the role of the dorsolateral prefrontal and anterior cingulate cortex in cognitive control. *Science*, 288(5472):1835–1838.
- Mai, J. K., Paxinos, G., and Voss, T. (2004). *Atlas of the human brain 2nd ed.* Academic Press Elsevier.
- Mathewson, K. E., Gratton, G., Fabiani, M., Beck, D. M., and Ro, T. (2009). To see or not to see: prestimulus alpha phase predicts visual awareness. *J Neurosci*, 29(9):2725–2732.
- Miller, E. K. and Cohen, J. D. (2001). An integrative theory of prefrontal cortex function. *Annu Rev Neurosci*, 24:167–202.
- Miller, K. J., Hermes, D., Honey, C. J., Hebb, A. O., Ramsey, N. F., Knight, R. T., Ojemann, J. G., and Fetz, E. E. (2012). Human motor cortical activity is selectively phase-entrained on underlying rhythms. *PLoS Comput Biol*, 8(9):e1002655.
- Mogenson, G. J., Jones, D. L., and Yim, C. Y. (1980). From motivation to action: functional interface between the limbic system and the motor system. *Prog Neurobiol*, 14(2-3):69–97.
- Morel, A. (2007). *Stereotactic Atlas of the Human Thalamus and Basal Ganglia.* Informa Health Care Inc.
- Muellbacher, W., Ziemann, U., Wissel, J., Dang, N., Kofler, M., Facchini, S., Boroojerdi, B., Poewe, W., and Hallett, M. (2002). Early consolidation in human primary motor cortex. *Nature*, 415(6872):640–644.
- Münte, T. F., Heldmann, M., Hinrichs, H., Marco-Pallares, J., Krämer, U. M., Sturm, V., and Heinze, H.-J. (2007). Nucleus Accumbens is Involved in Human Action Monitoring: Evidence from Invasive Electrophysiological Recordings. *Front Hum Neurosci*, 1:11.
- Nieuwenhuis, S., Ridderinkhof, K. R., Blom, J., Band, G. P., and Kok, A. (2001). Error-related brain potentials are differentially related to awareness of response errors: evidence from an antisaccade task. *Psychophysiology*, 38(5):752–760.
- Nissen, M. J. and Bullemer, P. (1987). Attentional Requirements of Learning: Evidence from Performance Measures. *Cognitive Psychology*, 19:1–32.

- Notebaert, W., Houtman, F., Opstal, F. V., Gevers, W., Fias, W., and Verguts, T. (2009). Post-error slowing: an orienting account. *Cognition*, 111(2):275–279.
- Nudo, R. J., Milliken, G. W., Jenkins, W. M., and Merzenich, M. M. (1996). Use-dependent alterations of movement representations in primary motor cortex of adult squirrel monkeys. *J Neurosci*, 16(2):785–807.
- O’Donnell, P. and Grace, A. A. (1995). Synaptic interactions among excitatory afferents to nucleus accumbens neurons: hippocampal gating of prefrontal cortical input. *J Neurosci*, 15(5 Pt 1):3622–3639.
- Okada, Y. C., Lahteenmki, A., and Xu, C. (1999). Experimental analysis of distortion of magnetoencephalography signals by the skull. *Clin Neurophysiol*, 110(2):230–238.
- Osipova, D., Takashima, A., Oostenveld, R., Fernández, G., Maris, E., and Jensen, O. (2006). Theta and gamma oscillations predict encoding and retrieval of declarative memory. *J Neurosci*, 26(28):7523–7531.
- Penhune, V. B. and Steele, C. J. (2012). Parallel contributions of cerebellar, striatal and M1 mechanisms to motor sequence learning. *Behav Brain Res*, 226(2):579–591.
- Pfurtscheller, G. and Cooper, R. (1975). Frequency dependence of the transmission of the EEG from cortex to scalp. *Electroencephalogr Clin Neurophysiol*, 38(1):93–96.
- Pfurtscheller, G. and da Silva, F. H. L. (1999). Event-related EEG/MEG synchronization and desynchronization: basic principles. *Clin Neurophysiol*, 110(11):1842–1857.
- Pierrot-Deseilligny, C., Müri, R. M., Ploner, C. J., Gaymard, B., Demeret, S., and Rivaud-Pechoux, S. (2003). Decisional role of the dorsolateral prefrontal cortex in ocular motor behaviour. *Brain*, 126(Pt 6):1460–1473.
- Poldrack, R. A., Sabb, F. W., Foerde, K., Tom, S. M., Asarnow, R. F., Bookheimer, S. Y., and Knowlton, B. J. (2005). The neural correlates of motor skill automaticity. *J Neurosci*, 25(22):5356–5364.
- Pollmann, S. (2008). *Allgemeine Psychologie*, chapter Lernen und Gedächtnis, page 183. Reinhardt UTB.
- Raghavachari, S., Kahana, M. J., Rizzuto, D. S., Caplan, J. B., Kirschen, M. P., Bourgeois, B., Madsen, J. R., and Lisman, J. E. (2001). Gating of human theta oscillations by a working memory task. *J Neurosci*, 21(9):3175–3183.
- Raghavachari, S., Lisman, J. E., Tully, M., Madsen, J. R., Bromfield, E. B., and Kahana, M. J. (2006). Theta oscillations in human cortex during a working-memory task: evidence for local generators. *J Neurophysiol*, 95(3):1630–1638.
- Ray, S., Crone, N. E., Niebur, E., Franaszczuk, P. J., and Hsiao, S. S. (2008). Neural correlates of high-gamma oscillations (60–200 Hz) in macaque local field potentials and their potential implications in electrocorticography. *J Neurosci*, 28(45):11526–11536.

Bibliography

- Ray, S. and Maunsell, J. H. R. (2011). Different origins of gamma rhythm and high-gamma activity in macaque visual cortex. *PLoS Biol*, 9(4):e1000610.
- Ridderinkhof, K. R., Ullsperger, M., Crone, E. A., and Nieuwenhuis, S. (2004). The role of the medial frontal cortex in cognitive control. *Science*, 306(5695):443–447.
- Sarnthein, J., Petsche, H., Rappelsberger, P., Shaw, G. L., and von Stein, A. (1998). Synchronization between prefrontal and posterior association cortex during human working memory. *Proc Natl Acad Sci U S A*, 95(12):7092–7096.
- Scheffer-Teixeira, R., Belchior, H., Leo, R. N., Ribeiro, S., and Tort, A. B. L. (2013). On high-frequency field oscillations (≈ 100 Hz) and the spectral leakage of spiking activity. *J Neurosci*, 33(4):1535–1539.
- Scheffers, M. K. and Coles, M. G. (2000). Performance monitoring in a confusing world: error-related brain activity, judgments of response accuracy, and types of errors. *J Exp Psychol Hum Percept Perform*, 26(1):141–151.
- Scheidt, R. A., Zimelman, J. L., Salowitz, N. M. G., Suminski, A. J., Mosier, K. M., Houk, J., and Simo, L. (2012). Remembering forward: neural correlates of memory and prediction in human motor adaptation. *Neuroimage*, 59(1):582–600.
- Schendan, H. E., Searl, M. M., Melrose, R. J., and Stern, C. E. (2003). An fMRI study of the role of the medial temporal lobe in implicit and explicit sequence learning. *Neuron*, 37(6):1013–1025.
- Siapas, A. G., Lubenov, E. V., and Wilson, M. A. (2005). Prefrontal phase locking to hippocampal theta oscillations. *Neuron*, 46(1):141–151.
- Simon, S. R., Meunier, M., Piettre, L., Berardi, A. M., Segebarth, C. M., and Bous-saoud, D. (2002). Spatial attention and memory versus motor preparation: premotor cortex involvement as revealed by fMRI. *J Neurophysiol*, 88(4):2047–2057.
- Singer, W. (1993). Synchronization of cortical activity and its putative role in information processing and learning. *Annu Rev Physiol*, 55:349–374.
- Sirota, A., Csicsvari, J., Buhl, D., and Buzsáki, G. (2003). Communication between neocortex and hippocampus during sleep in rodents. *Proc Natl Acad Sci U S A*, 100(4):2065–2069.
- Staudigl, T., Zaehle, T., Voges, J., Hanslmayr, S., Esslinger, C., Hinrichs, H., Schmitt, F. C., Heinze, H.-J., and Richardson-Klavehn, A. (2012). Memory signals from the thalamus: early thalamocortical phase synchronization entrains gamma oscillations during long-term memory retrieval. *Neuropsychologia*, 50(14):3519–3527.
- Sturm, V., Lenartz, D., Koulousakis, A., Treuer, H., Herholz, K., Klein, J. C., and Klosterkötter, J. (2003). The nucleus accumbens: a target for deep brain stimulation in obsessive-compulsive- and anxiety-disorders. *J Chem Neuroanat*, 26(4):293–299.

- Tombini, M., Zappasodi, F., Zollo, L., Pellegrino, G., Cavallo, G., Tecchio, F., Guglielmelli, E., and Rossini, P. M. (2009). Brain activity preceding a 2D manual catching task. *Neuroimage*, 47(4):1735–1746.
- Tort, A. B. L., Komorowski, R., Eichenbaum, H., and Kopell, N. (2010). Measuring phase-amplitude coupling between neuronal oscillations of different frequencies. *J Neurophysiol*, 104(2):1195–1210.
- Tort, A. B. L., Komorowski, R. W., Manns, J. R., Kopell, N. J., and Eichenbaum, H. (2009a). Theta-gamma coupling increases during the learning of item-context associations. *Proc Natl Acad Sci U S A*, 106(49):20942–20947.
- Tort, A. B. L., Komorowski, R. W., Manns, J. R., Kopell, N. J., and Eichenbaum, H. (2009b). Theta-gamma coupling increases during the learning of item-context associations. *Proc Natl Acad Sci U S A*, 106(49):20942–20947.
- Tort, A. B. L., Kramer, M. A., Thorn, C., Gibson, D. J., Kubota, Y., Graybiel, A. M., and Kopell, N. J. (2008). Dynamic cross-frequency couplings of local field potential oscillations in rat striatum and hippocampus during performance of a T-maze task. *Proc Natl Acad Sci U S A*, 105(51):20517–20522.
- Trepel, M., editor (2004). *Neuroanatomie*. Elsevier Urban & Fischer.
- Uhlhaas, P. J. and Singer, W. (2010). Abnormal neural oscillations and synchrony in schizophrenia. *Nat Rev Neurosci*, 11(2):100–113.
- van 't Wout, M., Kahn, R. S., Sanfey, A. G., and Aleman, A. (2005). Repetitive transcranial magnetic stimulation over the right dorsolateral prefrontal cortex affects strategic decision-making. *Neuroreport*, 16(16):1849–1852.
- Voges, J., Volkmann, J., Allert, N., Lehrke, R., Koulousakis, A., Freund, H.-J., and Sturm, V. (2002). Bilateral high-frequency stimulation in the subthalamic nucleus for the treatment of Parkinson disease: correlation of therapeutic effect with anatomical electrode position. *J Neurosurg*, 96(2):269–279.
- von Stein, A. and Sarnthein, J. (2000). Different frequencies for different scales of cortical integration: from local gamma to long range alpha/theta synchronization. *Int J Psychophysiol*, 38(3):301–313.
- Voytek, B., Canolty, R. T., Shestyuk, A., Crone, N. E., Parvizi, J., and Knight, R. T. (2010). Shifts in gamma phase-amplitude coupling frequency from theta to alpha over posterior cortex during visual tasks. *Front Hum Neurosci*, 4:191.
- Wang, X.-J. (2010). Neurophysiological and computational principles of cortical rhythms in cognition. *Physiol Rev*, 90(3):1195–1268.
- Wessel, K., Zeffiro, T., Lou, J. S., Toro, C., and Hallett, M. (1995). Regional cerebral blood flow during a self-paced sequential finger opposition task in patients with cerebellar degeneration. *Brain*, 118 (Pt 2):379–393.

Bibliography

- Whitham, E. M., Pope, K. J., Fitzgibbon, S. P., Lewis, T., Clark, C. R., Loveless, S., Broberg, M., Wallace, A., DeLosAngeles, D., Lillie, P., Hardy, A., Fronsco, R., Pulbrook, A., and Willoughby, J. O. (2007). Scalp electrical recording during paralysis: quantitative evidence that EEG frequencies above 20 Hz are contaminated by EMG. *Clin Neurophysiol*, 118(8):1877–1888.
- Willingham, D. B. and Goedert-Eschmann, K. (1999). The Relation between Implicit and Explicit Learning: Evidence for Parallel Development. *Psychological Science*, 10:531–534.
- Wilson, W. J. (1983). Nucleus accumbens inhibits specific motor but not nonspecific classically conditioned responses. *Brain Res Bull*, 10(4):505–515.
- Xing, D., Shen, Y., Burns, S., Yeh, C.-I., Shapley, R., and Li, W. (2012). Stochastic generation of gamma-band activity in primary visual cortex of awake and anesthetized monkeys. *J Neurosci*, 32(40):13873–13880.
- Yanagisawa, T., Yamashita, O., Hirata, M., Kishima, H., Saitoh, Y., Goto, T., Yoshimine, T., and Kamitani, Y. (2012). Regulation of motor representation by phase-amplitude coupling in the sensorimotor cortex. *J Neurosci*, 32(44):15467–15475.
- Zatorre, R. J., Chen, J. L., and Penhune, V. B. (2007). When the brain plays music: auditory-motor interactions in music perception and production. *Nat Rev Neurosci*, 8(7):547–558.

8 Appendix - ECoG recordings

Interpretation of partial and Pearson correlation

A geometric interpretation is given by the fact that Pearson correlation, as a similarity measure between random variables, is closely related to the angle between two vectors. The two vectors are the two possible regressions between the two variables. Correlation is high when the angle between the regressions is small. Partial correlation introduces a third variable, in our case time. It measures the angle of the two regression lines in the plane perpendicular to the third variable. Thus, in a 3D space spanned by TPR, performance, and time the plane in which the two possible regressions between TPR and performance can have different orientations with the time axis. If the time axis is orthogonal to the plane, then the correlation between TPR and performance is fully independent of time and unrelated to learning. On the contrary, if the two regression lines are in the same plane as the time axis, then the correlation between TPR and performance is fully time dependent and due to learning. In practice, we can expect to most likely observe mixed effects with regressions oriented between the extremes, indicating mixed contributions of learning and learning unrelated correlations. Importantly, our reasoning is that if we observe a significant Pearson correlation in an electrode that significantly changes if we discount time related correlations (in partial correlation), then the TPR with performance correlation in this electrode is at least partly due to learning related TPR with performance correlations.

Stability of coupling phase

The previous analyses showed that performance covaries with paCFC. However, calculating the paCFC at one phase (see Section 4.2) the changes with performance can either be a result of a shift of the HG amplitude peak relative to the θ trough or the result of simultaneous adaption of both frequency components. To test the hypothesis that the covariation is not a result of the HG peak shift we used the fitted phase angle of the trial-wise sine fit functions (see Figure 2) . By means of a linear regression we tested whether there are systematic changes of the phase angle over time. In each participant we compared the slope of the linear regression with an empirical distribution of slopes derived from randomizing the order of trials 500 times. Both for the channels showing correlation and partial correlation no systematic change was found as indicated by slopes within the confidence intervals. This suggests that performance/paCFC covariation is a result of simultaneous adaptation of both frequency components rather than a shift of the HG amplitude peak.

Specificity of θ -HG interaction

We investigated whether HG nested to the θ trough is exclusively predictive for performance. In the three experimental tasks we additionally assessed the specificity of the θ /HG coupling compared to θ/β or θ/γ coupling. For a broad frequency range encompassing β , γ , and high θ range we extracted all frequencies with a band width of 6 Hz and a resolution of 2 Hz; center frequencies: 13-190 Hz). For each sub band (Nsubbands = 89, 13 belonging to the β band, 21 the γ and 65 to the HG range) we calculated the paCFC with the θ activity and assessed the correlation with behavior for each channel across participants. The number of electrodes showing a significant ($p < .05$, uncorrected) performance/paCFC correlation varied as a function of frequency band ($N_{\theta/\beta} = 193$, $N_{\theta/\gamma} = 187$, $N_{\theta/HG} = 289$; $\chi^2 = 29.4$; $p < .0001$). The corresponding r-values were compared using a one-way ANOVA with the factor frequency band. The frequency bands predicted behavior differently ($F(2,666) = 10.9$, $p < .0001$). Posthoc tests revealed that the prediction of behavior by the θ /HG coupling was better than the prediction by θ/β coupling or θ/γ coupling (p corrected for Nsubbands $< .0001$), suggesting a specific effect of the θ /HG coupling for the prediction of motor behavior. Necessity of Interaction We then tested whether θ or HG alone predicted behavior. We compared performance/ θ , performance/HG, and performance/paCFC correlation coefficients. As for the specificity analysis, we calculated for each electrode the Pearson's r for correlation of performance with θ , HG, and paCFC and compared r-values of electrodes showing significant correlation. Since Pearson's r is not a metric measure we transformed r values using the inverse hyperbolic tangent

$$\operatorname{arctanh}(r) : \frac{1}{2} \ln \frac{(1+r)}{(1-r)} \text{ for } |r| < 1 \quad (8.1)$$

The levels covaried differently with behavior ($F(2,501) = 19.67$, $p < .0001$). Post-hoc tests revealed a significant difference between paCFC and θ ($t(373) = -4.81$; $p < .0001$) and paCFC and HG ($t(416) = -4.7$; $p < .0001$) at a Bonferroni corrected significance level. We did not find such difference comparing HG with θ ($p = .5$). Hence, paCFC predicted performance better than θ or HG activity alone. This indicates that the motor behavior automatization variation of θ -HG coupling is a result of cooperative modulation of neuronal activity in the two frequency bands rather than the result of a variation of either θ or HG band activity alone.

We next asked whether the trial-by-trial correlation strength depends on the θ phase at which the paCFC is calculated. The previous analysis showed that HG-amplitude varies with the θ phase. Importantly, a variation of performance/paCFC correlation strength as a function of θ phase, could underscore the neurophysiological relevance of paCFC for behavioral adaptation. Therefore, we determined trial-by-trial performance/paCFC correlations at 20 different equally spaced θ phase bins. To test the hypothesis we compared the probability to detect significant electrodes across θ phase bins for correlation and partial correlation. We compared the phase specificity by fitting a cosine function to the probability of significant electrodes (see Figure 8.1). Both for correlation and partial correlation the fit was highly significant ($p < .001$) with the

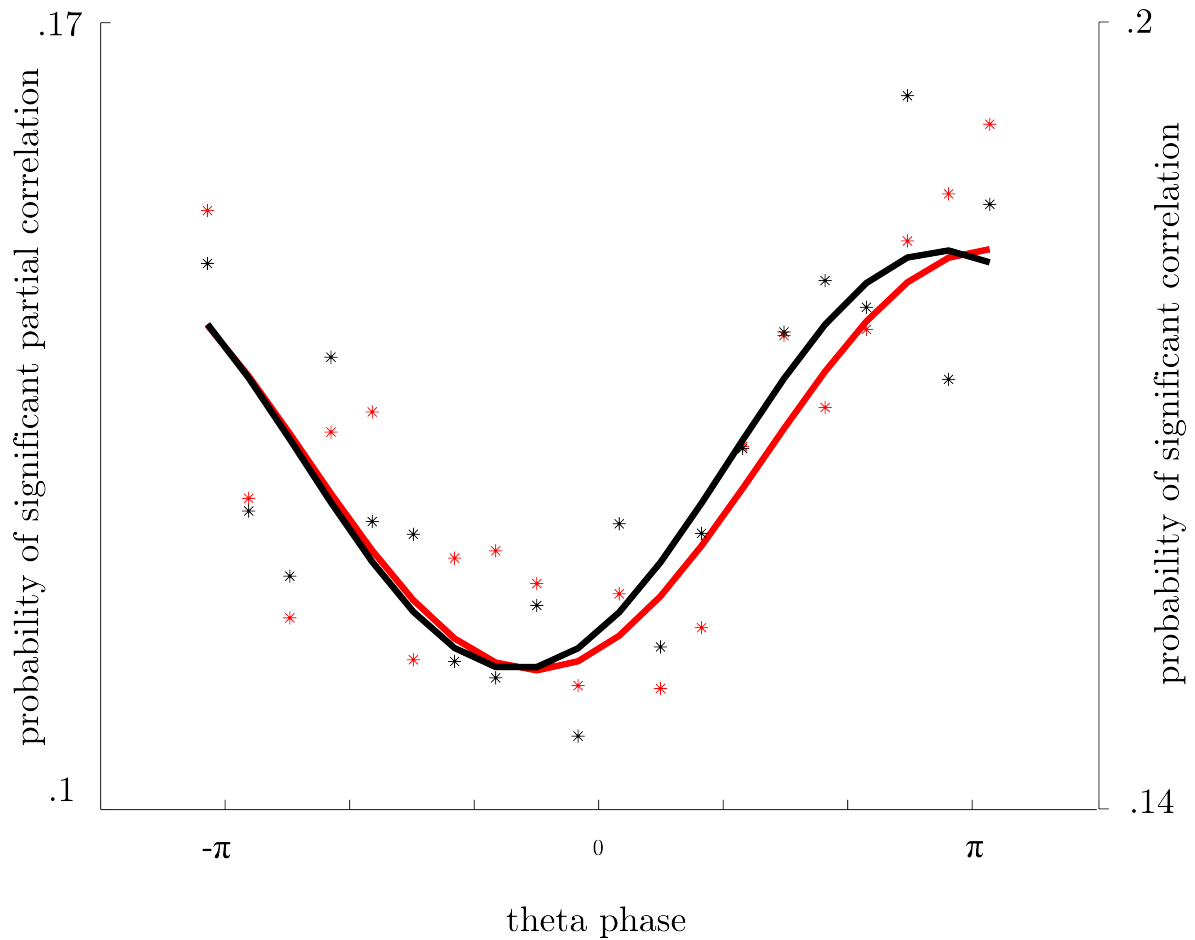


FIGURE 8.1:

Prediction of behavior changes as a function of the θ phase. Red and black asterisks show the number of significant electrodes for each of the 20 phase bins for the performance/paCFC correlation and partial correlation, respectively.

maximum of significant electrodes close to the trough ($\phi_{correlation} = .4$, $\phi_{partialcorrelation} = .6$). Figure 8.1 shows the probability of significant correlations both for the performance/paCFC correlation and partial correlation.

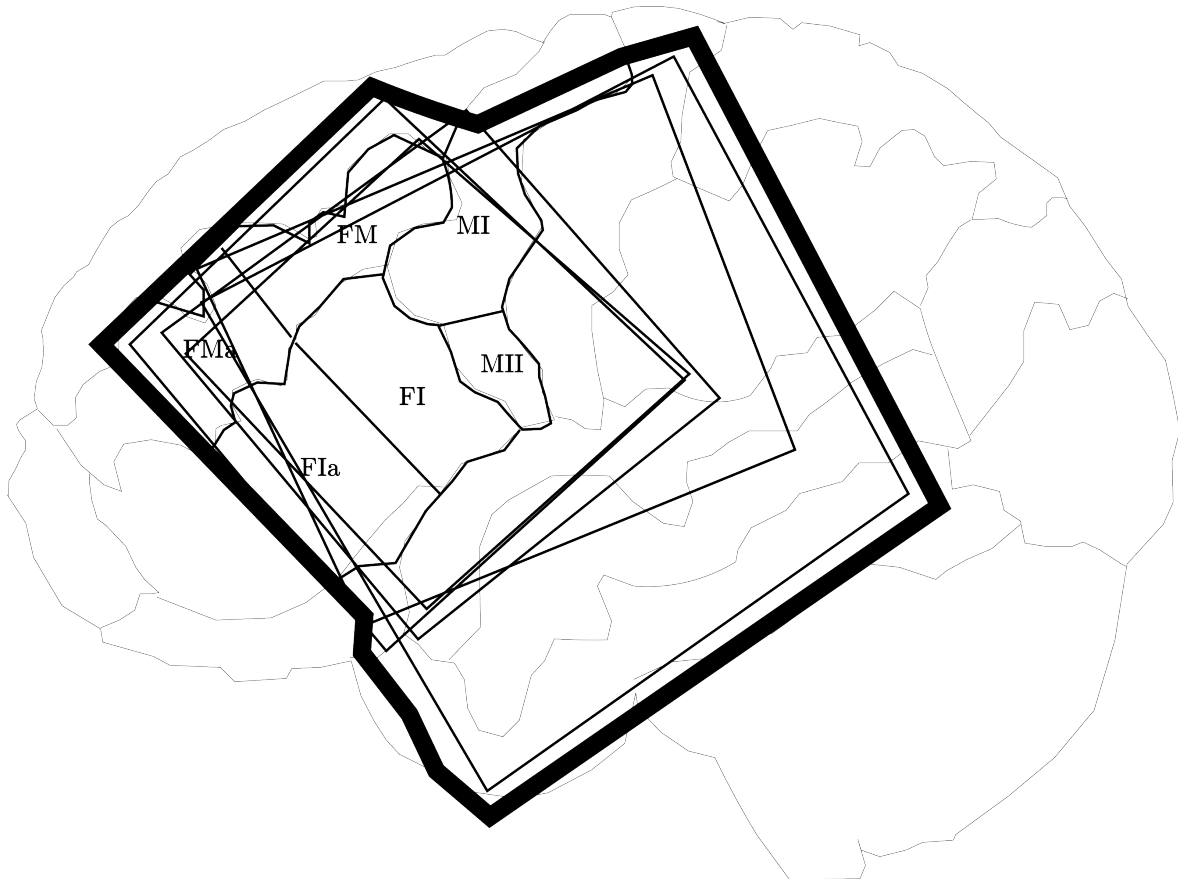


FIGURE 8.2:

We grouped electrodes into 6 regions of interest. Each outline denotes the grid coverage of one participant. The bold outline shows the summed coverage across all participants. The anterior and posterior medial frontal gyrus (FMa, FM), the anterior and the posterior inferior frontal gyrus (FIa, FI), and the superior and inferior sensorimotor cortex (MI, MII). The outline of the grid location of the AMCT participant is given in Figure 5.

9 Appendix - MEG recordings

9.1 Supplementary Methods

9.1.1 Calculation of Trough-to-Peak Ratio

The paCFC is a composite of the time series of a low frequency (trough frequency) and the analytic amplitude of a high frequency (amplitude frequency) of the same signal recorded at the same sensor. Therefore, the recorded signal was filtered both in a low frequency range providing the phase (phase-frequency) and in a high frequency range providing the amplitude (amplitude-frequency). Since we do not know the preferred frequency combination we split both the low phase-frequency and the high amplitude-frequency in sub-bands. For the phase-frequencies we choose three bands with the center frequencies 4, 6 and 8 Hz (θ range) all with a band width of 4 Hz . In each time series of the three bands the troughs were determined as the local minima in the time range of 600 ms after stimulus onset. We used the window of 600 ms since in each block across both sequence types the median of the reaction times fell below 600 ms after stimulus onset (see FIGURE 5.1). Around each trough a time range was defined in which the magnetic field values were averaged. These time ranges depended on the frequency of the filtered signal. In general these time ranges matched a half oscillation of the center frequency (time ranges: 4 $Hz - \frac{1}{8}$ sec, 6 $Hz - \frac{1}{12}$ sec, 8 $Hz - \frac{1}{16}$ sec). The amplitude frequencies were filtered in several frequency bands in the high γ range (center frequencies: 60 to 180 Hz with a resolution of 2 Hz and band width of 4 Hz). Separately, for each frequency band the analytic amplitude was calculated by means of the Hilbert transform. After this for each combination of trough frequencies ($N = 3$) and amplitude frequencies ($N = 60$) the paCFC was calculated as the θ -trough-to-high- γ -peak ratio (see SECTION 4.2.4). For example, for the coupling between 4 Hz and 80 Hz (paCFC_{4 Hz /80 Hz}) the analytic amplitude of the 80 Hz signal was averaged in the time window of 125 ms ($\frac{1}{8}$ sec) around each 4 Hz trough. The TPR measure

$$TPR_{\phi f, \hat{a} f, j} = \frac{|\overline{D_{\phi f, j}}|}{A_{\hat{a} f, j}} \quad (9.1)$$

was calculated for the combination of each phase-frequency ϕf with each amplitude-frequency $\hat{a} f$ separately for the 48 initial trials. The a priori hypothesis is that learning the fixed sequence is accompanied by temporal evolution of paCFC assuming that the θ -trough-to-high- γ -peak ratio increases particularly in the (pre-)motor cortex. To assess the temporal dynamics of paCFC (Δ paCFC) we applied a linear regression approach. For each phase-frequency \times amplitude-frequency combination we determined regression equation

$$y_{\phi f, \hat{a} f}(t) = a_{\phi f, \hat{a} f} * x_{\phi f, \hat{a} f}(t) + b_{\phi f, \hat{a} f} \quad (9.2)$$

9 Appendix - MEG recordings

with $x_{\phi,\hat{a}f}$ as the $TPR_{\phi,\hat{a}f}$ for all 48 trials, $a_{\phi,\hat{a}f}$ as the slope of the regression line and $b_{\phi,\hat{a}f}$ as the intercept. The slope a served as a measure for the change of paCFC. To assess the spatial patterns of ΔpaCFC $a_{\phi f,\hat{a}f,s}$ was calculated for each MEG-sensor s . $a_{\phi f,\hat{a}f,s}$ comprises the temporal evolution of all frequency combination at a spatial region defined by the sensor s . In each set of slopes $a_{\phi f,\hat{a}f,s}$ we determined the maximal slope value for the increase of paCFC (paCFC_{\uparrow}) and the minimal (maximal negative) slope value for the decrease of paCFC ($\text{paCFC}_{\downarrow}$). This leaves the possibility that for each sensor in each participant an individual frequency combination was chosen. To define regions of a significant increase and decrease of paCFC the maximal and minimal slope values were z-scored separately. Sensors with a maximal slope > 2 and or a minimal slope < -2 were considered showing significant temporal evolution of paCFC. Additionally, significant sensors without any adjacent sensor according to the spiral arrangement of MEG sensors greater or smaller than $z = 2 / -2$ (single sensors) were excluded from analysis. The paCFC is a measure which directly depends on temporal fluctuations of a high and low frequency subband. Therefore, it is possible that the temporal variation of the paCFC (ΔpaCFC) is the result of either the variation of the low or high frequency alone. To avoid that we carried out the same analysis as outlined above separately for the phase-frequency and amplitude-frequency. Sensors which showed a significant variation of the paCFC and additionally either the low or high frequency oscillations were excluded.

9.1.2 Granger Causality

The MVAR can be formulated by:

$$\mathbf{X}(t) = \sum_{j=1}^p \mathbf{A}(j)\mathbf{X}(t-j) + \mathbf{E}(t) \quad (9.3)$$

$\mathbf{X}(t)$ is a matrix of all MEG sensors of interest ($X_1(t), \dots, X_k(t)$). p refers to the model order. Here we used a model order of 5. This means that each time point in each channel is predicted out of the last 5 points in time of all time series ($\mathbf{X}(t-j)$). $\mathbf{A}(j)$ denotes the model coefficients. The advantage of this approach is that content of information can be ascribed to different frequency bands. Therefore, the MVAR equation has to be transformed to the frequency domain where the transfer function of the multi-channel system $\mathbf{H}(f)$ is calculated by

$$\mathbf{H}(f) = \left(\sum_{j=0}^p \mathbf{A}(j) \exp^{-1i*2\pi*j*f*\Delta t} \right)^{-1} \quad (9.4)$$

with i as the imaginary unit, f as the frequency of interest and Δt as the sampling interval ($\frac{1}{\text{samplingrate}}$). The causal influence from sensor a to sensor b is defined as

$$\theta_{ab}^2(f) = |\mathbf{H}_{ab}(f)|^2 \quad (9.5)$$

and the normalized information transfer function is defined according to Kamiński

and Blinowska (1991); Kamiński et al. (2001) as

$$\gamma_{ab}^2(f) = \frac{\theta_{ab}^2(f)}{\sum_{m=1}^k \theta_{am}^2(f)} \quad (9.6)$$

For each participant and experimental block we fitted the MVAR to the time series recorded at all sensors chosen according to significant paCFC changes as mentioned above. We have chosen to use the annotation used by Kamiński and Blinowska (1991); Kamiński et al. (2001) as $\theta_{ab}^2(f)$ and $\gamma_{ab}^2(f)$. Please note, that this is not the same as the θ and γ activity. For the calculation of the paCFC we restricted our analysis to the 600 ms after stimulus onset. Therefore, we only subjected the time series of the 13 sensors covering the PMC/MC and the rPFC in this interval to the MVAR. This was done for each trial separately and both the fixed and the random condition. For each trial the matrix $\mathbf{X}_{trial}(t)$ was z-scored and $\gamma_{ab}^2(f)$ was calculated for all frequencies between 1 and 200 Hz. This leads to 5 matrices containing the $\gamma_{ab}^2(f)$ - values for the fixed sequence for all channels in all trials for all participants and the same for the random condition (Nchannels \times Nchannels \times Ntrials \times Nparticipants). This matrix was averaged across trials and participants. We divided each Nchannels \times Nchannels matrix into sub-regions containing the causality within the PMC/MC (inmc: 6 \times 6), within the rPFC (inrpf: 7 \times 7), from the PMC/MC to the rPFC (mc2rpf: 6 \times 7) and from the rPFC to the PMC/MC (rpf2mc: 7 \times 6). Within each sub-region we determined the maximum causal influence in each frequency bin neglecting the the $\gamma_{ab}^2(f)$ -values for the causality of one and the same sensor. For each frequency bin we compared the maximal causal influence in the 5 random blocks with the maximal causal influence in the 5 fixed blocks with a two-sided t-test. We expected first that independent of the sequence type the causal influence between adjacent (inmc and indlpfc) sensors is greater compared to distant sensors (mc2dlpfc and dlpfc2mc). Second, we assume that the rPFC is the primary encoding unit and therefore, we suppose that differences between the random and the fixed conditions can be seen within the rPFC or the causality from the rPFC to the PMC/MC.

To prove the robustness of the Causality measure I repeated the the analysis with randomly shifted phase and amplitude time series 100 times. The resulting frequency specific t-values served as distribution for the estimation of confidence intervals.

9.2 Supplementary Results

The spatial patterns show no consistency with randomly generated spatial patterns. The distribution of the significant slopes over the scalp could lead one to conclude that during the task of finger tapping the strongest changes take place in the PMC/MC and the DLPFC. However, this spatial distribution of significant changes can only be a result of a random process and therefore, is independent of motor activity. If this is the case one should find comparable clusters of significant sensors even for a completely randomized time series. This means that the covariation of our spatial distribution with the spatial distribution derived from a random process should be the same as the covariation of the spatial distributions from two random processes.

Otherwise if our result is not a result of a complete random process the covariation between the original spatial distribution and the random distribution should be less than between two random distributions. If so this would show that the original spatial distribution shares less spatial characteristics with a random process than two random processes. We assessed this by comparing the original time series with randomized data. The randomization was carried out in the following way. First, for each subject and block of randomization the trials were shuffled independently of each other. Afterwards the time series were filtered in a high (60–180 Hz) and low frequency (4–8 Hz) each with a bandwidth of 4 Hz and a resolution of 2 Hz. These trialshuffled and filtered time series were randomly shifted in time and independent of each other with the restriction that the shift in time was maximally 600 ms. The paCFC of these shifted time series was calculated and the change of the paCFC over the shuffled trials was assessed by the slope of a linear regression for each frequency pair as explained for the actual data. This was repeated 21 times for each subject which results in 21 new random vectors containing 248 linear regression slopes. To assess whether the original slope distribution indeed shares less characteristics than two given random slope distributions, for each pair of vectors (vector matrix: 21 random + 1 original) we calculated Pearson's r . The correlation coefficients were used to compare the consistency of the original spatial distribution with all possible random distributions with the consistency of the a given random distribution with all possible random distribution (see A in FIGURE 9.1). This means that we have 22 r -values for the covariation with all 22 vectors. $r_{(original-vector_{v=1}^n)}$ contains the correlation of the original paCFC with all random paCFC and gives information of shared spatial characteristics of the original slope distribution with all given random vectors, whereas, $r_{(random_i-vector_{(1,\dots,n)})}$ contains the correlation of randomization i with all vectors in the vector matrix. This leads to a correlation matrix of 22-by-22 r values. We compared the first column in the correlation matrix $r_{(original-vector_{(1,\dots,n)})}$ with all remaining columns separately with a one-sided one-sampled t -test with the assumption that the original vector shares less spatial characteristics with all random vectors and hence, $r_{(original-vector_{(1,\dots,n)})} < r_{(random_i-vector_{(1,\dots,n)})}$. Single r values were Fishers- z -transformed, since the distribution of r -values is not symmetric. In each t -test between the original and the random vector i the autocorrelation values and the r -values for the correlation of the original and the random vector i were excluded. The significance level was Bonferroni-corrected for multiple comparisons ($p = .0025$). The correlation of the original spatial distribution with all random distributions was always smaller than the correlation of each random distribution with all random distributions, whereas there was no difference between two random distributions. This indicates that our spatial distribution of sensor specific linear regression slopes of the paCFC is not taken from a random distribution.

Spatial patterns are independent of the group constellation We defined clusters of sensors basically using the mean slopes across subjects. Therefore it is possible that spatial patterns can be a result of the combination of exactly those eleven subjects chosen. To verify the functional relevance of our finding it is necessary to preclude that this is the case and this result cannot be replicated with another group constellation. Within our entire set of subjects we formed all possible subgroups with $N_{members}$

= 3,10, since 3 is the smallest possible size of a group and 10 is the greatest possible group different from our group of 11. We calculated the z-scored mean slope for each sensor across subjects in each of our 1.980 subgroups (see R1-S2 and FIGURE 9.2). Subsequently, we averaged the mean slopes across all possible subgroups. This yields a distribution of slopes across all sensors in which consistencies collapsed across all subgroups are emphasized. Independently, of a given subgroup there is a high probability to show the same spatial pattern as in the entire group.

Cluster size Due to the spiral arrangement of the MEG sensors we have found clusters of sensors with a size $N_{sensors} \geq 6$. It is important to exclude the possibility that this size can be achieved by a mere random process. Therefore, we calculated $N_{sensors}$ in a cluster for each of 100.000 random vector of sensors. Each random vector contained 248 values according to the number of sensors. To a sample of 9 sensors within the vector a numerical value of $v = 1$ was allocated while the remainder was $v = 0$. $N_{positions} = 9$ was chosen since $N_{sensors} = 9$ for the increase of paCFC. Subsequently, only those sensors with $v = 1$ within a given random vector were retained which had at least one adjacent sensor with $v = 1$. $N_{sensors}$ for a given random vector was formulated as the sum of retained sensors. The probability of having $N_{sensors} \geq 6$ was $p < .0195$. Importantly, the conditional probability that those 6 sensors generate an uninterrupted pattern of adjacent sensors is $p = .009$.

Importantly, this shows that the highly specific pattern of Δ paCFC cannot be achieved by trialshuffled and frequency scrambled time series and occurs also with a high probability of each randomly chosen subgroup of our participants. Moreover, this significant increase of paCFC in these sensors is not a mere change of neither theta nor high gamma (see paragraph **Calculation of the theta-phase high gamma-amplitude Cross-Frequency Coupling**). This result is absent in EEG recordings and for the coupling between theta and the gamma frequency (30-60 Hz) in the MEG-recordings. This points to an effector-selective activity of paCFC changes (Donner et al., 2009).

9.3 Probability not to respond

Subjects did not respond in all trials where we zeroized the value of the reaction time. To anyhow analyze the trial-to-trial covariation of behavior and the paCFC we substituted missing reaction time values by the mean reaction time value across all subjects in the given trial. We opt for this way since we wanted to investigate not only in which block a covariation of individual values takes place but also the exact time point from which on the covariation starts. We assume that we do not distort the distribution of reaction times since both for the fixed and the random condition the probability to commit an error of omission was by chance across subjects. Separately for both conditions to calculate the probability of omission as

$$p_{omission} = \frac{N_{omission}}{N_{events}}$$

with $N_{events} = 11$ subjects \times 48 trials \times 5 blocks and $N_{omission}$ as the number of

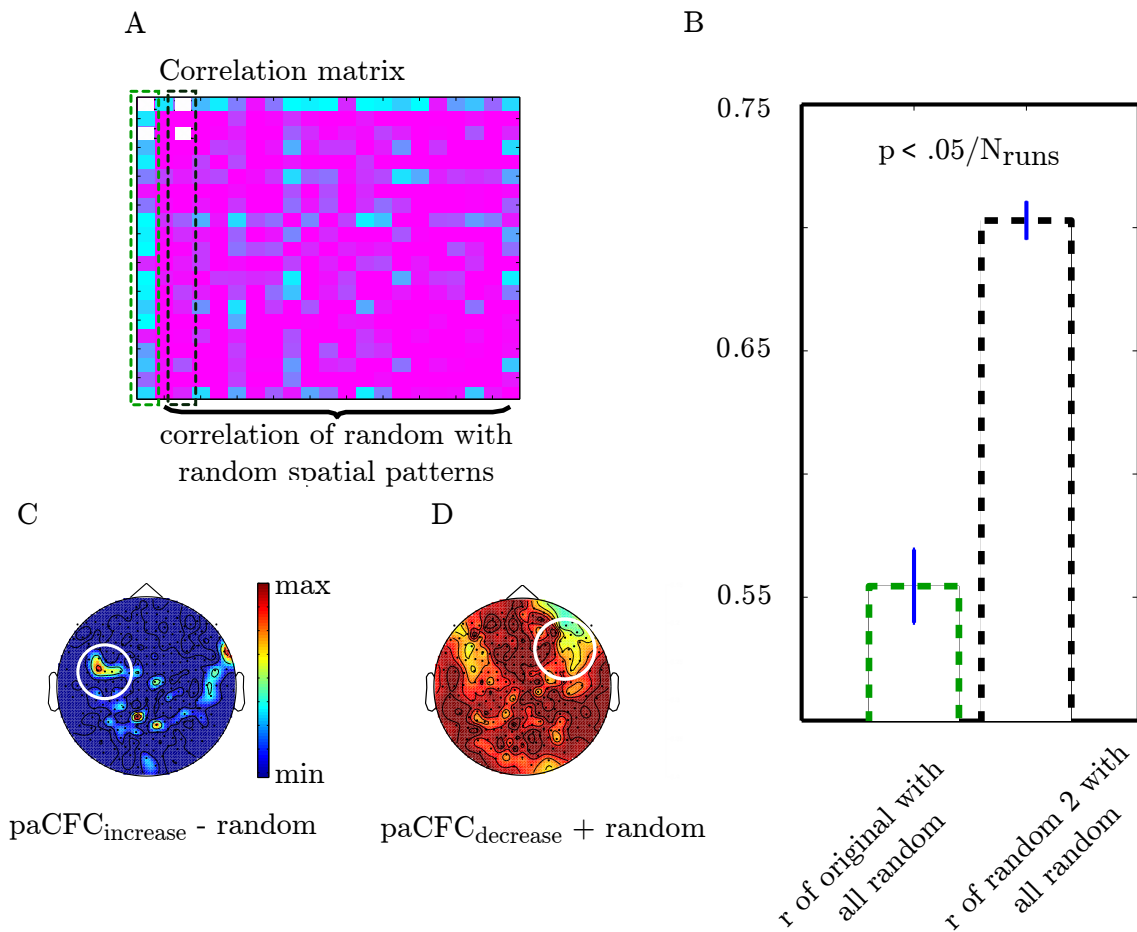


FIGURE 9.1: *A*: We calculated in 21 additional runs a random spatial pattern of paCFC slopes. These 21 random vectors and the one original vector are our vector matrix. From each pairwise correlations of all vectors in the vector matrix we calculated Pearson's r . This leads to a symmetric correlation matrix. In the first column (green dashed rectangular) there are the r -values for the original vector with all 20 random vectors. Remaining columns represent the r -values of one given random vector with all other random vector and the original vector. The first column was compared to all other columns. Blue refers to low values whereas pink refers to higher values. In *B* we depict this for the comparison with the second random vector (black dashed rectangular) with the original vector. The differences are depicted as barplots with the green dashed bar representing the mean r of the original with all random vectors except the second random vector. The blue line represents the standard error. The black dashed bar depicts the mean r of the second random vector with all other random. In those bars the r -values for the autocorrelation ($r = 1$) and the r -values with one another were excluded (white squares). The p -value was corrected for multiple comparisons. It is visible that the spatial pattern of the Δ paCFC from the original data set is different than the spatial patterns derived from the randomized data. In *C* and *D* we depict the difference between the paCFC change and the random change.

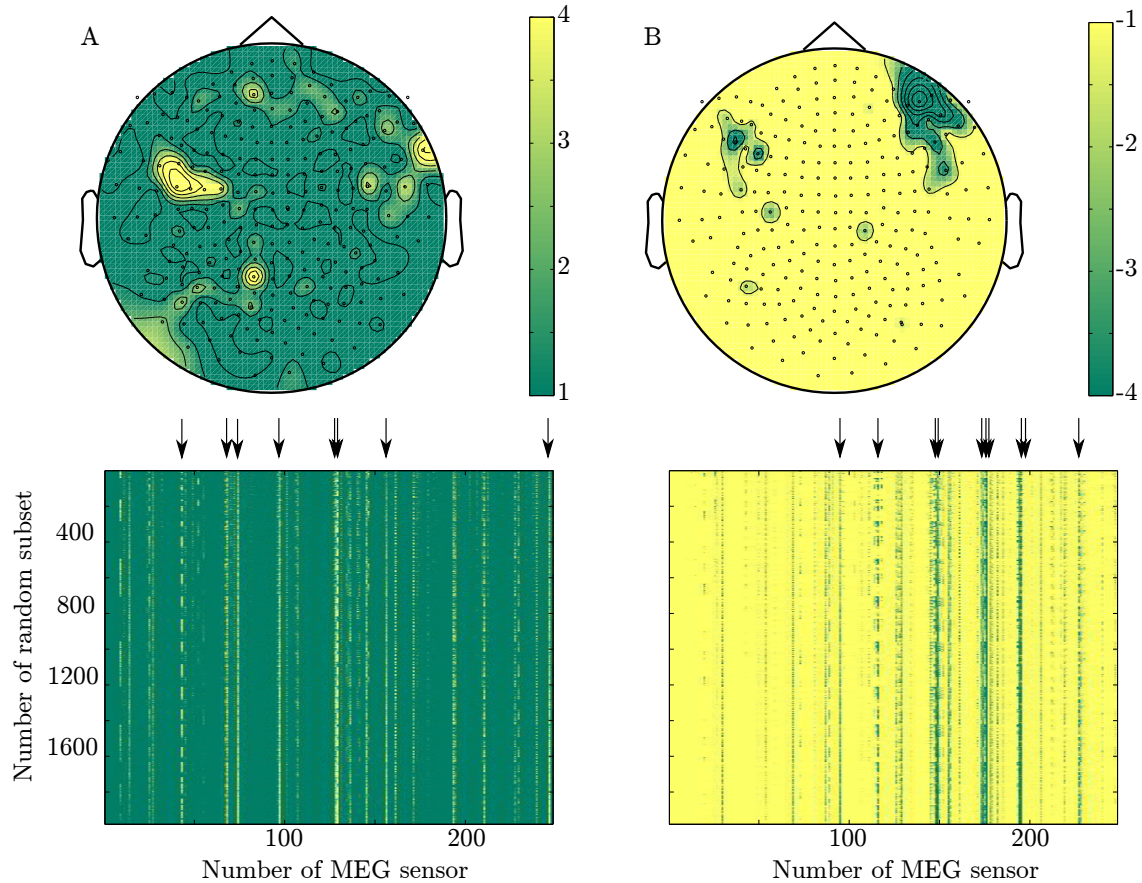


FIGURE 9.2: To preclude the possibility that the selection of sensors relies only on the mean of the entire group investigated here we calculated for each possible subgroup within the whole set of our participants the distribution of the slopes across all 248 MEG sensors. Subgroups consisted of $N = 3, \dots, 10$ participants. Each row in the lower right and left graphics represent the slope differences between sensors. Green regions represent low values whereas yellow regions represent higher regions. For each of the lower graphics it is obvious that there are some sensors (black arrows) which have a higher in the left and a lower slope in the right graphic as compared to all remaining sensors. And this is independent of the subgroup. For the upper plots of topography the whole matrix depicted in the lower graphics were averaged across all subgroups and plotted onto the head where spatial patterns are visible. For depiction the mean across all subgroups was squared to emphasize the differences across all slopes. The color bars refer to the squared z-scored slope values. For **B** the values were also multiplied by -1 to maintain the direction of change.

9 Appendix - MEG recordings

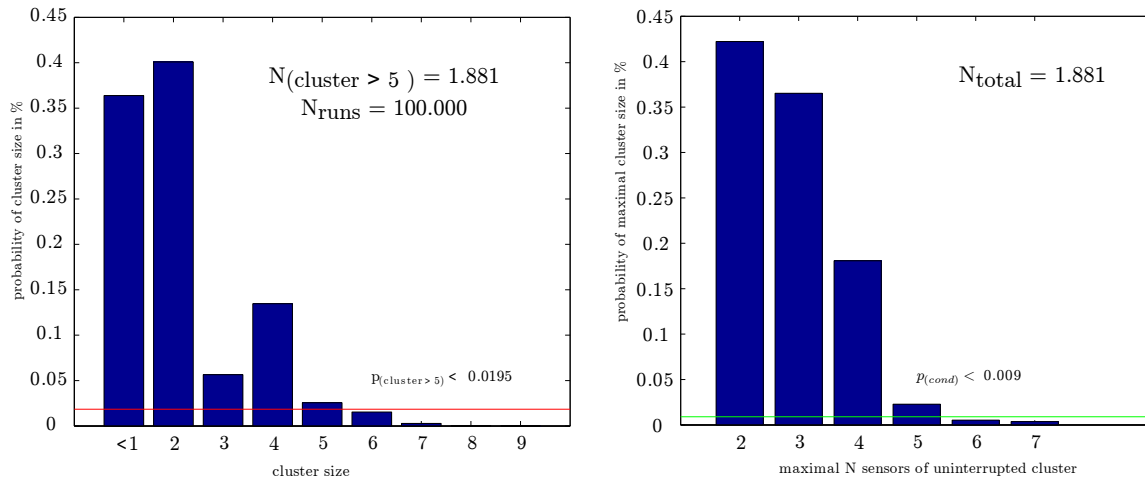


FIGURE 9.3: Depiction of the probability to find clusters of $N_{\text{sensors}} \geq 6$ by a random process.

trials with no response (fixed: $p_{\text{omission}} = .039$; random: $p_{\text{omission}} = .007$). And errors were evenly distributed across experimental blocks (fixed: $\chi^2 = 6.6$; $p > .05$; random: $\chi^2 = 5.47$; $p > .05$)

9.4 Equal variances

The correlation observed in the last block can be a mere result of differences of variance of the reaction time between our participants. We proved this by comparing the variance of reaction time between blocks across participants. An important issue is that the number of trials in scientific experiments is determined according to statistical considerations. However our primary interest is the time and number of trials necessary to learn a motor skill. Therefore, we repeated the analysis of equal variances in the following way. We averaged in each block for each participant across trials in steps of one trial. In the first run we averaged over the first two trials and in the last run over the 48 trials. This leads to 47 tests of equal variances between participants across blocks both for the reaction time and the paCFC values (see FIGURE 9.5). As result we see that independent of the number of averaged trials the variance within our population is the same across blocks for the reaction times and paCFC values, as well. We conclude that the covariation of paCFC and the inter-individual differences in reaction times in the last block is not a mere effect of greater variance between participants. Indeed we assume that this arises due to the individual differences in motor memory or differences in stimulus-response-mapping. However, one can state this only in the case that the covariation starts at least after the completion of one whole sequence and the cue for motor memory retrieval is given. We assessed this by a covariation analysis of the trialwise paCFC and reaction times as we did it in the analysis of equal variances. In a stepwise manner we averaged for each participant the paCFC values and the reaction times over trials starting with the average of the first two trials separately for each block and ending with the average across all trials separately for each block. Fur-

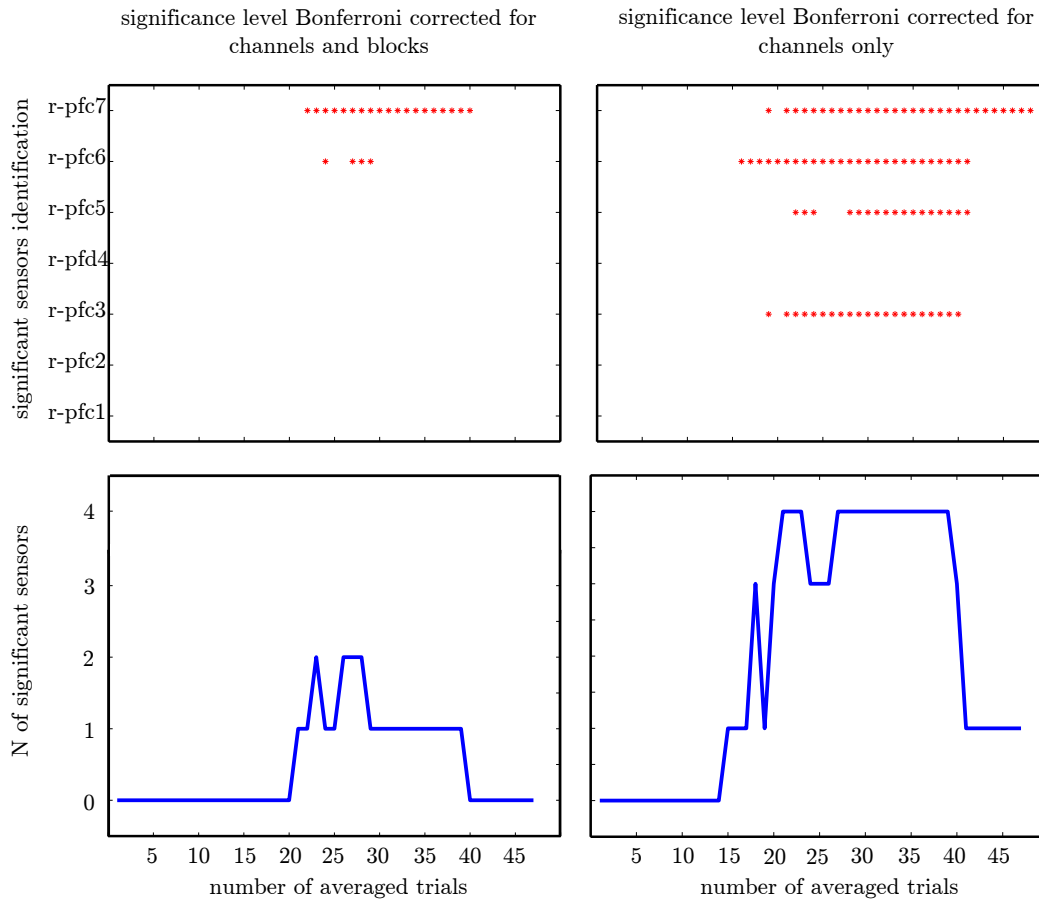


FIGURE 9.4: Depiction of channels correlating with memory retrieval in the last block. The left column shows the number and the location of the sensors whose recorded paCFC covaries significantly with behavioral differences between the participants. The significance level was corrected for multiple comparisons by number of channels (PMC/MC: 6; rPFC: 7) and the number of blocks of training ($N = 5$). In the right column the significance level was adjusted by the number of channels recorded in the block. An important note has to be made that only after the completion of at least 2 runs of the fixed sequence these individual differences of reaction times are represented in the paCFC of theta and high gamma activity. This effect is only observable in sensors covering the DLPFC and not the PMC/MC

thermore, we are interested in the location of sensors covarying with behavior. Hence, in all runs we averaged the paCFC separately for each sensor. The significance level was corrected for multiple comparisons ($p = \frac{.05}{N_{blocks} * N_{channels}}$). At this very conservative significance level we see that in the last block of training after the completion of three whole fixed sequences the paCFC of two sensors over the DLPFC (dlpfc.7 and dlpfc.6; see FIGURE 9.4) vary with individual performance. Since this is a very conservative level we also determined sensors whose paCFC covaries with individual performance. These were the 4 adjacent sensors dlpfc.3, dlpfc.5, dlpfc.6 and dlpfc.7 and this effect starts a little bit earlier but still after the complete passage of at least fixed sequences. This effect was only seen in the last block in the fixed condition and was completely

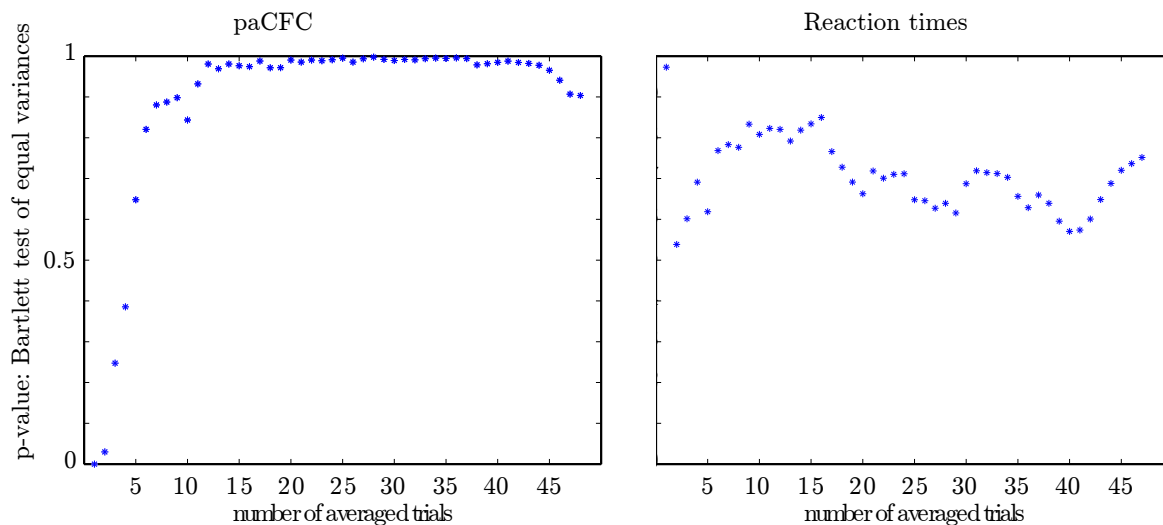


FIGURE 9.5: We conducted multiple test of equal variances both for the paCFC and the reaction times across blocks. This was done independent of the number of trials chosen. For each participant we averaged the paCFC in separated steps over 2, . . . , 48 trials in each of the blocks. The variance between the participants regarding the paCFC was compared across blocks. Each point in the left plot represents the significance level of the variance differences across blocks as a function of the number of averaged trials. p -values $< .05$ indicate that across blocks the variance of paCFC between participants differs across blocks. This shows that participants did not differ in their paCFC variance when the number of trials averaged is greater than 2. This is the result of very high inter-participant variance in the first trial of the first block of training. On the right side we show the same for the reaction times were independent of the number of averaged trials the between participant variance did not differ across blocks.

absent in the random condition.

10 Appendix - DBS recordings

10.1 Procedure: surgery and deep brain stimulation

We performed a bilateral stereotactically guided implantation of quadripolar brain electrodes (model 3387, Medtronic, Minneapolis, MI, USA) in the Nucleus Accumbens (NAcc) and in the anterior nuclear group of the thalamus (ANT) of 3 patients for treatment of a longterm pharmacoresistant epilepsy. General anesthesia was employed during the surgery. The implantation was conducted due to clinical reasons and as part of the treatment of the epilepsy.

Treatment planning standards and the surgical procedure are described elsewhere in detail *Voges et al. (2002)*. Briefly, the target for the deep brain stimulation electrode was defined using standard coordinates as the point 2 mm rostral to the anterior border of the anterior commissure at the level of the mid-sagittal plane, 3–4 mm ventral and 6–8 mm lateral of the midline (*Mai et al., 2004*), with these coordinates modified according to individual planning MRIs. An important landmark is the vertical limb of Broca diagonal band, which can be clearly visualized in coronal MRI-scans. The target was placed 2.5 mm lateral to this structure. Using a deep fronto-lateral approach, the two distal contacts of the DBS-electrode were placed in the caudo-medial accumbens, the third contact within the transition-area medial to the border of the abutting internal capsule, and the fourth highest contact in the most medial part of the capsule or in the transition area to the caudate. The contacts within the NAcc are placed in the caudo-medial part, which according to histochemical criteria represents the remnant of the shell area in the primate (*Sturm et al., 2003*). In contrast to rodents, in the primate the shell area has regressed and is no longer clearly distinguishable, except by the typical receptors that it carries.

In addition, electrodes were implanted in the bilateral anterior nuclei of thalamus (ANT) of all the patients. The anterior thalamic nucleus is located 5 mm lateral to and 12 mm above the midcommisural point according to the *Schaltenbrand atlas*. Since the anterior nucleus of the thalamus is readily visible on the floor of the lateral ventricle in MRI images, the exact location of this target could be directly specified in each patient. Intraoperatively the localization of the leads was documented by stereotactic x-ray imaging using x-ray tubes installed in the OR.

In addition, we performed postoperative CT-examination (2 mm slice thickness). After a transformation of postoperative CT- and X-ray images to align them with the stereotactic treatment planning-MRI, we defined the stereotactic coordinates of each electrode lead contact and visualized these anatomical positions on corresponding sections of two stereotactic brain atlases of (*Morel, 2007*). The localization of the electrodes is depicted in **Figure 10.1**. To further indicate the coordinates of the most caudal NAcc

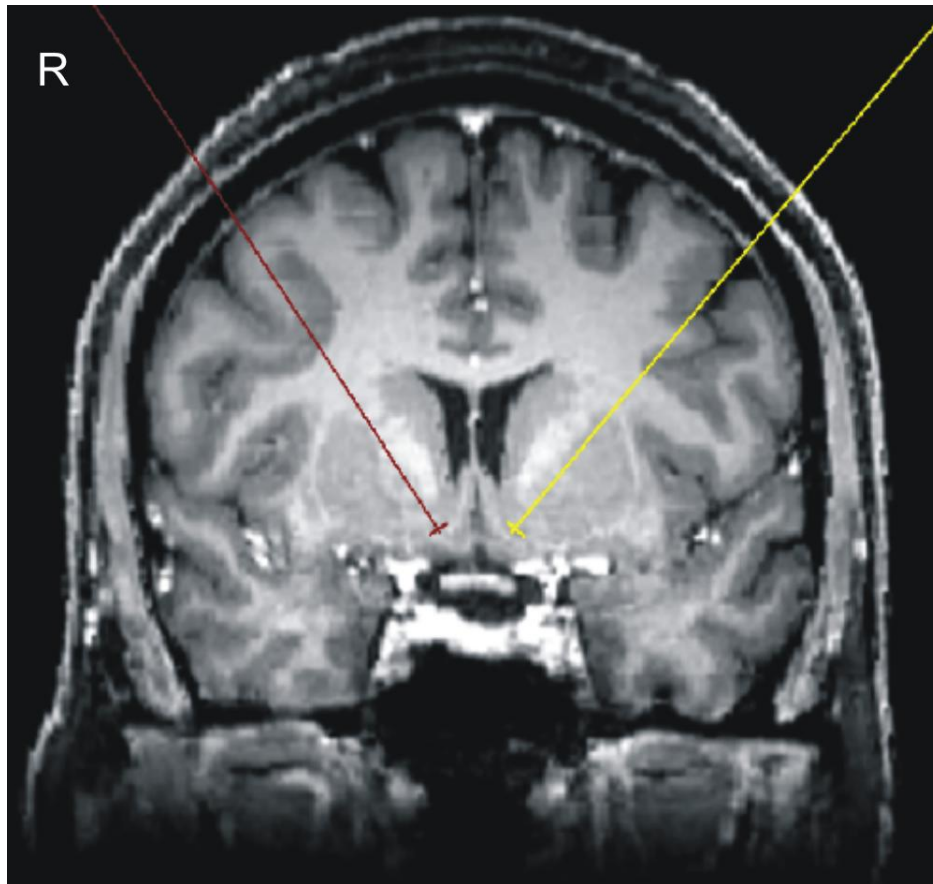


FIGURE 10.1: Anatomical location of bilateral NAccs.

electrode, we transformed all patients MRI images to MNI-space. The resulting individual MNI coordinates were (x, y, z): Pat 01: left (-6.9 5.2 -11.9), right (4.3 5.4 -10.4); Pat 02: left (-8.6 3.5 -8.6), right (9.6 3.7 -9.6); Pat 03: left (-8.3 7.5 -11.0), right (-6.2 7.3 -11.0). Postoperatively the electrode leads were externalized to allow electrical test stimulation with different parameters and recording from the depth contacts during different psychological tasks. Finally the four electrode-leads were connected to a single impulse-generator (IPG; Activa-PC, Medtronic placed subcutaneously beneath the right clavicle. To evaluate our hypotheses we analyzed data from the bilateral NAcc electrodes. To provide evidence of the specificity of our results for the NAcc we also performed a control analysis of the recordings from the bilateral thalamus. We found results described for the contralateral NAcc were not duplicated in the thalamus.

Patient	Gender, age, duration of epilepsy	Epilepsy			IQ (HAWIE-R)	Verbal memory		Figural memory (z-score)	Sustained Attention (z-score)		
		syndrome	laterali- zation	seizure onset		etiology	AEDs			Immediate free recall (z-score)	Delayed free recall (z-score)
Pat 01	F, 52, 19	multifocal	bilateral	mesio- temporal	cryptogenic	LCM 400mg LTG 200mg LEV	40(-.65)	5(-1.6)	9(-1)	8(-1.6)	199(-2.2)
Pat 02	M, 35, 9	focal	right	temporal	encephalocele	right temporal ESL 2000mg 1200mg LTB	57(-.65)	12(.2)	15(1.1)	39(-1)	486(0)
Pat 03	F, 28, 12	multifocal	bilateral	temporal	cryptogenic	200mg LCM 200mg	53(-.4)	13(.2)	15(1.1)	23(-1)	424(-.8)

TABLE 10.1:

F=female, M=male, AED = antiepileptic drugs, LCM=Lacosamide, OXC= Oxcarbazepine, LTG= Lamotrigine, LEV= Lev-
etiracetam, ESL= Eslicarbazepine acetate

TABLE 10.2:	comparison	p-value
The p-values refer	1-2	.81
to the pairwise	1-3	.64
comparisons of	1-4	.81
frequency by means	1-5	.25
of the χ^2 of the	2-3	.82
summed number	2-4	1
of errors across	2-5	.17
participants per	3-4	.82
block.	3-5	.11
	4-5	.17

11 Curriculum Vitae

Name:	Stefan Dürschmid
Date of birth:	August 26th,1979
Place of birth:	Magdeburg
Adress:	Wilhelm-Külz-Str. 4 39108 Madeburg Germany stefan.duerschmid@googlemail.com
Nationality	german
Education	1986 - 1991 POS "Karl-Wagner"- Magdeburg
	1991 - 1998 Bettina-von-Arnim Gymnasium (grammar school); Abitur
	1986 - 1998 Violin lessons, piano lessons, orchestra and chamber music, degree of upper stage at the music school
	1999 - 2001 Otto-von-Guericke University Magdeburg Major subject: Educational sciene; Minor subject: Psychology, English/Sociology
	2001 - 2005 University of applied sciences Magdeburg - Stendal (FH); Therapeutic Pedagogy
	2004 Diploma (exams)
	2002 Participation in Spanish lessons at the University of applied sciences (FH)
	2005 Participation in Spanish lessons (Unicert III) at the Otto-von-Guericke University
	2005 Advanced training of the German Alliance of Child welfare (Deutscher Kinderschutzbund) as a course instructor

11 Curriculum Vitae

	2005	Otto-von-Guericke University Magdeburg Psychology
	2007	Intermediate Diploma (Psychology) Participation in the workshop held by the University of Heidelberg. Topic: Responsibility - a useful illusion
	2009	Diploma (Psychology)
	2009	Participation in the workshop held by Dr. Michael Hanke Topic: multivariate patternanalysis with pyMVPA
Degree:	2005	Diplom-Heilpädagogin (FH)
	2009	Diplom-Psychologin
Work experience:	1993 - 1997	Participation in the German String Philharmonics (Deutsche Streicherphilharmonie) of the German Association of Music Schools (Deutscher Musikschulverband e.V.) Headman of the second violins
	2003 - 2004	Tutor at the University of applied sciences Magdeburg - Stendal (FH)
	2005 - 2006	Social facilitation for physically and mentally challenged persons at the Pfeifferschen Stiftungen Magdeburg
	2006	Teacher for Psychology, Education and Sociology (professional education Physiotherapy and Occupational Therapy) "Institut für Weiterbildung in Krankenberufen" (IWK Magdeburg)
	2006	Student assistant at the department of Biological Psychology at the Otto-von-Guericke University Magdeburg head: Prof. Dr. Chr. Herrmann
	2009 (since March)	PhD student at the department of Biological Psychology at the Otto-von-Guericke University Magdeburg head: Prof. Dr. Chr. Herrmann

	2009 (since October)	PhD student at the department of Experimental Psychology at the Carl-von-Ossietzky University Oldenburg head: Prof. Dr. Chr. Herrmann
	2010 (since January)	PhD student at the department of Neurology at the Otto-von-Guericke University Magdeburg head: Prof. Dr. H.-J. Heinze
Internships	2001	Internship at the Ministry for Labor, Health, and Women of Saxony-Anhalt (eight weeks)
	2002	Psychomotorik-Project "All the Senses" (three semesters)
	2003	10th Workshop Psychomotorik in Dortmund, Germany
	2003	Internship at the University Hospital for Psychiatry, Psychotherapy, and Psychosomatic Medicine Magdeburg (four weeks)
	2004	Internship at the service of child-welfare at the public health department Magdeburg (20 weeks)
	2004 - 2005	Internship at the <i>Universidad Peruana Cayetano Heredia</i> in Lima, Peru (six months)
Civilian service:	1998 - 1999	Civilian service at the Pfeiffersche Stiftungen Magdeburg
Programming language:		Matlab, python
Foreign language competence		Spanish English
Diploma thesis:	2004	Acceptance and Relevance of musictherapy in children with Attention-deficit hyperactivity disorder in a clinical context. Assesors: Dr. Thomas Wosch, Dr. Anette Mulkau
	2007	Neural Correlates of Localization and Identification of Visual Changes. Assesors: Prof. Dr. Christoph S. Herrmann, Dr. Niko A. Busch

12 Publikationen

- Journals**
- N.A. Busch, **S. Dürschmid**, C.S. Herrmann
ERP effects of change localization, change identification, and change blindness.Neuroreport. 2010 Mar 31;21(5):371-5.
- F. Quandt , C. Reichert, B. Schneider, **S. Dürschmid**,
D. Richter, H. Hinrichs, J.W. Rieger (2012)
**Fundamentals and Application of
Brain-Machine Interfaces.**
Klinische Neurophysiologie 43 (2): 158-167.
- S. Dürschmid**, T. Zaehle, K. Kopitzki,
J. Voges, F.C. Schmitt, H.-J. Heinze
R.T. Knight, H. Hinrichs
**Phase-Amplitude Cross-Frequency Coupling
in the Human Nucleus Accumbens
Tracks Action Monitoring during Cognitive Control.**
Frontiers in Human Neuroscience, 2013
- In Revision**
- S. Dürschmid**, Fanny Quandt, Ulrike Krämer
Hermann Hinrichs, Hans-Jochen Heinze, Reinhard Schulz
Heinz Pannek, Edward F Chang, Robert T Knight
**Oscillatory Dynamics Track Motor Automatization
in Human Cortex**
PLoS One.
- Book Chapter**
- C.S. Herrmann, **S. Dürschmid**.
**Von Libet zu einer Neuen Willensfreiheit:
Bewusste versus unbewusste Handlungsabsichten.**
In: T. Fuchs, G. Schwarzkopf (Hrsg.)
Verantwortlichkeit nur eine Illusion?, 127-146,
Universitätsverlag Heidelberg, 2010

13 Selbständigkeitserklärung

Stefan Dürschmid
Wilhelm-Külz-Straße 4
39108 Magdeburg

Hiermit erkläre ich, dass ich die von mir eingereichte Dissertation zu dem Thema: CROSS-FREQUENCY COUPLING TRACKS MOTOR AUTOMIZATION AND EXECUTION IN THE HUMAN MOTOR SYSTEM selbständig verfasst, nicht bereits als Dissertation verwendet habe und die benutzten Hilfsmittel und Quellen vollständig angegeben wurden. Weiterhin erkläre ich, dass ich weder diese noch eine andere Arbeit zur Erlangung des akademischen Grades doctor rerum naturalium (Dr. rer. nat.) an anderen Einrichtungen eingereicht habe.

Magdeburg, den 12.11.2013

Dipl.-Psych., Dipl.-Päd Stefan Dürschmid

14 Danksagung

Ich danke vor allem Herrn Prof. Hinrichs für die in fachlicher und menschlicher Hinsicht unkomplizierte, hilfreiche und wegweisende Unterstützung während der gesamten Arbeit.

Besonderer Dank gilt meinem Lebenspartner Dr. Hagen Bönigk und unserem Sohn Paul Bönigk für den Blick auf das Relevante.